Decoherence of spatially separated quantum bits

Dissertation

zur Erlangung des akademischen Grades eines
Doktors der Naturwissenschaften,

vorgelegt der Mathematisch-Naturwissenschaftlichen Fakultät
der Universität Augsburg

von

Roland Doll

Augsburg, im Januar 2008

Prüfungskommission

Priv. Doz. Dr. Sigmund Kohler	(Erstgutachter)
Prof. Dr. Stefan Kehrein	(Zweitgutachter)
Prof. Dr. Peter Hänggi	
Prof. Dr. Achim Wixforth	
Tag der mündlichen Prüfung:	22.02.2008

Contents

1

Introduction

Substantial technical progress in the last two decades enabled the development and fabrication of nanoscale devices that exhibit explicit quantum mechanical properties on a macroscopic level. The ability to gain external control of such devices allows one to put the fundamental laws of quantum mechanics to a test. A lot of effort in this direction certainly was driven by the emerging discipline of quantum information processing whose basic aim is not only to test quantum mechanics, but rather to understand how its principles can actually be used for the manipulation, storage, and communication of information.

Computers based on intrinsic quantum mechanical devices will not only process information faster than today's computers. Rather, they are able to run specially designed quantum algorithms to perform tasks that go beyond the capability of any classical approach. For the implementation of a quantum algorithm it is necessary to ensure and control the unitary evolution of an array of quantum mechanical two-level systems, i.e. a qubit register. Solid-state quantum systems using charge or spin degrees of freedom of confined electrons or holes, and also superconducting qubits based on Josephson junctions are currently very promising candidates for its realization. However, one of the major remaining challenges is decoherence: The interaction of the qubits with their environment affects the indispensable quantum coherence and entanglement of the quantum states. Thus, understanding of decoherence in quantum computer architectures is crucial for the development of successful qubit operations in scalable solid state systems.

Several strategies are pursued to beat decoherence [1, 2]. An active scheme is quantum error correction [3–5], which requires a redundant encoding of a logical qubit by several two-level systems, so-called physical qubits. Standard error correction protocols are designed to work efficiently if the physical qubits are subject to independent errors. This condition can be realized by putting the qubits far apart so that it is reasonable to assume that they couple to uncorrelated noise sources. Decoherence-free subspaces are a passive variant of quantum error correction [6–9]. In this scheme, one logical qubit is encoded by several physical qubits in such a way that the logical qubit states do not couple to the environment at all. Consequently, the quantum code works perfectly coherent and neither the detection nor the active correction of errors is needed. Ideal decoherence-free subspaces occur when the qubit-environment coupling exhibits symmetries such that the physical qubits interact with perfectly correlated noise, an idealized situation that can be achieved by co-located qubits. In several physical situations,

however, spatial correlations in the fluctuations of the environment can be present and neither of the ideal cases outlined above is perfectly realized. In the present thesis we focus on these non-ideal situations. Our goal is to study the consequences of spatially correlated quantum noise for the dissipative entanglement dynamics and the fidelity of a qubit register. We investigate the interplay of decoherence and spatial qubit separation.

The following sections give an overview of the basics of quantum information processing and briefly review the ideas of quantum error correction and decoherence-free subspace encoding and their respective relations to independent and collective noise models. We then present in Chap. 2 a system-bath model that takes spatial separations of qubits explicitly into account. It is shown how various physical situations can be mapped to our model. For the case in which the environment induces pure phase noise, the reduced qubit dynamics possesses an exact solution which we present in an explicit form in Chap. 3. Since it is not always feasible to achieve exact results for the dissipative system dynamics, we consider in Chap. 4 a time-convolutionless master equation approach and derive a non-Markovian master-equation for weak qubit-bath coupling. An application of this approximate equation to our pure phase noise model allows for an unambiguous comparison with an exact solution and shows that the emerging results can even be exact, despite the fact that they are based on second-order perturbation theory. As a first application of the analytical results, we discuss in Chap. 5 the dephasing of a single qubit for various spectral densities of the environment. We concentrate on the short-time dynamics of the qubit coherence. It is shown that algebraic decay laws lead to a fast initial loss of the coherence which in the standard description with exponential decay rates shows up as a reduced initial amplitude of coherent qubit oscillations. Analytical expressions quantifying the amount of this reduced visibility are derived and its dependence on temperature and qubit-bath coupling strength is studied. In Chap. 6 the entanglement dynamics of two spatially separated qubits is considered and the robustness of the two-qubit decoherence-free subspace with respect to physical parameters such as temperature, qubit-bath coupling strength and qubit separation is investigated. We then focus on the time evolution of a spatially extended N-qubit register with linear qubit arrangement. Explicit expressions for the fidelity loss of the register are presented and the scaling of decoherence as a function of the number of qubits and their separations is studied.

Since the exact solution for the reduced dynamics of a qubit register subject to pure phase noise involves rather complex expressions, an intuitive picture of the observed behavior can be hard to find. For a more qualitative understanding we study in Chap. 7 the reduced dynamics in an approximate treatment in the spirit of the Bloch-Redfield theory. It is shown that a direct application of the Bloch-Redfield theory to a spatially extended system of qubits leads to a violation of causality and predicts spurious decoherence-free subspaces. We reveal why this approach fails and derive a non-Markovian causal master equation that captures the main effects of the spatial separation. Compared to general non-Markovian master equations, our causal master equation has the advantage of being more intuitive and of allowing for algebraic methods, e.g. within a symmetry analysis. In Chapter 8 two qubits subject to bit-flip noise are studied using the causal master equation approach. We investigate how spatial noise correlations influence the relaxation of solid-state qubits. It is shown that by collective exchange of bosons via a thermal environment effects similar to superradiance and subradiance are possible even

for rather large qubit distances and at high temperatures.

1.1 Quantum information processing

Quantum mechanics since its birth in the 1920s became one of the most successful theories of modern science. It sheds light on a vast number of physical phenomena that are not accessible by purely classical methods. Although the concepts of quantum theory often appear to have little relation with the human experience of nature, it is capable to correctly describe physical effects on the nanometer scale.

Entanglement is one of those inherently quantum mechanical properties that can emerge when individual parts of a bi- or multipartite quantum system interact with each other [10, 11]. It leads to correlations between observable physical properties of the quantum systems that, from a classical point of view, appeared to Einstein as a "spooky action at a distance" and caused him, Podolsky, and Rosen in 1935 to formulate the so-called "EPR paradox" [12], a quantum-mechanical Gedankenexperiment with a highly counterintuitive and apparently nonlocal outcome. Indeed, entanglement is a phenomenon in which the quantum states of two or more objects have to be described with reference to each other, even though the individual objects may be spatially separated and not interacting anymore. It can emerge already for the simple case of two quantum mechanical two-level systems: As a consequence of the superposition principle of quantum mechanics, each two-level system individually can be in a superposition of two basis states $|0\rangle$ and $|1\rangle$, but once both systems have interacted with each other, a possible state of the two systems as a whole is $(|01\rangle + |10\rangle)/\sqrt{2}$. This state vector contains the full information about the total system. However, all information is contained in joint properties and only by a projective measurement on either of the two-level systems, the state of the other one can be predicted with certaincy. It is this "spooky action" on which quantum teleportation and quantum cryptography are based on [1, 13–15].

Quantum mechanics is required to understand and also tailor properties of micro- and optoelectronic devices as for example semiconductor based integrated circuits and microprocessors used in the electrical industry nowadays. However, once these properties are established, the actual operation of such devices can be described on the basis of classical theories, e.g. by classical electrodynamics. Put differently, even though the components of a classical computer are designed and developed by using the knowledge about quantum mechanical effects, they are operated classically and consequently implement classical Boolean logic, i.e. process a unit of information in the form of a classical bit which carries either the value 0 or 1. A thrilling question is what happens when the physical basis for the computer becomes explicitly quantum so that the classical approximation fails. Will such a quantum computer be more powerful than a classical one? In 1982, Feynman put this question in another form by asking whether a classical computer ever could efficiently simulate quantum mechanical systems [16]. To simulate N interacting two-level systems one generally has to keep track of 2^N complex numbers. Thus, the problem size grows exponentially with N which renders it unrealistic to classically simulate even a few hundred two-level systems in a reasonable time. On the other hand, this line of argumentation demonstrates the large amount of information that is present in a quantum system. It led to the conclusion that only quantum systems can be

able to efficiently simulate themselves [16–18] and thus outperform classical computers.

For a device that is supposed to process quantum information, one has to define how information is stored and in which way an input can be transformed into the desired output. These decisions are still hardware independent and the most natural approach is the network model [1, 2, 16, 19, 20]: In analogy to the way in which classical binary information is processed, quantum information can be stored in a register of quantum mechanical two-level systems. In this context the two-level system is called a quantum bit or qubit. The qubit register is initially prepared in a definite state, the input. By controlling the Hamiltonian of the register and hence its time evolution, the input register state is in a prescribed way changed to an output state, i.e. a computation is performed. It turns out that all possible unitary operations in the Hilbert space of the qubit register can be decomposed to a sequence of universal quantum gates [1] which only involve single- and conditional two-qubit operations. Such a sequence of gates defines a quantum algorithm. Modifications and alternatives to the network model have been proposed that can efficiently run quantum algorithms, among them are quantum cellular automata, the one-way quantum computer, and adiabatic as well as topological quantum computers [21–28].

The speedup that can be gained by doing a computation quantum mechanically is a consequence of what is termed "quantum parallelism": A classical gate g which, for example, processes a binary string of two digits $N = 2$ has to be evaluated four times to get all possible output values $g(00)$, $g(01)$, $g(10)$, and $g(11)$. Due to linearity of quantum mechanics, a corresponding quantum gate can be fed with the superposition of all possible input states, i.e. $g(|00\rangle + |01\rangle + |10\rangle + |11\rangle)$ and returns a superposition of all possible outcomes at the same time, $g(|00\rangle) + g(|01\rangle) + g(|10\rangle) + g(|11\rangle)$. The initial creation of the superposition is efficient since its complexity grows linearly with the number N of qubits [2]. The single computational step of the quantum gate, however, replaces 2^N steps of the classical counterpart [19]. However by a measurement, the superposition of all possible outcomes is reduced to one actual outcome so that it seems that the computational power, though present, is not accessible. In fact, the advantage of the quantum parallelism manifests itself when one is interested not to find all answers to all possible inputs but rather to find global characteristics, e.g. to decide whether a function is constant or not, or to find its period [18, 29, 30]. Prominent examples for efficient and quite useful quantum algorithms that outperform all known classical variants are the search in an unsorted database with a quadratic speed-up [31, 32], and the factorization of integers [33] with exponential performance gain. In particular the latter has gained much interest, since most forms of encryption technology today as for example the widely-used RSA public key cryptography are based on the fact that it is easy to quickly perform multiplications of prime numbers, but – by classical means – hard to do the opposite, i.e. to factorize a large integer into its prime factors [34].

An exponential speedup of a quantum algorithm over any classical algorithm for the same computational task is fundamentally a feature of quantum entanglement [35]. It is possible to imitate some important properties of quantum computing by using classical waves, e.g. classical light beams, since they admit the possibility of superpositions of modes [36]. However, regardless of how much the waves interact with each other, their joint state is always a product state. The total state space of all classical waves is the Cartesian product of the individual spaces, whereas quantum-mechanically it is the ten-

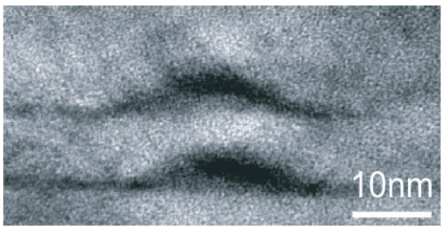

Figure 1.1: Image of a vertically stacked pair of self-assembled quantum dots (dark gray) taken by cross-sectional transmission electron microscopy [47].

sor product. Only in the latter case linear combinations of product states can be formed such that they give rise to quantum entanglement, i.e. an exponential performance gain is not only due to superposition and interference, but also entanglement [37, 38]. Note that algorithms that are based solely on single-qubit superpositions exist [39, 40]. Although they involve only separable states, they may outperform classical variants with polynomial speedup. Nevertheless, it is in principle still possible to simulate them efficiently on a classical computer.

1.2 Qubit realizations

A vast variety of different physical systems have been considered for the experimental realization of quantum bits [41]. One approach is the encoding of qubits in ensembles of nuclear spins of dissolved molecules [42]. Well established techniques of nuclear magnetic resonance are used to manipulate the spin states. Although based on an ensemble rather than on single qubits, an important proof-of-principle of quantum computation was achieved by this setup in factoring the number 15 into its prime factors 3 and 5 based on a quantum algorithm [43]. Another possibility is to use a chain of trapped ions to encode quantum information in the internal states of the ions as well as in the vibrational modes of the chain; the qubit register is then manipulated by means of external lasers [44]. Optical implementations of qubits encoding the information in photons also play an important role for quantum information processing [45]. They have been among the first physical systems to enable the realization of multipartite entanglement and are successfully applied for experimentally realizing quantum cryptography [15].

A common problem of the aforementioned approaches is the difficulty to scale up the architecture from a few-qubit system to a many-qubit system. This requirement is one of the five Di-Vincenzo criteria for the implementation of a quantum computer [46]:

- A scalable physical system with well-defined qubits
- The ability to initialize the qubits in a known pure state
- The ability to realize a universal set of quantum gates
- Decoherence times much longer than the gate operation times
- A qubit-specific possibility to perform a measurement with high fidelity

In current setups, ion trap quantum registers of at most 8 qubits have been realized [48]. However, it is believed that at least 20-50 qubits are needed to perform non-trivial quantum computational tasks beyond proof-of-principle applications [1, 2]. Solid-state based realizations of qubits may reach the criterion of scalability more easily. Very promising candidates are for example superconducting qubits based on Josephson junctions [49] and quantum dot qubits. In the following, we will focus on the latter.

A quantum dot is an artificially structured system in which charge carriers (electrons

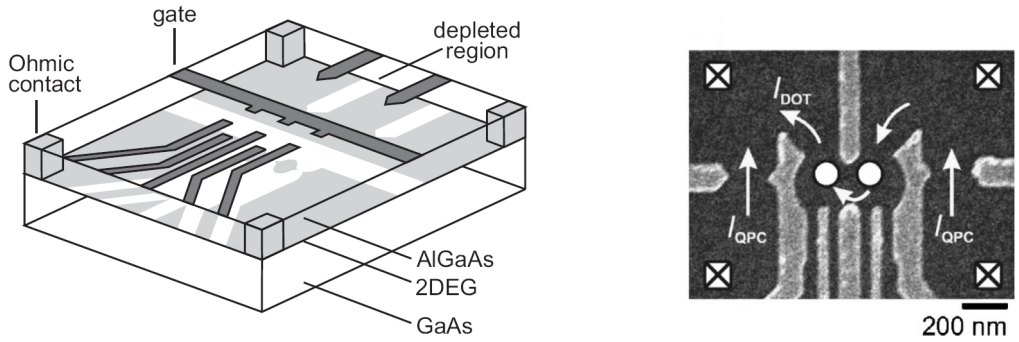

Figure 1.2: Lateral double quantum dot defined by metal surface electrodes, taken from Ref. [58]. Left: Schematic view. Negative voltages applied to metal gate electrodes (dark gray) lead to depleted regions (white) in the two-dimensional electron gas (2DEG). Right: Scanning electron micrograph for a slightly different layout showing the gate electrodes (light gray) on top of the surface (dark gray). The white dots indicate the location of the two quantum dots.

or holes) can strongly be confined in three spatial directions to exhibit a discrete level structure. Depending on whether charge or the spin degrees of freedom of the confined carriers are utilized to form the qubit, one differs between charge or spin qubits. There is a rich variety of approaches to realize the desired confinement. For example, self-assembled quantum dots are grown epitaxially by depositing layers of lattice-mismatched materials, like InAs on a GaAs substrate [50]. Due to the lattice strain the layers assemble into small self-organized islands with typical confinement lengths of the order of a few to tens of nanometers, see Fig. 1.1. Quantum information may then be encoded in neutral and charged excitonic states and probed and manipulated optically [47,51–54]. Several dots can, for example, be vertically stacked [55] so that quantum dot molecules are formed whose coupling is controllable by static electric fields [56, 57].

Another sort of quantum dots is realized by means of semiconductor heterostructures such as GaAs/AlGaAs, see Fig. 1.2. The dots are defined by locally depleting the two-dimensional free electron gas at the heterointerface with electric fields that are created by applying negative voltages to metal gate electrodes on top of the heterostructure. In this way, small islands of electrons can be isolated from the rest of the two-dimensional electron gas. The gate voltages allow one to precisely control the number of free electrons from several hundreds down to zero [59, 60]. Qubits based on the charge degree of freedom use an odd number of electrons confined in a double quantum-dot structure [61–63]. The excess electron moves between the dots like in a double-well potential whose asymmetry and tunneling barrier can be controlled by the gate voltages. The logical qubit states are defined by the localization of the unpaired electron in the left or right dot. In such double-dot charge qubits, coherent oscillations have been realized experimentally [64–66], and strong decoherence was observed due to the coupling of the electron to external degrees of freedom, in particular to phonons and charge fluctuations in the substrate, as well as to electromagnetic noise in the environment [62,67–72]. By contrast, in the quantum dot spin qubit the quantum information is encoded in the spin state of a single electron or in the singlet and triplet states of two electrons [53,58,73,74]. The spin

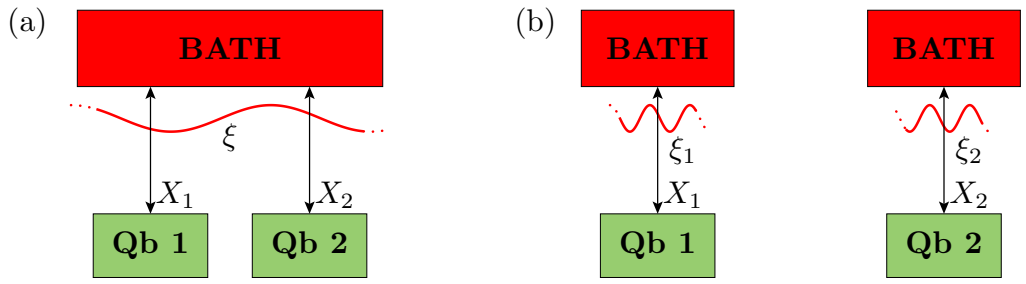

Figure 1.3: Schematic representation of two qubits (green boxes) interacting (a) with a common bath, and (b) with two independent baths.

degree of freedom is expected to be better isolated from the environment, although at the same time it is harder to control and readout. Nevertheless, substantial experimental progress enabled the readout and the coherent manipulation of single electron spins, as well as the realization of two-qubit gates, see Ref. [58] for a recent review. Relevant decoherence mechanisms in spin qubits based on GaAs/AlGaAs heterostructures are spin-phonon coupling [75, 76] and in particular hyperfine interaction with nuclear spins of the bulk material [77–80]. Recently, a lot of efforts exist to form gated quantum dots in alternative materials for which nuclear spins are supposed to be less detrimental, as for example carbon nanotubes [81–83] and Si/SiGe heterostructures [84]. There are alternative approaches for qubits in semiconductors based on donor impurities embedded in a crystal matrix, e.g. buried phosphorus dopants in silicon [85]. In such systems, a qubit can be defined by the nuclear spin states of the dopant [86] or, similar to the gated double quantum dot, by the charge degree of freedom of a single electron shared by two donor atoms [87, 88].

1.3 Collective vs. independent noise

As mentioned above, one major obstacle for realizing quantum bits in the solid state is decoherence, i.e. the inevitable coupling of the quantum system to environmental degrees of freedom (or bath) which causes unwanted errors of the qubit state. Decoherence here means both dephasing, i.e. loss of phase coherence in superpositions of the logical qubit states $|0\rangle$ and $|1\rangle$, as well as dissipation, i.e. processes in which the populations of the quantum states are modified so that bit flips $|0\rangle \leftrightarrow |1\rangle$ occur.

For a theoretical description of decoherence in many-qubit systems it is frequently assumed that depending on the qubit separation either all qubits couple via a collective coordinate to one common bath or each qubit couples to a separate heat bath, see Fig. 1.3. In the former model the qubits experience perfectly correlated noise which allows for a qubit-permutation symmetry in the system-environment coupling. In such situations the quantum information eventually can be preserved by the use of decoherence-free subspaces $\mathcal{S} = \{|s_k\rangle\}$ of the qubits' Hilbert space $\mathcal{H}_\mathrm{s}$ that effectively decouple from the influence of the environment [6–9]. For a qubit-environment coupling of the form

$$H_\mathrm{sb} = \sum_\nu X_\nu \otimes \xi_\nu \,, \tag{1.1}$$

where X_ν and ξ_ν are qubit operators and bath operators, respectively, the states $|s_k\rangle$ are decoherence-free if they are degenerate eigenstates to all coupling operators [9],

$$X_\nu |s_k\rangle = \lambda_\nu |s_k\rangle , \quad \text{for all } \nu \text{ and } k . \tag{1.2}$$

Furthermore, the coherent evolution of the qubits by a system Hamiltonian H_s has to leave the subspace $\mathcal{S}$ invariant.

As an example which explains nicely the idea of decoherence-free subspace encoding, let us consider the situation depicted in Fig. 1.3a in which two qubits $\nu = 1, 2$ with Hilbert space $\mathcal{H}_\mathrm{s} = \mathcal{H}_{\mathrm{s},1} \otimes \mathcal{H}_{\mathrm{s},2}$ couple collectively to a common environment such that

$$H_\mathrm{sb} = (X_1 + X_2) \otimes \xi . \tag{1.3}$$

Suppose that by this interaction the qubits undergo a pure dephasing process that puts a random phase between the logical qubit states $|0\rangle_\nu$ and $|1\rangle_\nu$ of each qubit ν, which we define as the eigenstates of the Pauli matrix σ_z with respective eigenvalues $+1$ and -1. To this end, the first qubit couples via $X_1 = \sigma_z \otimes \mathbb{1}$ and the second via $X_2 = \mathbb{1} \otimes \sigma_z$. Condition (1.2) implies that there exists a decoherence-free subspace $\mathcal{S}$ spanned by the two states $|s_1\rangle = |01\rangle = |0\rangle \otimes |1\rangle$, and $|s_2\rangle = |10\rangle$ which both are eigenstates of the collective coupling operator $X_1 + X_2$ with zero eigenvalue. Hence it is possible to encode one logical qubit in the two-dimensional subspace $\mathcal{S}$ of two physical qubits by using the states $|s_k\rangle$ as new logical basis states. Since the noise acts collectively on both qubits, the states in the subspace $\mathcal{S}$ acquire random, but equal phase shifts so that the relative phase of any linear combination of them remains stable.

Since the first observations of such "subdecoherence" [6], the idea of avoiding errors by decoherence-free subspace encoding has been put to a general mathematical framework, for a review see Ref. [9]. It turned out that decoherence-free subspaces are a particular case of quantum error correcting codes [1,3–5], where again a logical qubit is encoded in a subspace $\mathcal{S}$ (the code space) of several physical qubits. The encoding is such that the information represented in the code can actively be restored after any one of the errors occurred for which the code was designed. To restore the information, first a syndrome is measured that identifies which error has to be corrected for, and then a conditional subsequent recovery operation is applied that projects the erroneous qubit state back to the code space. This procedure is repeatedly performed with a rate $1/t_\mathrm{cycle}$ which must be kept high enough to sufficiently suppress uncorrectable errors. For decoherence-free subspaces, the existence of symmetries in the system-bath coupling manifests itself in the absence of errors to any order in error rate p, that is the probability of an error per cycle time [1, 89]. By contrast, error correcting codes are based on a perturbative treatment, i.e. they are designed to prevent decoherence to a given order in the error rate but allow for residual errors to take place. The underlying key assumption for the efficient use of quantum error correcting codes is that errors in different qubits occur independently [4, 5], i.e. it is presumed that physical qubits couple to different heat baths, see Fig. 1.3b. Then the interaction Hamiltonian takes the form (1.1) with totally uncorrelated bath coordinates ξ_ν. This constitutes the limiting case of independent decoherence for which no decoherence-free subspace can be found [8].

To exemplify the idea of quantum error correction let us again consider the case of phase noise as discussed above. In contrast to collective decoherence, the phase

coherence of each qubit ν now gets randomized independently. This process may be interpreted in terms of rotations $R_\nu(\varphi) = \mathrm{diag}(\mathrm{e}^{\mathrm{i}\varphi}, \mathrm{e}^{-\mathrm{i}\varphi})$ around the z axis by a random angle. Although the influence of noise is continuous, the repeated application of the error measurement introduces a natural discretization of the possible errors [4]. For the example of phase noise, the effective rotation R_ν of qubit ν after time t_{cycle} may be understood as a linear combination of two basic errors, namely no error [the identity $\mathbb{1} = R_\nu(0)$] and phase flip error $\sigma_z = R_\nu(\pi)$, i.e. a state is transformed according to

$$\alpha\,|0\rangle_\nu + \beta\,|1\rangle_\nu \xrightarrow{\sigma_z} \alpha\,|0\rangle_\nu - \beta\,|1\rangle_\nu \ . \tag{1.4}$$

An adequate error-correcting code must be designed such that its protocol can detect and correct those basic errors up to the probability at which they occur. Suppose that in the linear combination of errors for a single qubit, a phase flip occurs with relative probability p, i.e. the probability of no error is $1-p$. We look for a protocol that encodes one logical qubit into several physical qubits such that the probability that we cannot recover the correct logical qubit state is less than the probability p of an error without any encoding. To this end, it is convenient to represent the phase flips in the basis

$$|+\rangle = \frac{1}{\sqrt{2}}(|0\rangle + |1\rangle), \quad |-\rangle = \frac{1}{\sqrt{2}}(|0\rangle - |1\rangle)\,, \tag{1.5}$$

with $\sigma_x\,|\pm\rangle = \pm\,|\pm\rangle$. Thus, a phase flip in the standard basis appears in the $|\pm\rangle$ basis as a bit flip $|+\rangle \leftrightarrow |-\rangle$. We then can use the repetition code [3]

$$\alpha\,|+\rangle + \beta\,|-\rangle \ \rightarrow\ |s\rangle = \alpha\,|+++\rangle + \beta\,|---\rangle \ , \tag{1.6}$$

which maps one logical qubit to an entangled state of three physical qubits, i.e. the code space $\mathcal{S}$ is spanned by the two states $|+++\rangle$ and $|---\rangle$. Note that this encoding operation does not copy the quantum state since the latter is prohibited by the no-cloning theorem [90].

Let us assume that an error occurred in at most one of the three qubits. One has to decide which qubit, if any, is erroneous without destroying the encoded information. This error syndrome can be determined by a measurement of the parity $\sigma_{x\nu}\sigma_{x\nu'}$ for each qubit pair $\nu\nu'$. If, for instance, the erroneous state is $|s'\rangle = \alpha\,|-++\rangle + \beta\,|+--\rangle$, the parity of pair 12 is equal to the parity of pair 13, but it is different from pair 23. From that we can deduce that the first qubit was affected and the state can be corrected by the projection

$$\left[|+++\rangle\langle-++| \ + \ |---\rangle\langle+--|\right] |s'\rangle = |s\rangle \ . \tag{1.7}$$

It is clear that if all qubits acquired an error, which happens for independent qubits with probability p^3, the legal codeword $|+++\rangle$ cannot be distinguished from the legal codeword $|---\rangle$ and vice versa, i.e. no error can be detected at all. If the phase of two qubits was flipped, a spurious single-qubit error is detected and, thus, wrongly corrected. This happens with probability $3p^2(1-p)$. In total, the probability of an error remaining uncorrected is $3p^2 - 2p^3$ and, thus, one benefits from error correction if $p < 1/2$, provided that the errors in different qubits are independent of each other.

The two examples above demonstrate that passive error protection by decoherence-free subspace encoding and active quantum error correction work efficiently in mutually

exclusive limiting cases. Ideas exist to concatenate both strategies by forming clusters of qubits [89], i.e. groups of nearby qubits are formed and protected by decoherence-free subspaces and quantum error correction is applied to the set of groups. In experimental realizations, however, physical qubits will never be exactly co-located; first, they must be individually addressable and, second, the system which implements the qubit will have a natural finite extension. We cannot put the qubits arbitrarily far apart, as well, since in order to get them entangled, we must be able to control their mutual interaction. If correlations in the fluctuations of the environment are present, i.e. if their length scales and the distances between qubits are comparable, neither a collective decoherence model nor an independent decoherence model is justified. For example for charge qubits based on quantum dots or donor impurities, a relevant source of decoherence is the coupling to substrate phonons [64, 66–68, 72, 87, 91–93]. Widely separated dots at high temperatures will experience uncorrelated noise due to the phonon bath. However, at lower temperatures and smaller separations, spatial correlations become important. In a typical solid-state substrate, the sound velocity is of the order of $c \approx 10^3$m/s. At a temperature of $T = 1$K phonons with long wavelengths of at most $\lambda \approx 50$nm are dominant and typical donor or dot separations are of the order of several tens to hundreds of nanometer. Thus, for low temperatures and multi-qubit setups the identification of a crossover regime between collective and independent decoherence requires models in which the qubit separation and the phonon bath are taken explicitly into account. The development and the study of such models is the topic of this thesis.

2

Coupling qubits to bosonic fields

We will now present a heat-bath model which allows for spatial noise correlations with the collective and independent noise models as limiting cases for vanishing and infinite qubit separation, respectively. This constitutes the starting point for our calculations in the subsequent chapters. We formally derive the model for the case of a one-dimensional environment starting from an appropriate Lagrangian and then generalize it to higher dimensions. Finally, we relate it to various microscopic coupling mechanisms that are important for specific qubit realizations.

2.1 Heat-bath model

A successful approach to the description of irreversible dynamics within quantum mechanics is the use of system-bath theories. The system of interest interacts with its environment, i.e. external degrees of freedom which act as a heat bath. The combined set, system plus bath, is considered as a closed system so that the usual rules of quantum mechanics apply. In particular, the dynamics governed by the total Hamiltonian H (of the system, the environment, and their interaction) is unitary. However, due to the interaction the system and the bath may get entangled and energy may be exchanged. These processes lead to dephasing and dissipation in the reduced system dynamics.

The total Hamiltonian of a heat-bath model reads

$$H = H_{\mathrm{s}} + H_{\mathrm{b}} + H_{\mathrm{int}} \,, \tag{2.1}$$

where H_{s} describes the system of interest, H_{b} is the Hamiltonian of the heat-bath and H_{int} their interaction. A macroscopic environment usually has many more degrees of freedom than the system of interest. For that reason, it is plausible to argue that the coupling of the system to a single environmental degree of freedom is weak, i.e. it is reasonable to assume that H_{int} is a bi-linear interaction between system operators X_ν and bath operators ξ_ν [94]. Note that this assumption does not immediately imply that also the total system-environment coupling is weak, since a single degree of freedom of the system is generally influenced by many external ones. The interaction Hamiltonian may also include an additive counter term H_{c}, which is a function of system operators and depends on the properties of the system-bath coupling. It typically removes a

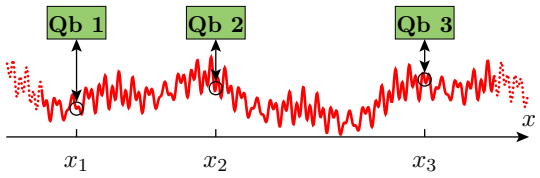

Figure 2.1: Schematic representation of three qubits (green boxes) interacting via a coupling to the bosonic field (red line) at their positions $\mathbf{x}_\nu$.

renormalization stemming from the coupling,

$$H_{\mathrm{int}} = H_{\mathrm{sb}} + H_{\mathrm{c}} = \sum_\nu X_\nu \xi_\nu + H_{\mathrm{c}}\,. \tag{2.2}$$

2.2 System-bath coupling

In this work we are interested in the influence of an environment to a system of qubits. Assuming that the environment itself is only weakly perturbed by the presence of the qubits, its response to the perturbation exerted by the system is linear and one may model the environment by a set of independent harmonic oscillators. Modelling a quantum heat bath by independent bosons has a long standing history in quantum dissipation [95–101] and is usually referred to as Ullersma, Caldeira-Leggett, or independent-boson model [94, 102–109]. To achieve a microscopic model for quantum dissipation that takes also the wave propagation in the bath into account, we couple the qubits to a bosonic field. Locally, at a fixed point in space, the modes of the quantized field can be regarded as a set of independent bosons. In addition, the wave nature of the field allows for spatial correlations between different points in space. We describe the space in which the field propagates by coordinates $\mathbf{x}$ and denote the qubit positions in this d-dimensional space by $\mathbf{x}_\nu$, where $\nu = 1, 2, \ldots N$ labels the qubits. The aim of this section is to give a general motivation for the model we are going to use and to highlight its relation to the problem of atom-photon interaction which provides a natural example for the coupling of a system to a bosonic field [110]. Subsequently, in Sect. 2.3 we show in more detail how various physical situations can be mapped to the model, in particular we consider the coupling of solid-state qubits to the bosonic environment formed by substrate phonons.

2.2.1 The one-dimensional case

To ease the presentation we restrict ourselves to a one-dimensional environment $d = 1$ where the field $\psi(x)$ is a scalar function of the position coordinate. It can be considered as the displacement of a string at position x. The model obtained for this case will then be generalized to higher dimensions.

We first consider only a single system that couples to this field, but for the moment we do not specify the system any further. We assume that it can be described by a Lagrangian $L_s(q, \dot{q})$ where q is the generalized coordinate and $\dot{q}$ the corresponding velocity. Motivated by the minimal-coupling (mc) scheme of quantum electrodynamics

we start with the total Lagrangian [111]

$$L_{\mathrm{mc}} = L_{\mathrm{s}}(q,\dot{q}) + \int \mathrm{d}x\, \mathcal{L}_{\mathrm{b}}(\psi,\dot{\psi},\partial_x\psi) + \int \mathrm{d}x\, \dot{q}h(x)\psi\,. \tag{2.3}$$

The integrand of the second term in Eq. (2.3) is the Lagrangian density of the field. For instance, for a free bosonic field, i.e. a massless Klein-Gordon field, the Lagrangian density is $\mathcal{L}_{\mathrm{b}} = (\dot{\psi})^2/2 - c^2(\partial_x\psi)^2/2$, where c is the field velocity. The last term in Eq. (2.3) describes the coupling of the field to the velocity $\dot{q}$ where $h(x)$ is an interaction range function that typically peaks at the position of the system. For an electron interacting with the electromagnetic field, $h(x)\dot{q}$ corresponds to the current density $-e\dot{q}\delta(x-q)$. Note, however, that q is not necessarily a spatial coordinate and in general has to be distinguished from x. Thus, in the following we avoid mixing the variables q and x by writing expressions as $\delta(x-q)$. In other words, we will distinguish between the q-space and the space in which the field propagates. We formally write the Lagrangian $L_{\mathrm{mc}} = \int \mathrm{d}x\, \mathcal{L}_{\mathrm{mc}}$ with the total Lagrangian density $\mathcal{L}_{\mathrm{mc}} = L_{\mathrm{s}}\delta(x-x_1) + \mathcal{L}_{\mathrm{b}} + \dot{q}h\psi$.

Coupling the field to the velocity $\dot{q}$ brings along the disadvantage that the conjugate momentum of the system coordinate q is not purely kinetic,

$$p_{\mathrm{mc}} = \frac{\partial L_{\mathrm{mc}}}{\partial \dot{q}} = \frac{\partial L_{\mathrm{s}}}{\partial \dot{q}} + \int \mathrm{d}x\, h(x)\psi\,. \tag{2.4}$$

Hence, the resulting system Hamiltonian $H_{\mathrm{s}} = p_{\mathrm{mc}}\dot{q} - L_{\mathrm{s}}$ does not coincide with the proper energy of the system defined as sum of its kinetic and potential energies [111]. To bring the Lagrangian in line with our intention, we transform it by adding the time derivative of a function $f(q,\psi,t)$. This transformation is always possible without altering the corresponding Euler-Lagrange equations. We choose $f(q,\psi,x,t) = -qh(x)\psi$ which in the quantum optics literature is known as the Göppert-Mayer transformation [111,112]. The new Lagrangian density then reads $\mathscr{L} = \mathscr{L}_{\mathrm{mc}} + \frac{\mathrm{d}}{\mathrm{d}t}f = \mathscr{L}_{\mathrm{s}} + \mathscr{L}_{\mathrm{b}} - qh(x)\dot{\psi}$ so that the field couples to the generalized coordinate q rather than to the velocity $\dot{q}$, as expected. This type of Lagrangian was used by Unruh already in an early investigation of decoherence in a qubit register [113]. Note that the canonical momentum $\partial\mathscr{L}/\partial\dot{q}$ is now determined solely by the Lagrangian density $\mathscr{L}_{\mathrm{s}}$ of the system.

We now apply the transformed Lagrangian density to model the coupling of N qubits to the field,

$$\mathscr{L} = \mathscr{L}_{\mathrm{s}} + \mathscr{L}_{\mathrm{b}} - \sum_{\nu=1}^{N} X_\nu h_\nu(x)\dot{\psi}\,. \tag{2.5}$$

The first term represents the system of N qubits and the second term models the field. The last term is the time-derivative coupling between the field and generalized system coordinates X_ν with $h_\nu(x)$ being an interaction range function for qubit ν. Typically this function peaks at the qubit position $x = x_\nu$. The corresponding Hamiltonian density is obtained in a straightforward manner. The conjugate momenta of the system coordinates do not mix with the field so that the Lagrangian density $\mathscr{L}_{\mathrm{s}}$ directly transforms to the corresponding Hamiltonian density of the system, $\mathscr{L}_{\mathrm{s}} \to \mathscr{H}_{\mathrm{s}}$. The field variable $\Pi(x)$ conjugate to $\psi(x)$ is $\Pi = \partial\mathscr{L}/\partial\dot{\psi} = \partial\mathscr{L}_{\mathrm{b}}/\partial\dot{\psi} - \sum_\nu X_\nu h_\nu$. For the Klein-Gordon field, we find the full Hamiltonian density

$$\mathscr{H} = \mathscr{H}_{\mathrm{s}} + \mathscr{H}_{\mathrm{b}} + \mathscr{H}_{\mathrm{sb}} + \mathscr{H}_{\mathrm{c}}\,, \tag{2.6}$$

with

$$\mathscr{H}_{\mathrm{b}} = \frac{1}{2}\left[\Pi^2 + c^2(\partial_x\psi)^2\right] , \tag{2.7}$$

$$\mathscr{H}_{\mathrm{sb}} = \sum_{\nu=1}^{N} X_\nu h_\nu(x)\Pi \,, \tag{2.8}$$

$$\mathscr{H}_{\mathrm{c}} = \frac{1}{2}\left[\sum_{\nu=1}^{N} X_\nu h_\nu(x)\right]^2 . \tag{2.9}$$

Finally, the total Hamiltonian is obtained by integration,

$$H = \int \mathrm{d}x\, \mathscr{H} \,. \tag{2.10}$$

For the example of a qubit register in the absence of a direct interaction between the qubits, the first term in Eq. (2.6) denotes the system Hamiltonian

$$H_{\mathrm{s}} = \int \mathrm{d}x\, \mathscr{H}_{\mathrm{s}} = \frac{\hbar}{2}\sum_{\nu=1}^{N} \Omega_\nu \sigma_{\nu z} \,, \tag{2.11}$$

where $\sigma_{\nu z}$ is a Pauli matrix for qubit ν with energy splitting $\hbar\Omega_\nu$. The last term in Eq. (2.6) results in a counter term $H_{\mathrm{c}} = \int \mathrm{d}x\, \mathscr{H}_{\mathrm{c}}$. In the language of quantum optics, this term can be interpreted as dipolar self-energy [111]. The qubit-qubit distance is typically larger than the interaction range of a qubit with the field, i.e. the width of $h_\nu(x)$. Then the overlap between the interaction ranges of different qubits is small and only the pure quadratic terms $h_\nu^2(x)X_\nu^2$ contribute to the counter term. For two-level systems, the coupling operators are Pauli matrices so that X_ν^2 is a c-number and the counter term results in a renormalization of the energy scale.

To obtain a quantized description of the field, let us consider the Fourier-transform Π_k and ψ_k of $\Pi(x)$ and $\psi(x)$, respectively. For example, we have $\Pi_k = \int \mathrm{d}x\, \Pi(x)\mathrm{e}^{-\mathrm{i}kx}/\sqrt{2\pi}$. It is convenient to introduce normal coordinates b_k and b_k^* by the following linear combinations

$$b_k = \frac{1}{\sqrt{2\hbar\omega_k}}\left(\Pi_k + \mathrm{i}\omega_k\psi_k\right), \quad b_k^* = \frac{1}{\sqrt{2\hbar\omega_k}}\left(\Pi_k^* - \mathrm{i}\omega_k\psi_k^*\right) , \tag{2.12}$$

with the dispersion relation $\omega_k = c|k|$. In a quantized picture, the real-valued field variables Π and ψ are represented by hermitian operators. Note that in reciprocal space the fields are complex valued so that for instance Π_k^* corresponds to the non-hermitian operator $\Pi_k^\dagger$. We restrict ourselves to a bosonic commutation relation $[\Pi(x), \psi(x')] = \mathrm{i}\hbar\,\delta(x-x')$ which in reciprocal space translates to $[\Pi_k, \psi_{k'}^\dagger] = \mathrm{i}\hbar\,\delta(k-k')$. The prefactors in the definition of the normal variables b_k and b_k^* have been chosen so that in the quantized picture their corresponding operators b_k and $b_k^\dagger$ obey the usual commutation relation $[b(k), b^\dagger(k')] = \delta(k-k')$. Hence, the operators $b_k^\dagger$ and b_k are the familiar creation and annihilation operators for mode k. After a back-transform to the x-space, we find

for the displacement $\psi(x)$ and its conjugate momentum $\Pi(x)$

$$\psi(x) = \frac{-\mathrm{i}}{\sqrt{2\pi}} \int \mathrm{d}k \sqrt{\frac{\hbar}{2\omega_k}} \left(b_k \mathrm{e}^{\mathrm{i}kx} - b_k^\dagger \mathrm{e}^{-\mathrm{i}kx} \right) , \tag{2.13}$$

$$\Pi(x) = \frac{1}{\sqrt{2\pi}} \int \mathrm{d}k \sqrt{\frac{\hbar\omega_k}{2}} \left(b_k \mathrm{e}^{\mathrm{i}kx} + b_k^\dagger \mathrm{e}^{-\mathrm{i}kx} \right) . \tag{2.14}$$

Using the expansions (2.13) and (2.14), the bath Hamiltonian in Eq. (2.6) reads $H_\mathrm{b} = \int \mathrm{d}x\, \mathscr{H}_\mathrm{b} = \int \mathrm{d}k\, \hbar\omega_k b_k^\dagger b_k$ where we have set the ground state energy to zero. As expected, the bath consists of a set of independent harmonic oscillators with frequencies ω_k. The interaction Hamiltonian $H_\mathrm{sb} = \int \mathrm{d}x\, \mathscr{H}_\mathrm{sb}$ is obtained likewise and reads

$$H_\mathrm{sb} = \sum_{\nu=1}^{N} X_\nu \int \mathrm{d}k\, h_{\nu,-k} \Pi_k \,, \tag{2.15}$$

where $h_{\nu,k}$ is the Fourier transform of the interaction range function $h_\nu(x)$. In a dipole approximation one assumes $h_\nu(x) \propto \delta(x - x_\nu)$, i.e. $h_{\nu k} \propto \exp(-\mathrm{i}kx_\nu)$. The interaction then takes the form

$$H_\mathrm{sb} = \hbar \sum_{\nu=1}^{N} X_\nu \int \mathrm{d}k\, g_k \left(b_k \mathrm{e}^{\mathrm{i}kx_\nu} + b_k^\dagger \mathrm{e}^{-\mathrm{i}kx_\nu} \right) , \tag{2.16}$$

where for convenience, we introduced a prefactor $\hbar$. In many cases, the interaction range function $h_\nu(x)$ peaks at the qubit position and shows a broadening. Regarding the coupling of an confined electron to phonons, the width is determined by the localization of the electron's wavefunction, e.g. the size of the quantum dot. As a consequence, the coupling to modes of large wavevectors k gets suppressed, i.e. $|g_k|$ vanishes for large k. Typically one recasts the properties of the qubit-bath coupling into the spectral density [99, 100]

$$J(\omega) = \int \mathrm{d}k\, |g_k|^2 \delta(\omega - \omega_k) \,. \tag{2.17}$$

The finite extension of the interaction range thus results in a decay of the spectral function for large frequencies ω, providing a cutoff frequency ω_c. The analytical form of the decay depends much on the nature of the coupling but is often assumed to be exponentially [97], i.e. $J(\omega) \propto \exp(-\omega/\omega_c)$ for large ω.

Typically, the environment of the qubits is of a finite volume, like for example the substrate that hosts the quantum dots. One may employ periodic boundary conditions so that the wavenumber k assumes discrete values. The integral in Eq. (2.16) then converts into a sum, $\int \mathrm{d}k \ldots \to \sqrt{2\pi/L} \sum_k \ldots$, where L is the length of the string. We adopt this notation in the following and write

$$H = \frac{\hbar}{2} \sum_{\nu=1}^{N} \Omega_\nu \sigma_{\nu z} + \sum_k \hbar\omega_k b_k^\dagger b_k + \hbar \sum_{\nu=1}^{N} X_\nu \xi_\nu \,, \tag{2.18}$$

with the bath coordinate

$$\xi_\nu = \sum_k g_k \left(b_k \mathrm{e}^{\mathrm{i}kx_\nu} + b_k^\dagger \mathrm{e}^{-\mathrm{i}kx_\nu} \right) . \tag{2.19}$$

For $N = 1$ qubit located at $x_1 = 0$, Eq. (2.18) is identical to the standard spin-boson Hamiltonian [97].

2.2.2 Generalization to higher dimensions

The model presented in the last section is easily generalized to higher bath dimensions $d = 2, 3$. We now also include the possibility that there may be different boson branches $\kappa = 1, 2, \ldots$, analogously to the description of phonons in a crystal [114]. Furthermore, we also allow that a qubit ν couples via multiple operators $X_{\nu 1}, X_{\nu 2}, \ldots$ to the bath. The number of these operators can in general be different from the dimension d and we collect them formally by a vector $\mathbf{X}_\nu$. The generalized total Hamiltonian, which provides the starting point for our discussions in the subsequent chapters reads

$$H = H_\mathrm{s} + H_\mathrm{b} + H_\mathrm{sb}\,, \tag{2.20}$$

$$H_\mathrm{b} = \sum_{\mathbf{k},\kappa} \hbar\omega_{\mathbf{k}\kappa} b^\dagger_{\mathbf{k}\kappa} b_{\mathbf{k}\kappa}\,, \tag{2.21}$$

$$H_\mathrm{sb} = \hbar \sum_{\nu=1}^{N} \mathbf{X}_\nu \cdot \boldsymbol{\xi}_\nu\,, \tag{2.22}$$

with a vector-valued bath coordinate

$$\boldsymbol{\xi}_\nu = \sum_{\mathbf{k},\kappa} \left(\mathbf{g}_{\nu,\mathbf{k}\kappa} b_{\mathbf{k}\kappa} + \mathbf{g}^*_{\nu,\mathbf{k}\kappa} b^\dagger_{\mathbf{k},\kappa} \right)\,. \tag{2.23}$$

Assuming equal coupling strengths for all qubits ν, the vector $\mathbf{g}_{\nu,\mathbf{k}\kappa}$ depends on ν only through a phase that determines the position of the qubit, $\mathbf{g}_{\nu,\mathbf{k}\kappa} = \mathbf{g}_{\mathbf{k}\kappa} \exp(\mathrm{i}\mathbf{k}\cdot\mathbf{x}_\nu)$. Then we define the spectral density $J_\kappa(\omega)$ for branch κ and the total spectral density $J(\omega)$ by

$$J(\omega) = \sum_\kappa J_\kappa(\omega) = \sum_\kappa \sum_{\mathbf{k}} |\mathbf{g}_{\mathbf{k}\kappa}|^2 \delta(\omega - \omega_{\mathbf{k}\kappa})\,. \tag{2.24}$$

2.3 Microscopic coupling mechanism

For different physical realizations of qubits the relevant noise sources of the environment and the nature of the coupling can be quite different. The model presented in the preceding section is generic enough to capture a broad range of different possibilities. Before we proceed using our model Hamiltonian (2.20), we will give an overview of some important microscopic coupling mechanisms and their relation to our model.

2.3.1 Interaction with photons

For many realizations of qubits in the optical regime, the electromagnetic background radiation forms a relevant source of decoherence that leads, for example, to relaxation or spontaneous emission. The model presented in the last section directly relates to the microscopic coupling of a two-level system to the quantized electromagnetic field. Here, we demonstrate this fact for the example of a single-electron atom. The field operator of the electron is denoted as $\phi(\mathbf{x}) = \sum_n a_n \varphi_n(\mathbf{x})$, where $\varphi_n(\mathbf{x})$ is the wavefunction that

belongs to the nth bound state of the electron with energy E_n. With the electronic creation and annihilation operators $a_n^\dagger$ and a_n, respectively, we can write the electronic Hamiltonian in the second-quantized form $H_\mathrm{s} = \sum_n E_n a_n^\dagger a_n$. For the atom at position $\mathbf{x}_1$, the interaction with the field in dipole-approximation reads [111, 115]

$$H_\mathrm{sb} = -e \int \mathrm{d}^3x\, \phi^\dagger(\mathbf{x})[\mathbf{x}\cdot\mathbf{E}(\mathbf{x}_1)]\phi(\mathbf{x})\,, \tag{2.25}$$

where the center-of-mass motion was neglected. The electric field operator is given by

$$\mathbf{E}(\mathbf{x}) = \mathrm{i}\sum_\mathbf{k} \sqrt{\frac{\hbar\omega_\mathbf{k}}{2\epsilon_0 V}}\,\mathbf{u}_\mathbf{k}\left(b_\mathbf{k}\mathrm{e}^{\mathrm{i}\mathbf{k}\cdot\mathbf{x}} - b_\mathbf{k}^\dagger \mathrm{e}^{-\mathrm{i}\mathbf{k}\cdot\mathbf{x}}\right)\,, \tag{2.26}$$

with real mode vectors $\mathbf{u}_\mathbf{k}$. In the two-level approximation, one keeps only the two lowest energy levels $n = 1, 2$ of the atom. We can shift the energy scale by $-(E_2 + E_1)/2$ and write the system Hamiltonian in the basis $\{|\varphi_2\rangle, |\varphi_1\rangle\}$ in the convenient form $H_\mathrm{s} = \hbar\Omega\sigma_z/2$ with Ω being the transition frequency. In terms of creation and annihilation operators we find for the interaction $H_\mathrm{sb} = \sum_{n,n'=1}^2 a_n^\dagger a_{n'}\mathbf{d}_{nn'}\cdot\mathbf{E}(\mathbf{x}_1)$ with the dipole matrix element $\mathbf{d}_{nn'} = -e\,\langle\varphi_n|\mathbf{x}|\varphi_{n'}\rangle$. Since the energy eigenstates have a well-defined parity, elements with $n = n'$ vanish and we can write $H_\mathrm{sb} = \mathbf{E}(\mathbf{x}_1)\cdot[\mathbf{d}_{12}\,|\varphi_1\rangle\langle\varphi_2| + \mathbf{d}_{12}^*\,|\varphi_2\rangle\langle\varphi_1|]$. Using the notation $\mathbf{u}_\mathbf{k}\cdot\mathbf{d}_{12} = |\mathbf{u}_\mathbf{k}\cdot\mathbf{d}_{12}|\exp(\mathrm{i}\eta_\mathbf{k})$ the atom-field interaction corresponds to the model (2.22) with

$$\mathbf{X}_\nu = \begin{pmatrix}\sigma_{\nu x}\\ \sigma_{\nu y}\end{pmatrix}, \qquad \text{and} \quad \mathbf{g}_{\nu,\mathbf{k}} = \mathrm{i}\mathrm{e}^{\mathrm{i}\mathbf{k}\cdot\mathbf{x}_\nu}\sqrt{\frac{\omega_\mathbf{k}}{2\hbar\epsilon_0 V}}|\mathbf{u}_\mathbf{k}\cdot\mathbf{d}_{12}|\begin{pmatrix}\cos\eta_\mathbf{k}\\ -\sin\eta_\mathbf{k}\end{pmatrix}. \tag{2.27}$$

Note that after a rotating-wave approximation and by assuming $\mathbf{g}_{\nu,\mathbf{k}} \propto \delta(\mathbf{k}-\mathbf{k}_0)$ we obtain the Jaynes-Cummings model as a special case.

2.3.2 Carrier-phonon interaction

For solid-state based quantum information processing, the qubit is embedded in a condensed matter environment and the interaction with phonons of the crystal is one important source of decoherence. Depending on how the qubit and its logical states are realized, the microscopic origin of the qubit-phonon coupling can be different. For instance, for a charge qubit in a semiconductor double-dot structure, the two positions of a confined (excess) electron, either in the left or the right dot form the qubit. Phonons that directly couple to the position of the electron thus influence its coherence. By contrast, if the qubit is realized by the spin states of a confined electron, the coupling to phonons is typically mediated by an admixture mechanism like the spin-orbit interaction. Note, however, that a qubit-phonon interaction can be relevant also for other setups that are not directly solid-state based, for instance in an ion-trap experiment where the motional bus provides a source of decoherence since it is subject to heating and dissipation [44].

In semiconductors, there are three major mechanisms for an interaction of confined carriers with phonons [114,116,117]: deformation potential coupling to longitudinal acoustic phonons, piezoelectric coupling to longitudinal and transversal acoustic phonons, and polar (Fröhlich) coupling to optical phonons. We here concentrate on the first two mechanisms.

Deformation potential coupling

The lattice vibrations cause local shifts in the band structure of the semiconductor which lead to changes in the potential energy of the carrier, i.e. the electron or hole. These deformations are due to acoustic phonons and result in an effective electron-phonon (and hole-phonon) interaction called deformation potential coupling. For long wavelengths the contribution to the energy of the electron is proportional to the relative volume change $\boldsymbol{\nabla}\cdot\boldsymbol{\psi}(\mathbf{x})$, where $\boldsymbol{\psi}(\mathbf{x})$ is the phonon displacement operator given by [114]

$$\boldsymbol{\psi}(\mathbf{x}) = \mathrm{i}\sum_{\mathbf{k},\kappa}\sqrt{\frac{\hbar}{2\rho V\omega_{\mathbf{k}\kappa}}}\mathbf{u}_{\mathbf{k}\kappa}\mathrm{e}^{\mathrm{i}\mathbf{k}\cdot\mathbf{x}}\left(b_{\mathbf{k}\kappa}+b^{\dagger}_{-\mathbf{k},\kappa}\right), \tag{2.28}$$

with $\mathbf{u}_{\mathbf{k}\kappa}$ being the real polarization vector, $\mathbf{u}_{-\mathbf{k},\kappa}=-\mathbf{u}_{\mathbf{k},\kappa}$. In terms of the stress tensor

$$S_{ij} = \frac{1}{2}\left(\frac{\partial\psi_i}{\partial x_j}+\frac{\partial\psi_j}{\partial x_i}\right) = \sum_{\mathbf{k},\kappa} S_{\mathbf{k}\kappa,ij}\,, \tag{2.29}$$

where

$$S_{\mathbf{k}\kappa,ij} = -\sqrt{\frac{\hbar}{8\rho V\omega_{\mathbf{k}\kappa}}}[u_{\mathbf{k}\kappa,i}k_j+u_{\mathbf{k}\kappa,j}k_i]\mathrm{e}^{\mathrm{i}\mathbf{k}\cdot\mathbf{x}}\left(b_{\mathbf{k}\kappa}+b^{\dagger}_{-\mathbf{k},\kappa}\right), \tag{2.30}$$

one can write the deformation potential as $V(\mathbf{x}) = -D\boldsymbol{\nabla}\cdot\boldsymbol{\psi}(\mathbf{x}) = -D\,\mathrm{tr}\,S$. The deformation potential constant D depends on the properties of the material and generally is different for electrons and holes because of their different effective masses. Only longitudinal polarizations contribute to $\boldsymbol{\nabla}\cdot\boldsymbol{\psi}$ so that we can consider the branch $\kappa=\parallel$ with polarization $\mathbf{u}_{\mathbf{k}\parallel}=\mathbf{k}/k$. Then one finds

$$V(\mathbf{x}) = D\sum_{\mathbf{k}}\sqrt{\frac{\hbar}{2\rho V\omega_{\mathbf{k}\parallel}}}k\mathrm{e}^{\mathrm{i}\mathbf{k}\cdot\mathbf{x}}\left(b_{\mathbf{k}\parallel}+b^{\dagger}_{-\mathbf{k},\parallel}\right), \tag{2.31}$$

and the carrier-phonon interaction is given by $H_{\mathrm{sb}}=\int\mathrm{d}^3x\,\rho_c(\mathbf{x})V(\mathbf{x})$, where the carrier density $\rho_{\mathrm{c}}(\mathbf{x}) = \sum_{nn'}a^{\dagger}_n a_{n'}\varphi^*_n(\mathbf{x})\varphi_{n'}(\mathbf{x})$ in second quantization with respect to the carrier states. Hence, the deformation coupling reads

$$H_{\mathrm{sb}} = \sum_{nn'}a^{\dagger}_n a_{n'}\sum_{\mathbf{k}}M^{\mathrm{d}}_{\mathbf{k}}\mathcal{F}_{\mathbf{k},nn'}\left(b_{\mathbf{k},\parallel}+b^{\dagger}_{-\mathbf{k},\parallel}\right), \tag{2.32}$$

with the coupling matrix element

$$M^{\mathrm{d}}_{\mathbf{k}} = D\sqrt{\frac{\hbar}{2\rho V\omega_{\mathbf{k}\parallel}}}k\,, \tag{2.33}$$

and the form factor

$$\mathcal{F}_{\mathbf{k},nn'} = \int\mathrm{d}^3x\,\varphi^*_n(\mathbf{x})\mathrm{e}^{\mathrm{i}\mathbf{k}\cdot\mathbf{x}}\varphi_{n'}(\mathbf{x})\,. \tag{2.34}$$

Piezoelectric interaction

A crystal deformation in a piezoelectric material induces an electric field which affects a charge carrier by means of the Coulomb potential. The deformation can be caused by lattice vibrations and, thus, gives rise to an effective carrier-phonon interaction, called piezoelectric interaction [114]. Consequently, it is only present for piezoelectric materials which lack inversion symmetry like GaAs, but not for Ge or Si. Using the piezoelectric tensor $\boldsymbol{\epsilon}$ which depends on the crystal structure, the polarization relates to the strain by $\mathbf{P} = \boldsymbol{\epsilon} S$. By Maxwell's equations the polarization is in turn related to an electrical field. It turns out that the component of the piezoelectric field transversal to $\mathbf{k}/k$ is proportional to $(c_\mathrm{s}/c)^2$ where c_s and c are the sound velocity and the speed of light, respectively [117]. Thus, the piezoelectric field is nearly longitudinal and one can introduce an corresponding electric potential $V = -\mathrm{i}e\mathbf{k}\cdot\mathbf{P}/k^2\epsilon_0\epsilon_1$, where ϵ_1 is an effective dielectric constant that accounts for screening effects caused by electron-electron interactions and optical phonons [118]. For a zincblende structure like in GaAs, the piezoelectric tensor depends only on a constant $h_{14} = \epsilon_{xyz} = \epsilon_{yzx} = \epsilon_{zxy}$ and the other components vanish. Then the piezoelectric potential reads

$$V(\mathbf{x}) = \sum_{\mathbf{k}} \sqrt{\frac{\hbar}{2\rho V \omega_{\mathbf{k}\kappa}}} \frac{2\mathrm{i}h_{14}e}{\epsilon_0\epsilon_1} A_{\mathbf{k}\kappa} \mathrm{e}^{\mathrm{i}\mathbf{k}\cdot\mathbf{x}} \left(b_{\mathbf{k}\kappa} + b^\dagger_{-\mathbf{k},\kappa}\right) , \tag{2.35}$$

with a geometrical factor $A_{\mathbf{k}\kappa} = -A_{-\mathbf{k},\kappa}$ that takes the anisotropy of the piezoelectric tensor into account. For the zincblende structure $A_{\mathbf{k}\kappa} = k_x k_y u_{\mathbf{k}\kappa,z} + k_y k_z u_{\mathbf{k}\kappa,x} + k_x k_z u_{\mathbf{k}\kappa,y}$. One can now proceed as for the deformation potential to obtain the piezoelectric interaction

$$H_\mathrm{sb} = \sum_{nn'} a^\dagger_n a_{n'} \sum_{\mathbf{k},\kappa} M_{\mathbf{k}\kappa} \mathcal{F}_{\mathbf{k},nn'} \left(b_{\mathbf{k}\kappa} + b^\dagger_{-\mathbf{k},\kappa}\right) , \tag{2.36}$$

with the coupling matrix element

$$M^\mathrm{pz}_{\mathbf{k}\kappa} = \sqrt{\frac{\hbar}{2\rho V \omega_{\mathbf{k}\kappa}}} \frac{2\mathrm{i}h_{14}e}{\epsilon_0\epsilon_1} A_{\mathbf{k}\kappa} . \tag{2.37}$$

The form factor is given in Eq. (2.34). Note that in general longitudinal as well as transversal phonons couple to the charged carrier. In contrast to the deformation potential, the matrix element (2.37) for electrons and holes is the same (besides the sign of the electrical charge e), but it depends on the direction k of the wavenumber due to the geometrical factor $A_{\mathbf{k}\kappa}$. Often an effective isotropic piezoelectric interaction is constructed by averaging over the solid angle [119]. In relevant quantities like the spectral bath density, it enters the absolute value squared of the coupling matrix element, i.e. the average of $|A_{\mathbf{k}\kappa}|^2$ over the solid angle is needed.

The deformation potential and the piezoelectric interaction matrix elements (2.33) and (2.37) may be combined into a total matrix element $M_{\mathbf{k}\kappa} = M^\mathrm{dp}_{\mathbf{k}} + M^\mathrm{pz}_{\mathbf{k}\kappa}$. Note that because the matrix element of the deformation potential is real and the matrix element of the piezoelectric interaction is purely imaginary and both mechanisms do not interfere, $|M_{\mathbf{k}\kappa}|^2 = (M^\mathrm{dp}_{\mathbf{k}})^2 + |M^\mathrm{pz}_{\mathbf{k}\kappa}|^2$. Assuming a linear dispersion relation $\omega_{\mathbf{k}} = c_\mathrm{s} k$

for the acoustic phonon branch, one finds for the coupling matrix element (2.33) of the deformation potential $M_{\mathbf{k}}^{\mathrm{dp}} \propto \sqrt{k}$ whereas for the piezoelectric interaction $M_{\mathbf{k}}^{\mathrm{pz}} \propto 1/\sqrt{k}$. Thus, it is generally expected that for transitions involving low frequency phonons the interaction via the piezoelectric component is dominant whereas the deformation potential becomes relevant for transitions involving higher energies. In quantum dots, the localization a of the carrier wavefunction provides a natural cutoff frequency $\omega_{\mathrm{c}} \approx c_{\mathrm{s}}/a$ for the phonon spectrum due to the form factor, i.e. the contribution of phonons with higher frequencies than ω_{c} is suppressed. Thus, the relative contributions of the deformation potential and piezoelectric interactions depend stronly on the temperature as well as the dot size, and neglecting one of these mechanisms can be justified in certain parameter regimes [71, 120–122].

Example: double-dot charge qubits

To relate the above discussed coupling mechanisms to our model, let us consider a double-dot charge qubit [61, 67, 71, 123]. Typically, the system Hamiltonian is written in the tunnel basis, i.e. the state $|0\rangle$ refers to the situation where an (excess) electron is in the left dot whereas $|1\rangle$ is the state where the electron is in the right dot. Then the qubit Hamiltonian takes the form

$$H_{\mathrm{s}} = \frac{\epsilon}{2}\sigma_z + \frac{\Delta}{2}\sigma_x \,, \tag{2.38}$$

where ϵ is the energy level difference of the dots and Δ the tunnel amplitude connecting the dots. We denote by a_n and $a_n^\dagger$ the annihilation and creation operators for state $n = 0, 1$ so that the interaction Hamiltonian reads

$$H_{\mathrm{sb}} = \sum_{nn'} a_n^\dagger a_{n'} \sum_{\mathbf{k}\kappa} \mathcal{F}_{\mathbf{k},nn'} (M_{\mathbf{k}}^{\mathrm{dp}} + M_{\mathbf{k}\kappa}^{\mathrm{pz}}) \left(b_{\mathbf{k}\kappa} + b_{-\mathbf{k},\kappa}^\dagger \right) . \tag{2.39}$$

In the simplest case, one may assume a small tunneling between the dots [123], i.e. the overlap between the wavefunctions $\varphi_0(\mathbf{x}) = \langle \mathbf{x}|0\rangle$ and $\varphi_1(\mathbf{x})$ of the electron in the left and the right dot to be small so that the form factors $\mathcal{F}_{\mathbf{k},nn'}$ associated to the non-diagonal elements with $n \neq n'$ can be neglected [67, 72, 123]. The diagonal elements are determined by the electron density $|\varphi_{0,1}(\mathbf{x})|^2$ in the left (right) dot that we assume to have equal shape, i.e. $|\varphi_1(\mathbf{x})|^2 = |\varphi_0(\mathbf{x}-\mathbf{d})|^2$ where $\mathbf{d}$ is the vector connecting the centers of the dots. For quantum dots in semiconductor heterostructures, the two-dimensional free electron gas is strongly confined in z-direction. The charge distribution in the x-y-plane can typically be assumed to be Gaussian so that for the left dot, located at $\mathbf{x}_1$, one obtains the form factor

$$\mathcal{F}_{\mathbf{k},00} = \int \mathrm{d}^3x \, |\varphi_0(\mathbf{x})|^2 \mathrm{e}^{\mathrm{i}\mathbf{k}\cdot\mathbf{x}} = \int \mathrm{d}^3x \, \delta(z - z_1) \frac{1}{2\pi a^2} \mathrm{e}^{\mathrm{i}\mathbf{k}\cdot\mathbf{x} - \frac{(x-x_1)^2+(y-y1)^2}{2a^2}} \tag{2.40}$$

$$= \mathrm{e}^{\mathrm{i}\mathbf{k}\cdot\mathbf{x}_1 - (k_x^2+k_y^2)a^2/2} \,, \tag{2.41}$$

and accordingly for the right dot $\mathcal{F}_{\mathbf{k},11} = \mathcal{F}_{\mathbf{k},00} \exp(\mathrm{i}\mathbf{k}\cdot\mathbf{d})$. By keeping in Eq. (2.39) only terms with $n = n'$, we can write the interaction in the form

$$H_{\mathrm{sb}} = \sigma_z \sum_{\mathbf{k}\kappa} \frac{\mathcal{F}_{\mathbf{k},00}(1 - \mathrm{e}^{\mathrm{i}\mathbf{k}\cdot\mathbf{d}})}{2} (M_{\mathbf{k}}^{\mathrm{dp}} + M_{\mathbf{k}\kappa}^{\mathrm{pz}}) \left(b_{\mathbf{k}\kappa} + b_{-\mathbf{k},\kappa}^\dagger \right) , \tag{2.42}$$

where an irrelevant energy shift has been ignored. Thus, this (single-qubit) interaction Hamiltonian corresponds to our model (2.20) by setting

$$X = \sigma_z, \quad \text{and} \qquad g_{\nu,\mathbf{k}\kappa} = \frac{\mathcal{F}_{\mathbf{k},00}}{2\hbar}(1 - \mathrm{e}^{\mathrm{i}\mathbf{k}\cdot\mathbf{d}})(M^{\mathrm{dp}}_{\mathbf{k}} + M^{\mathrm{pz}}_{\mathbf{k}\kappa})\,. \tag{2.43}$$

As it turns out, the corresponding spectral density (2.24) features characteristic oscillations with a frequency scale $\omega = c_\mathrm{s}/d$ resulting from the phase factor $\exp(\mathrm{i}\mathbf{x}\cdot\mathbf{d})$ in (2.42) [67]. In recent works, the interaction of a double-dot charge qubit with phonons via the piezoelectric coupling [67,71,123] and also via deformation potential coupling was studied [68]. Assuming a three-dimensional Gaussian charge density, the spectral density was considered to be ohmic for the piezoelectric coupling mechanism [67,123], and super-ohmic $\propto \omega^3$ for the deformation potential coupling [69]. However, for semiconductor heterotructures where electrons are strongly confined in the interface, a two-dimensional Gaussian shape of the charge density seems more realistic, and the spectral density for the piezoelectric interaction was found to be super-ohmic $\propto \omega^3$ with an analytical decay $\propto 1/\omega$ for large frequencies [71, 92].

2.3.3 Spin-phonon interaction

Finally, let us also briefly discuss the interaction of phonons with the spin of an electron. Hereby, we focus on the mechanisms that are the most relevant ones for electron spins localized at a donor atom or confined in a quantum dot. One may divide the different types of spin-phonon interaction into two groups: direct spin-phonon interactions and by admixture mechanisms like spin-orbit coupling mediated indirect spin-phonon interactions [75, 124].

Direct spin-phonon interactions

Direct spin-phonon interactions can result from parameter fluctuations in the spin-dependent parts of the electronic Hamiltonian caused by lattice vibrations. Two important examples are (i) the modulation of an anisotropic g-factor and (ii) a direct coupling of the spin to the lattice strain by fluctuations of the electron-phonon potential in the spin-orbit interaction [124–128].

With an external magnetic field $\mathbf{B} = (B_x, B_y, B_z)$ the interaction of the former mechanism takes the form [129]

$$H_\mathrm{sb} = \mu_\mathrm{B} \sum_{i,j=x,y,z} g_{ij}\sigma_i B_j\,, \tag{2.44}$$

where μ_B is Bohr's magneton and the tensor g_{ij} is sensitive to lattice deformations. This coupling was considered in recent calculations for P-donor electron spins in Si-Ge type materials [129, 130]. For donor states with tetrahedral symmetry like P in Si or Ge, the interaction can be written as [129]

$$\begin{aligned} H_\mathrm{sb} = a\mu_\mathrm{B}\left[\tilde{S}_{xx}\sigma_x B_x + \tilde{S}_{yy}\sigma_y B_y + \tilde{S}_{zz}\sigma_z B_z\right] \\ + b\mu_\mathrm{B}\left[\tilde{S}_{xy}(\sigma_x B_y + \sigma_y B_x) + \text{c.p.}\right], \end{aligned} \tag{2.45}$$

where c.p. means cyclic permutations and a and b are material constants [125, 126, 130]. The tensor $\tilde{S}_{ij}$ is the strain tensor (2.29) averaged over the orbital wavefunction of the donor, i.e. $\tilde{S}_{ij} = \sum_{\mathbf{k}\kappa} \mathcal{F}_{\mathbf{k}} S_{\mathbf{k}\kappa,ij}$. Thus, the interaction (2.45) is related to our model (2.20) by taking $\mathbf{X} = (\sigma_x, \sigma_y, \sigma_z)$ and the x-component of $\mathbf{g}_{\mathbf{k}\kappa}$ as

$$g_{\mathbf{k}\kappa,x} = \mathcal{F}_{\mathbf{k}} \left[a\mu_{\mathrm{B}} S_{\mathbf{k}\kappa,xx} B_x + b\mu_{\mathrm{B}} (S_{\mathbf{k}\kappa,xy} B_y + S_{\mathbf{k}\kappa,zy} B_z) \right] , \tag{2.46}$$

and the other components follow from cyclic permutation.

Another mechanism exists due to which the spin can couple directly to phonons [75, 127, 131–133]: An electron with momentum $\mathbf{p}$ moving in an electrical field $\mathbf{E}$ experiences (in its rest frame) an effective magnetic field $\propto \mathbf{E} \times \mathbf{p}$. The spin of the electron interacts with this magnetic field with a Zeeman energy, i.e. spin and orbital degrees of freedom are coupled. For an electron in a solid, the lattice strain causes local electrical fields and the spin-orbit interaction directly couples them to the electron spin. The interaction can be written as [127, 133]

$$H_{\mathrm{sb}} = \frac{1}{2} V_0 \left[\sigma_x (S_{xy} p_y + S_{xz} p_z) + \text{c.p.} \right] , \tag{2.47}$$

where S_{ij} is the lattice stress tensor (2.29) and $V_0 = 8 \times 10^7 \mathrm{cm/s}$ for GaAs. This Hamiltonian has to be averaged over the relevant spatial (orbital) part $\varphi(\mathbf{x})$ of the electron wavefunction, where the position $\mathbf{x}$ in the stress tensor (2.29) and $\mathbf{p}$ in the interaction (2.47) have to be considered as position- and momentum operator of the electron. In the presence of an external magnetic field with vector potential $\mathbf{A}$, we have to replace the kinetic momentum $\mathbf{p}$ in Eq. (2.47) by $\mathbf{p} + e\mathbf{A}/c$. With the definition

$$f_{\mathbf{k}\kappa,ij} = -\left(u_{\mathbf{k}\kappa,i} k_j + u_{\mathbf{k}\kappa,j} k_i\right) \int \mathrm{d}^3 x \, \varphi^*(\mathbf{x}) \frac{1}{2} \left\{ \mathrm{e}^{\mathrm{i}\mathbf{x}\cdot\mathbf{k}}, \frac{-\mathrm{i}}{\hbar} \frac{\partial}{\partial x_j} + \frac{e A_j}{c} \right\} \varphi(\mathbf{x}) \tag{2.48}$$

where $\{\cdot,\cdot\}$ is the anti-commutator, we arrive at our model (2.20) by identifying

$$\mathbf{X} = \begin{pmatrix} \sigma_x \\ \sigma_y \\ \sigma_z \end{pmatrix} , \qquad \mathbf{g}_{\mathbf{k}\kappa} = \frac{V_0}{2} \sqrt{\frac{\hbar}{8\rho V \omega_{\mathbf{k}\kappa}}} \begin{pmatrix} f_{\mathbf{k}\kappa,xy} \\ f_{\mathbf{k}\kappa,yz} \\ f_{\mathbf{k}\kappa,zx} \end{pmatrix} . \tag{2.49}$$

Spin-phonon interaction via spin-orbit coupling

The second group of spin-phonon interactions that we want to discuss here are indirect couplings of lattice vibrations to the spin via an admixture mechanism, i.e. a term in the electronic Hamiltonian that does not allow to define a common spin quantization axis, with the spin-orbit coupling being the most important example [134–136]. For electron spins in GaAs quantum dots, this mechanism for spin relaxation due to phonons is actually the dominant one [58, 75, 76, 133].

An electron in the conduction band of a semiconductor subject to an additional confining potential may be described in an effective mass approximation: Assuming that the characteristic extension of the confining potential is larger than the typical periodicity of the lattice potential, the electron wavefunction is approximated by a product of an oscillating Bloch function with fixed band index and a modulating envelope function.

For the envelope function one can derive an effective Hamiltonian that models a free electron with renormalized mass, i.e. the influence of the lattice is recast to an effective mass and the presence of other bands is neglected. Multi-band $\mathbf{k}\cdot\mathbf{p}$ -theory [135,137,138] provides a generalization to this scheme and also takes the effects of more bands into account. The influence of couplings between different bands leads to additional spin-dependent interactions in the effective Hamiltonian. A prominent and important example is the Dresselhaus spin-orbit coupling. It results from a lack of inversion symmetry of the crystal (bulk inversion asymmetry) [134, 135]. It is, thus, relevant for materials like GaAs with zincblende structure, but is absent for Si. With x, y, and z pointing along the main crystallographic axis, the Dresselhaus term for bulk GaAs reads [134] $H_{\mathrm{SO,D}} \propto \sigma_x p_x (p_y^2 - p_z^2) + \text{c.p.}$

In the case of a semiconductor heterostructure based on a material with bulk inversion asymmetry (e.g. GaAs/AlGaAs quantum dots), one is interested in the spin-orbit coupling in the two-dimensional electron gas. The relevant two-dimensional Dresselhaus term can be obtained by averaging the bulk term over the electron wavefunction along the growth direction. For a GaAs/AlGaAs heterostructure grown along the [001] direction, we can replace in the bulk Dresselhaus spin-orbit coupling p_z by $\langle p_z \rangle \approx 0$ and p_z^2 by $\langle p_z^2 \rangle \approx \text{const.}$ to obtain

$$H_{\mathrm{SO,D}} = \lambda_{\mathrm{D}}^{(1)} (-\sigma_x p_x + p_y \sigma_y) + \lambda_{\mathrm{D}}^{(3)} (p_x p_y^2 \sigma_x - p_y p_x^2 \sigma_y) \,, \tag{2.50}$$

with the coupling constants $\lambda_{\mathrm{D}}^{(i)}$. The linear-in-$p$ Dresselhaus term typically dominates the cubic term for a strong spatial confinement in the z-direction, since the former is proportional to $\langle p_z^2 \rangle$.

The interface potential in the heterostructure itself is usually asymmetric along the growth direction. This asymmetry leads to a further spin-dependent correction in the effective Hamiltonian of the electron and is called Rashba-Bychkov spin-orbit coupling (spin-orbit coupling due to structure asymmetry) [134, 135]. It reads

$$H_{\mathrm{SO,R}} = \lambda_{\mathrm{R}} (-p_y \sigma_x + p_x \sigma_y) \,. \tag{2.51}$$

The form of this contribution can be explained in terms of the standard expression for spin-orbit coupling $\propto \boldsymbol{\sigma} \cdot (\mathbf{E} \times \mathbf{p})$ when one considers the potential asymmetry in the heterointerface as an effective local electrical field in z-direction, $\mathbf{E} = (0, 0, E_z)$ [58]. Very recently, the Rashba and Dresselhaus coefficients λ_{R} and $\lambda_{\mathrm{D}}^{(i)}$ have been measured in GaAs/InGaAs quantum wells using opical detection schemes [139].

The two spin-orbit terms in the effective Hamiltonian lead to an admixture of spin-up and spin-down states (assuming a magnetic field parallel to the growth direction that defines the Pauli spin quantization axis) [75,124]. The spin-orbit interaction is typically small so that virtual "spin-up" and "spin-down" states can still be defined, e.g. by the sign of the spin expectation value along the magnetic field. Nevertheless, the small admixture allows phonons (which interact with the orbital degrees of freedom of the electron via the deformation potential and piezoelectric coupling discussed above) to flip the spin state. Thus, there is an indirect spin-phonon interaction mediated by the spin-orbit coupling. To obtain an effective spin-phonon interaction Hamiltonian, one may treat the spin-orbit terms perturbatively, e.g. in first order by a Schrieffer-Wolf

transformation [76]. This eliminates the spin-orbit terms making the carrier-phonon interaction Hamiltonian dependent on the spin state. It can be shown [76, 140] that after projecting to the orbital ground state of the electron, the interaction assumes the form (2.20) with

$$\mathbf{X} = \begin{pmatrix} \sigma_x \\ \sigma_y \end{pmatrix}, \quad \text{and} \quad \mathbf{g}_{\mathbf{k}\kappa} = \begin{pmatrix} g_{\mathbf{k}\kappa,1} \\ g_{\mathbf{k}\kappa,2} \end{pmatrix}, \tag{2.52}$$

where the coupling matrix elements $g_{\mathbf{k}\kappa,i}$ depend on the carrier-phonon interaction constants, the spin-orbit coupling parameters as well as the external magnetic field. When recast to a spectral density, one finds for spin qubits realized in a semiconductor heterostructure a super-ohmic behaviour $J(\omega) \propto \omega^5$ for the spin-orbit mediated deformation-potential coupling and $J(\omega) \propto \omega^3$ for the piezoelectric mechanism [140,141].

3

Pure phase noise

The system-bath model presented in the previous chapter describes a spatially extended quantum system coupled to a bosonic field. Like in our case, the environment of a quantum system can frequently be modeled as an ensemble of harmonic oscillators. If the coupling is linear in the oscillator coordinates, one can formally eliminate the environment to obtain a closed equation for the dissipative quantum system. Such equations are in general not easy to deal with and, accordingly, only a few exact solutions exist in dissipative quantum mechanics, e.g. for the dissipative harmonic oscillator [142–145] and its parametrically driven version [146]. Recently, an exact solution has been found also for the dissipative Landau-Zener problem at zero temperature [147]. A whole class of system-bath models that can be solved exactly are those in which the system Hamiltonian and the system-bath coupling commute [6,148–160,162,163]. In the present section, we focus on such a pure phase-noise model. On short time scales, phase noise is considered as the main source of decoherence in solid state environments; on longer time scales, bit-flip noise, i.e. relaxation becomes relevant as well [49, 130]. The former case is characterized by a system-bath coupling $H_{\rm sb}$ that commutes with the system Hamiltonian,

$$[H_{\rm s}, H_{\rm sb}] = 0\,. \tag{3.1}$$

Although pure phase noise allows an exact solution of the system dynamics, the evaluation of the exact expressions can be rather complex and often relies on approximations. We here evaluate the exact solution in explicit form [159].

3.1 Exact reduced dynamics

We consider a system-bath Hamiltonian of the form (2.20) as discussed in the previous chapter. To ease the notation we assume that each part ν of the system couples via a single operator X_ν to the field, i.e. the interaction

$$H_{\rm sb} = \hbar \sum_{\nu=1}^{N} X_\nu \xi_\nu\,. \tag{3.2}$$

The system operators X_ν are assumed to commute pairwise with each other since for N qubits coupled to the bosonic field the operators X_ν act on different parts of the

total N-qubit Hilbert space. The qubits couple to the field at positions $\mathbf{x}_\nu$ and the corresponding field operators ξ_ν read

$$\xi_\nu = \xi(\mathbf{x}_\nu) = \sum_{\mathbf{k}\kappa} \left(g_{\mathbf{k}\kappa} b_{\mathbf{k}\kappa} \mathrm{e}^{\mathrm{i}\mathbf{k}\cdot\mathbf{x}_\nu} + g^*_{\mathbf{k}\kappa} b^\dagger_{\mathbf{k}} \mathrm{e}^{-\mathrm{i}\mathbf{k}\cdot\mathbf{x}_\nu} \right) . \tag{3.3}$$

For ease of notation we will henceforth suppress the explicit notation of the branch index κ.

At time $t = t_0$ we choose an initial condition of the Feynman-Vernon type, i.e. one for which the total density operator R of the system and the bath can be factorized into a system and a bath contribution ρ and ρ_b, respectively,

$$R(t_0) = \rho(t_0) \otimes \rho_\mathrm{b}(t_0). \tag{3.4}$$

The factorizing initial condition is a standard assumption in the theory of open quantum systems [99–101]. Moreover, it is expected in most applications of quantum information processing because a proper implementation of quantum algorithms in a quantum computer requires the ability to prepare the qubits in well defined pure states [1]. In other words, we must be able to assume that at a certain instance of time the state of the qubits is well known and, thus, uncorrelated with the environment. Another justification for a factorizing initial state in view of quantum computation is the following [129]: The application of operations like single qubit rotations and two-qubit gates typically involve temporary interactions with external controls that are strong compared to interactions with sources of quantum noise being always present. Usually, it is assumed that these control functions will erase the fragile entanglement that qubits develop with the bath modes at times during which they were left alone, i.e. during the system evolves with purely bath induced interactions. One may expect that only a part of the environment, the low frequency modes, can be prepared factorized from the qubits [164], whereas the high-frequency components lead to renormalization effects. Nevertheless, for evaluating the relative importance of the quantum noise effects on the internal qubit dynamics, we assume that the qubit-bath system is set to uncorrelated at $t = t_0$.

Typically, the bath is initially at thermal equilibrium. If the initial expectation value of the coupling operators X_ν do not vanish, the coupling (3.2) entails a force on the bath oscillators. Then the natural initial state $\rho_\mathrm{b} = \rho_\mathrm{b}(t_0)$ of the bath is rather a displaced thermal state which falls in the class of non-squeezed Gaussian states. A convenient basis for these states is provided by the coherent states $\{|\beta_\mathbf{k}\rangle\}$ defined by the eigenvalue equation $b_\mathbf{k}|\beta_\mathbf{k}\rangle = \beta_\mathbf{k}|\beta_\mathbf{k}\rangle$. Owing to the overcompleteness of this basis, any hermitian operator can be written in a diagonal form, which assigns to each operator a P-function [101, 165]. In particular, the bath density operator can be written as

$$\rho_\mathrm{b} = \int \prod_\mathbf{k} \mathrm{d}^2\beta_\mathbf{k}\, P_\mathbf{k}(\beta_\mathbf{k}, \beta^*_\mathbf{k}) |\beta_\mathbf{k}\rangle\langle\beta_\mathbf{k}| \,, \tag{3.5}$$

where $\mathrm{d}^2\beta_\mathbf{k}$ denotes integration over the complex plane. Henceforth, we assume that the P-function of each mode $\mathbf{k}$ is a Gauss function, such that

$$P_\mathbf{k}(\beta_\mathbf{k}, \beta^*_\mathbf{k}) = \frac{1}{\pi n_\mathbf{k}} \exp\left(\frac{-(\beta_\mathbf{k} - \bar\beta_\mathbf{k})(\beta_\mathbf{k} - \bar\beta_\mathbf{k})^*}{n_\mathbf{k}} \right) . \tag{3.6}$$

As a central property of a Gaussian state, all expectation values are fully determined by $\bar{\beta}_{\mathbf{k}} = \langle b_{\mathbf{k}} \rangle_{\mathrm{b}}$ and $n_{\mathbf{k}} = \langle b_{\mathbf{k}}^\dagger b_{\mathbf{k}} \rangle_{\mathrm{b}} - |\langle b_{\mathbf{k}} \rangle_{\mathrm{b}}|^2$, where

$$\langle \ldots \rangle_{\mathrm{b}} = \mathrm{tr}_{\mathrm{b}}(\rho_{\mathrm{b}} \ldots) \tag{3.7}$$

denotes the expectation value with respect to the bath state ρ_{b}. An important particular case is the canonical ensemble of the bath at temperature T for which

$$\rho_{\mathrm{b}}(t_0) = \rho_{\mathrm{b}}^{\mathrm{eq}} \propto \exp\Big(- \sum_k \frac{\hbar \omega_k b_k^\dagger b_k}{k_{\mathrm{B}} T} \Big) . \tag{3.8}$$

It corresponds to the P-function (3.6) with $\bar{\beta}_{\mathbf{k}} = 0$ and $n_{\mathbf{k}}$ being the Bose distribution function, i.e. $2n_{\mathbf{k}} = \coth(\hbar\omega_{\mathbf{k}}/2k_{\mathrm{B}}T) - 1$.

It is convenient to set the initial time $t_0 = 0$ and to work in the interaction-picture representation with respect to the uncoupled system and bath $H_0 = H_{\mathrm{s}} + H_{\mathrm{b}}$. Operators A in this representation are denoted by a tilde, i.e. they transform to $\tilde{A}(t) = U_0^\dagger(t) A\, U_0(t)$, where $U_0(t) = \exp(-\mathrm{i}H_0 t/\hbar)$. The condition (3.1) for pure phase noise implies that $[H_{\mathrm{sb}}, U_0] = 0$, i.e. the interaction-picture coupling operators remain time-independent, $\tilde{X}_\nu(t) = X_\nu$. For the bosonic annihilation and creation operators one finds $\tilde{b}_{\mathbf{k}}(t) = b_{\mathbf{k}} \exp(-\mathrm{i}\omega_{\mathbf{k}} t)$ and $\tilde{b}_{\mathbf{k}}^\dagger(t) = b_{\mathbf{k}}^\dagger \exp(\mathrm{i}\omega_{\mathbf{k}} t)$, respectively.

The dynamics of the system plus the environment is governed by the Liouville-von Neumann equation

$$\mathrm{i}\hbar \frac{\mathrm{d}}{\mathrm{d}t} \widetilde{R}(t) = \big[\widetilde{H}_{\mathrm{sb}}(t), \widetilde{R}(t) \big] . \tag{3.9}$$

We are exclusively interested in the state of the system, so our goal is to find the time evolution of the reduced density operator $\tilde{\rho}(t) = \langle \tilde{R}(t) \rangle_{\mathrm{b}}$. The system Hamiltonian H_{s} and the set of coupling operators X_ν possess a complete set of common eigenstates, that is the product eigenbasis $|\mathbf{n}\rangle = |n_1, n_2, \ldots, n_N\rangle$ of the coupling operators which we define by $X_\nu |\mathbf{n}\rangle = \chi_{\nu,n_\nu} |\mathbf{n}\rangle$ where χ_{ν,n_ν} is the n_ν-th eigenvalue of the operator X_ν. In what follows, we consider the reduced matrix elements $\tilde{\rho}_{\mathbf{m},\mathbf{n}} = \langle \mathbf{m} | \tilde{\rho} | \mathbf{n} \rangle$ in this basis. The explicit solution of the Liouville-von Neumann equation is deferred to App. A, where we find for the density matrix elements the closed exact expression

$$\begin{aligned} \tilde{\rho}_{\mathbf{m},\mathbf{n}}(t) = \rho_{\mathbf{m},\mathbf{n}}(0)\, \mathrm{e}^{\mathrm{i}\phi_{\mathbf{m},\mathbf{n}}(t) - \sum_{\mathbf{k}} \left| \sum_\nu (\chi_{\nu,m_\nu} - \chi_{\nu,n_\nu}) y_{\mathbf{k}\nu} \right|^2} \\ \times \prod_{\mathbf{k}} \mathcal{C}_{\mathbf{k}} \Big(\sum_\nu \left[\chi_{\nu,m_\nu} - \chi_{\nu,n_\nu} \right] y_{\mathbf{k}\nu} \Big) . \end{aligned} \tag{3.10}$$

with the quantum characteristic function [101]

$$\mathcal{C}_{\mathbf{k}}(z) = \int \mathrm{e}^{z\beta_{\mathbf{k}}^* - z^* \beta_{\mathbf{k}}} P_{\mathbf{k}}(\beta_{\mathbf{k}}, \beta_{\mathbf{k}}^*) \mathrm{d}^2 \beta_{\mathbf{k}} , \tag{3.11}$$

and the complex numbers $y_{\mathbf{k}\nu} = g_{\mathbf{k}}^* \mathrm{e}^{-\mathrm{i}\mathbf{k}\cdot\mathbf{x}_\nu} (1 - \mathrm{e}^{\mathrm{i}\omega_{\mathbf{k}} t})/\omega_{\mathbf{k}}$. The time-dependent phase $\phi_{\mathbf{m},\mathbf{n}}(t)$ corresponds to a Lamb-shift and is brought about by time-ordering. It depends on the separations $\mathbf{x}_{\nu\nu'} = \mathbf{x}_\nu - \mathbf{x}_{\nu'}$ and reads

$$\phi_{\mathbf{m},\mathbf{n}}(t) = \sum_{\mathbf{k}} |g_{\mathbf{k}}|^2 \frac{\omega_{\mathbf{k}} t - \sin(\omega_{\mathbf{k}} t)}{\omega_{\mathbf{k}}^2} \sum_{\nu\nu'} \mathrm{e}^{\mathrm{i}\mathbf{k}\cdot\mathbf{x}_{\nu\nu'}} \left[\chi_{\nu,m_\nu} \chi_{\nu',m_{\nu'}} - \chi_{\nu,n_\nu} \chi_{\nu',n_{\nu'}} \right] . \tag{3.12}$$

This phase corresponds to an effective coherent evolution with Hamiltonian

$$H_{\mathrm{s,eff}} = \sum_{\nu\nu'} f_{\nu\nu'} X_\nu X_{\nu'} \,, \tag{3.13}$$

where the function $f_{\nu\nu'}$ depends on the separations $\mathbf{x}_{\nu\nu'}$, but not on the temperature. Put differently, the phase arises from an indirect pairwise interaction between different parts ν and ν' of the system mediated by the vacuum fluctuations of the bosonic field. This interaction gives rise to interesting effects, for example the creation of entanglement between initially unentangled and spatially separated qubits [162, 166].

For the case of a Gaussian distribution (3.6) of the bath modes, it is possible to calculate the integral in the characteristic function (3.11) explicitly. We then obtain our final result

$$\tilde{\rho}_{\mathbf{m},\mathbf{n}}(t) = \rho_{\mathbf{m},\mathbf{n}}(0)\, \mathrm{e}^{-\Lambda_{\mathbf{m},\mathbf{n}}(t) + \mathrm{i}[\phi_{\mathbf{m},\mathbf{n}}(t) + \varphi_{\mathbf{m},\mathbf{n}}(t)]} \,. \tag{3.14}$$

The amplitudes of the density matrix elements (3.14) are changed by the time-dependent damping amplitude

$$\Lambda_{\mathbf{m},\mathbf{n}}(t) = \sum_{\mathbf{k}} |g_{\mathbf{k}}|^2 \frac{1-\cos(\omega_{\mathbf{k}} t)}{\omega_{\mathbf{k}}^2} \left[1 + 2n_{\mathbf{k}}\right] \left| \sum_\nu \mathrm{e}^{\mathrm{i}\mathbf{k}\cdot\mathbf{x}_\nu} \left[\chi_{\nu,m_\nu} - \chi_{\nu,n_\nu}\right] \right|^2 \,. \tag{3.15}$$

The phase $\varphi_{\mathbf{m},\mathbf{n}}(t)$ depends on the shifts $\bar{\beta}_{\mathbf{k}}$ of the Gaussian initial state (3.6) and reads

$$\varphi_{\mathbf{m},\mathbf{n}}(t) = 2 \sum_{\mathbf{k}} \sum_\nu \mathrm{Im} \left(\frac{\bar{\beta}_{\mathbf{k}} g_{\mathbf{k}}^*}{\omega_{\mathbf{k}}} \mathrm{e}^{\mathrm{i}\mathbf{k}\cdot\mathbf{x}_\nu} \left[1 - \mathrm{e}^{\mathrm{i}\omega_{\mathbf{k}} t}\right] \right) \left(\chi_{\nu,m_\nu} - \chi_{\nu,n_\nu}\right) . \tag{3.16}$$

Note that it vanishes for a thermal bath state. At time $t = 0$ both the damping (3.15) as well as the phases (3.12) and (3.16) vanish, so that Eq. (3.14) is consistent with the initial condition. As expected for pure dephasing, populations are preserved, i.e. the diagonal matrix elements obey $\tilde{\rho}_{\mathbf{m},\mathbf{m}}(t) = \tilde{\rho}_{\mathbf{m},\mathbf{m}}(0)$. This implies that generally neither the reduced nor the total system will reach thermal equilibrium. However, the relative phases between system eigenstates $|\mathbf{n}\rangle$ will be randomized so that off-diagonal density matrix elements — the so-called coherences — may decay, which reflects the process of decoherence.

3.2 Exact results in explicit form

Given the physical parameters of the qubit-bath coupling, i.e. the microscopic coupling constants $g_{\mathbf{k}}$, the dispersion relation $\omega_{\mathbf{k}}$, and the variations $n_{\mathbf{k}}$ of the bath state $\rho_{\mathrm{b}}^{\mathrm{eq}}$, the exact time evolution of the reduced density matrix can be computed. In doing so, the remaining summations in the expressions for the damping (3.15) and the phase (3.12) have to be carried out. In principle, this can be established numerically. However, for a detailed theoretical study of the reduced dynamics and the influence of a nonlocal system-bath coupling, the knowledge of the matrix elements in an explicit form is desirable. We thus evaluate explicit expressions for various spectral bath densities. Thereby, we focus on a thermal initial state (3.8) for which the phases (3.16) vanish and where $1 + 2n_{\mathbf{k}} = \coth(\hbar\omega_{\mathbf{k}}/2k_{\mathrm{B}}T)$ in the damping (3.15). Moreover, we consider acoustic

bosons, i.e. branches with dispersion relation $\omega_{\mathbf{k}} = ck$, where $k = |\mathbf{k}|$. Here, c is the velocity of the field, which defines the transit time $t_{\nu\nu'} = |\mathbf{x}_{\nu\nu'}|/c$ of the field from the coupling ν to ν'.

For the evaluation of the damping and phase factors it is convenient to introduce the spectral bath density

$$J(\omega) = \sum_{\mathbf{k}} |g_{\mathbf{k}}|^2 \delta(\omega - ck)\,. \tag{3.17}$$

With the help of the spectral density, summations over the wave vector $\mathbf{k}$ can now be replaced by a frequency integral plus an integration over the solid angle. The angle integral can be carried out explicitly only when the dependence of the microscopic coupling strengths on the angle, i.e. its anisotropy, is known. To proceed further one may construct an effective isotropic interaction by averaging the coupling constants $|g_{\mathbf{k}}|^2$ over the solid angle. This procedure is exact for isotropic coupling mechanisms like the electron-phonon interaction via the deformation potential (see Sect. 2.3), and it turns out that it is reasonable even for anisotropic couplings like the piezoelectric interaction [71, 114, 120]. Thus, we define an angular averaged coupling constant g_k, e.g. for the three-dimensional model by

$$|g_k|^2 = \frac{1}{4\pi} \int_0^{2\pi} \mathrm{d}\varphi \int_0^{\pi} \mathrm{d}\theta\, \sin(\theta) |g_{\mathbf{k}}|^2\,, \tag{3.18}$$

where the wave vector is expressed in spherical coordinates $\mathbf{k} = (k, \theta, \varphi)$. We then find for the time-dependent phase (3.12) in the continuum limit

$$\phi^{(d)}_{\mathbf{m},\mathbf{n}}(t) = \sum_{\nu,\nu'} [\chi_{\nu,m_\nu} \chi_{\nu',m_{\nu'}} - \chi_{\nu,n_\nu} \chi_{\nu',n_{\nu'}}] \phi^{(d)}(\tau, \tau_{\nu\nu'})\,, \tag{3.19}$$

$$\phi^{(d)}(\tau, \tau_{\nu\nu'}) = \int_0^{\infty} \mathrm{d}\omega\, J(\omega) G^{(d)}\left(\omega t_{\nu\nu'}\right) \frac{\omega t - \sin(\omega t)}{\omega^2}\,. \tag{3.20}$$

Here, $G^{(d)}(x)$ denotes a dimension-dependent geometrical factor stemming from the integration over the solid angle for which we obtain

$$G^{(1)}(x) = \cos(x)\,, \tag{3.21a}$$

$$G^{(2)}(x) = J_0(x)\,, \tag{3.21b}$$

$$G^{(3)}(x) = \frac{\sin(x)}{x}\,, \tag{3.21c}$$

with J_0 beinh the zeroth-order Bessel function of the first kind. Note that $G^{(d)}(0) = 1$ for all dimensions, and for large arguments $G^{(d)}$ decays to zero for $d = 2, 3$ but not for $d = 1$. For the damping rate (3.15), we find in the continuum limit

$$\Lambda^{(d)}_{\mathbf{m},\mathbf{n}}(t) = \sum_{\nu,\nu'} [\chi_{\nu,m_\nu} - \chi_{\nu,n_\nu}][\chi_{\nu',m_{\nu'}} - \chi_{\nu',n_{\nu'}}] \Lambda^{(d)}(\tau, \tau_{\nu\nu'})\,, \tag{3.22}$$

$$\Lambda^{(d)}(\tau, \tau_{\nu\nu'}) = \int_0^{\infty} \mathrm{d}\omega\, J(\omega) G^{(d)}(\omega t_{\nu\nu'}) \frac{1 - \cos(\omega t)}{\omega} \coth\left(\frac{\hbar\omega}{2k_{\mathrm{B}}T}\right)\,. \tag{3.23}$$

Note that only pairwise terms contribute to the phase (3.19) and the damping (3.22). The evaluation of the remaining frequency integrals crucially depends on the geometrical factor $G^{(d)}$ and thus on the dimension of the environment. Furthermore, the spectral bath density needs to be specified. In the following, we outline the derivation for the important cases $d = 1$ and $d = 3$ and we consider spectral densities of the form

$$J(\omega \geq 0) = \alpha \frac{\omega^s}{\omega_{\mathrm{c}}^{s-1}} \, \mathrm{e}^{-\omega/\omega_{\mathrm{c}}} \,, \tag{3.24}$$

with the dimensionless qubit-bath coupling parameter α, the cutoff frequency ω_{c} and the exponent s that depends on the dimension and the microscopic origin of the coupling. For instance, in Sec. 2.3 we have seen that for the coupling of a confined electron to phonons via the deformation potential $|g_k|^2 \propto k$. With a factor k^2 for a three-dimensional environment we obtain a super-ohmic spectral density with $s = 3$. By contrast, for a quasi one-dimensional environment we end up with an ohmic spectral density $s = 1$. A more detailed discussion on the relation of the spectral density to the geometry of the environment, in particular in the context of semiconductor quantum dots, can be found in Refs. [71,72,120,162]. Here we will focus on both ohmic as well as super-ohmic spectral densities with integer $s = 1, 2, ...$ In particular, we do not discuss sub-ohmic damping with $s < 1$.

The cutoff frequency ω_{c} provides a natural scaling of time and energy, so that for ease of notation, we introduce the dimensionless time $\tau = \omega_{\mathrm{c}} t$, transit times $\tau_{\nu\nu'} = \omega_{\mathrm{c}} t_{\nu\nu'}$, and temperature $\theta = k_{\mathrm{B}} T / \hbar\omega_{\mathrm{c}}$. The calculation of the integral in Eq. (3.23) is deferred to App. B, where we obtain the explicit expressions for the damping

$$\Lambda^{(1)}(\tau, \tau_{\nu\nu'}) = \alpha \, \mathrm{Re} \, I^{\Lambda}_{\nu\nu'}(s, \tau) \,, \tag{3.25}$$

$$\Lambda^{(3)}(\tau, \tau_{\nu\nu'}) = \alpha \begin{cases} \mathrm{Re} \, I^{\Lambda}_{\nu\nu}(s, \tau), & \text{for } \tau_{\nu\nu'} = 0 \\ \frac{1}{\tau_{\nu\nu'}} \, \mathrm{Im} \, I^{\Lambda}_{\nu\nu'}(s-1, \tau) & \text{otherwise.} \end{cases} \tag{3.26}$$

The function $I^{\Lambda}_{\nu\nu'}$ reads

$$\begin{aligned} I^{\Lambda}_{\nu\nu'}(s, \tau) = (-\theta)^{s-1} \Big[& 2F^{(s-1)}\big(\theta[1 - \mathrm{i}\tau_{\nu\nu'}]\big) - F^{(s-1)}\big(\theta[1 - \mathrm{i}(\tau_{\nu\nu'} - \tau)]\big) \\ & - F^{(s-1)}\big(\theta[1 - \mathrm{i}(\tau_{\nu\nu'} + \tau)]\big) \Big] \\ & + \Gamma(s-1) \left(\frac{\cos\big[(s-1) \arctan\big(\frac{\tau}{1 - \mathrm{i}\tau_{\nu\nu'}}\big)\big]}{[\tau^2 + (1 - \mathrm{i}\tau_{\nu\nu'})^2]^{\frac{s-1}{2}}} - (1 - \mathrm{i}\tau_{\nu\nu'})^{1-s} \right) , \end{aligned} \tag{3.27}$$

where $\Gamma(z)$ denotes Euler's Gamma function, $F(z) = \log \Gamma(z)$ and $F^{(m)}$ is its m-th derivative, which equals the Polygamma function $\Psi_{m-1}(z)$. Note that the expression $I_{\nu\nu'}(1, \tau)$ for the ohmic case is obtained by taking the limit $s \to 1$. The phase shift (3.20) reads

$$\phi^{(1)}(\tau, \tau_{\nu\nu'}) = \alpha \, \mathrm{Re} \, I^{\phi}_{\nu\nu'}(s, \tau) \,, \tag{3.28}$$

$$\phi^{(3)}(\tau, \tau_{\nu\nu'}) = \alpha \begin{cases} \mathrm{Re} \, I^{\phi}_{\nu\nu}(s, \tau), & \text{for } \tau_{\nu\nu'} = 0 \\ \frac{1}{\tau_{\nu\nu'}} \, \mathrm{Im} \, I^{\phi}_{\nu\nu'}(s-1, \tau) & \text{otherwise} \,, \end{cases} \tag{3.29}$$

with the function

$$I^{\phi}_{\nu\nu'}(s,\tau) = \frac{\tau\Gamma(s)}{(1+\mathrm{i}\tau_{\nu\nu'})^s} - \frac{\sin\left[(s+1)\arctan\left(\frac{\tau}{1-\mathrm{i}\tau_{\nu\nu'}}\right)\right]}{[\tau^2-(1-\mathrm{i}\tau_{\nu\nu'})^2]^{(s-1)/2}}\,. \tag{3.30}$$

4

Exact solutions from approximate master equations

Although pure dephasing constitutes an important contribution to the decoherence of a quantum system, it is not always feasible to achieve exact results for the dissipative system dynamics. In such cases, one can benefit from an approximate treatment in the spirit of a perturbative master equation approach. To this end we first revisit the time-convolutionless master equation approach and present a non-Markovian master equation for weak system-bath coupling, which is typically termed "Born master equation" [100]. By neglecting memory effects of the heat bath, one eventually obtains from the Born master equation a Markovian description of the reduced system known as Bloch-Redfield theory [167].

By applying the Born master equation to the pure phase noise model we show that the results of this approximate equation can even be exact [168], despite the fact that it is based on second-order perturbation theory. We reveal that this equivalence holds if and only if the initial state of the bath can be mapped to a Gaussian phase-space distribution function, which for example is the case for a thermal bath initial state.

4.1 Time-local master equation approach

A common and successful approach to dissipative quantum dynamics is provided by master equations, i.e. differential or integro-differential equations of motion for the reduced density operator $\tilde{\rho}$ [100, 101, 169]. There exist various formally exact quantum master equations in time-convolutionless [170–181] and time-nonlocal form [182–184] which, however, generally cannot be solved explicitly so that one often has to resort to a perturbative treatment, see App. C for an overview.

In the following, we employ the time-convolutionless version of such master equations. It is of the form

$$\dot{\tilde{\rho}}(t) = \mathcal{K}(t)\tilde{\rho}(t)\,, \tag{4.1}$$

with a time-dependent superoperator $\mathcal{K}(t)$. Note that there arises no inhomogeneity since we are assuming a factorizing initial state (3.4), which leads to a linear equation of motion [185]. Equation (4.1) is formally exact and possesses an apparently simple form, but it generally cannot be solved analytically. Thus, it is convenient to expand the

generator $\mathcal{K}(t)$ in powers of the interaction, i.e. $\mathcal{K}(t) = \sum_\ell \mathcal{K}_\ell(t)$. By a direct calculation [173,174,186] or by using a time convolutionless projection operator technique [100,177, 181,187] it is possible to obtain an expression for the ℓth order generator $\mathcal{K}_\ell$. In doing so, we assign to a superoperator $\mathcal{G}$ of the total system a reduced superoperator $\langle\mathcal{G}\rangle$ defined by its action on a system operator X, that is $\langle\mathcal{G}\rangle X = \mathrm{tr_b}\{\mathcal{G}(X\rho_\mathrm{b})\}$. With this notation, the time-convolutionless generators read $\mathcal{K}_1(t) = \langle\mathcal{L}(t)\rangle$, and

$$\mathcal{K}_\ell(t) = \int_{t_0}^{t} \mathrm{d}t_1 \int_{t_0}^{t_1} \mathrm{d}t_2 \ldots \int_{t_0}^{t_{\ell-2}} \mathrm{d}t_{\ell-1} \langle\langle \mathcal{L}(t)\mathcal{L}(t_1)\ldots\mathcal{L}(t_{\ell-1})\rangle\rangle_\mathrm{oc} \tag{4.2}$$

for $\ell = 2, 3, \ldots$ The symbol $\langle\langle\ldots\rangle\rangle_\mathrm{oc}$ denotes an ordered cumulant [169,174], i.e. a sum of certain products of reduced superoperators of the form $\langle\mathcal{L}(t)\mathcal{L}(t_1)\ldots\rangle$.

4.1.1 Weak system-bath coupling: Born master equation

The fact that the Liouvillians at different times generally do not commute makes it practically impossible to write down an explicit expression for the ℓth cumulant for large ℓ. However, for weak system-bath coupling it is possible to employ the so-called Born approximation, i.e. to neglect higher than second order terms in the expansion of the generator. Thus, we may approximate $\mathcal{K}(t) \approx \mathcal{K}_1(t) + \mathcal{K}_2(t)$. Fortunately the second time-ordered cumulant takes the simple form $\langle\langle\mathcal{L}(t)\mathcal{L}(t_1)\rangle\rangle_\mathrm{oc} = \langle\mathcal{L}(t)\mathcal{L}(t_1)\rangle - \langle\mathcal{L}(t)\rangle\langle\mathcal{L}(t_1)\rangle$. Using the explicit expression (3.2) for the bi-linear coupling H_sb we obtain the standard time-local Born master equation

$$\frac{d}{dt}\tilde{\rho}(t) = -\mathrm{i}\sum_\nu \langle\tilde{\xi}_\nu(t)\rangle_\mathrm{b}\left[\widetilde{X}_\nu(t), \tilde{\rho}(t)\right] - \sum_{\nu,\nu'}\int_0^{t-t_0} \mathrm{d}t'\, \kappa_{\nu\nu'}(t,t')\tilde{\rho}(t)\,, \tag{4.3}$$

with $t \geq t_0$, the superoperator

$$\begin{aligned}\kappa_{\nu\nu'}(t,t')[\ldots] = {}& \mathcal{S}_{\nu\nu'}(t,t-t')\big[\widetilde{X}_\nu(t), \big[\widetilde{X}_{\nu'}(t-t'), \ldots\big]\big] \\ & + \mathrm{i}\mathcal{A}_{\nu\nu'}(t,t-t')\big[\widetilde{X}_\nu(t)\big\{\widetilde{X}_{\nu'}(t-t'), \ldots\big\}\big]\,,\end{aligned} \tag{4.4}$$

and the anti-commutator $\{A, B\} = AB + BA$. In Eq. (4.4) we have defined the symmetric and anti-symmetric bath correlation functions

$$\mathcal{S}_{\nu\nu'}(t,t') = \frac{1}{2}\langle\{\Delta\tilde{\xi}_\nu(t), \Delta\tilde{\xi}_{\nu'}(t')\}\rangle_\mathrm{b}\,, \tag{4.5}$$

$$\mathcal{A}_{\nu\nu'}(t,t') = \frac{1}{2}\langle[\Delta\tilde{\xi}_\nu(t), \Delta\tilde{\xi}_{\nu\nu'}(t')]\rangle_\mathrm{b}\,. \tag{4.6}$$

Here, the operator-valued fluctuation $\Delta\tilde{\xi}_\nu(t) = \tilde{\xi}_\nu(t) - \langle\tilde{\xi}_\nu(t)\rangle_\mathrm{b}$. Note that for a thermal initial state (3.8) of the bath, the mean value $\langle\tilde{\xi}_\nu(t)\rangle_\mathrm{b}$ of the bath coordinate vanishes. For the more general Gaussian initial state (3.5) this is not the case so that the mean value explicitly appears in the master equation (4.3).

Although this master equation is in a time-convolutionless form, it still is non-Markovian owing to the explicit dependence on the initial time t_0. Using the coherent state representation (3.6) for a Gaussian bath state, we can evaluate the mean value of the bath

coordinate $\tilde{\xi}_\nu$ and the correlation functions (4.5) and (4.6) in an explicit form and find

$$\langle\tilde{\xi}_\nu(t)\rangle_\mathrm{b} = \sum_{\mathbf{k}} \left(g_{\mathbf{k}}\bar{\beta}_{\mathbf{k}} \mathrm{e}^{\mathrm{i}(\mathbf{k}\cdot\mathbf{x}_\nu - \omega_{\mathbf{k}}t)} + g_k^*\bar{\beta}_{\mathbf{k}}^* \mathrm{e}^{-\mathrm{i}(\mathbf{k}\cdot\mathbf{x}_\nu - \omega_{\mathbf{k}}t)} \right) , \tag{4.7}$$

$$\mathcal{S}_{\nu\nu'}(t, t-t') = \sum_{\mathbf{k}} |g_{\mathbf{k}}|^2 \cos(\omega_{\mathbf{k}}t' - \mathbf{k}\cdot\mathbf{x}_{\nu\nu'})(1+2n_{\mathbf{k}}) \,, \tag{4.8}$$

$$\mathcal{A}_{\nu\nu'}(t, t-t') = -\sum_{\mathbf{k}} |g_{\mathbf{k}}|^2 \sin(\omega_{\mathbf{k}}t' - \mathbf{k}\cdot\mathbf{x}_{\nu\nu'}) \,. \tag{4.9}$$

Note that the correlation functions $\mathcal{S}_{\nu\nu'}(t,t')$ and $\mathcal{A}_{\nu\nu'}(t,t')$ depend on time differences $t-t'$ only, with $\mathcal{A}_{\nu\nu'}(t,t')$ independent of the initial state of the bath.

4.1.2 The Markov approximation: Bloch-Redfield theory

If the correlation functions vanish sufficiently fast, it is convenient to employ a Markov approximation, i.e. to neglect the memory effects of the heat bath [99, 100, 167]. This is reasonable if the typical time scale t_dec with which the system decoheres is large compared to the correlation time t_b of the heat bath. The latter can be defined by the time scale over which the correlation functions are effectively non-vanishing. Then one may extend the upper integration limits in Eq. (4.3) to infinity,

$$\int_0^{t-t_0} \mathrm{d}t' \, \kappa_{\nu\nu'}(t,t') \approx \int_0^{\infty} \mathrm{d}t' \, \kappa_{\nu\nu'}(t,t') \,, \tag{4.10}$$

which constitutes the long-time limit of the Born master equation. This approximation leads to a coarse graining of time, i.e. the Markovian master equation will be valid for time steps $\mathrm{d}t \gg t_\mathrm{b}$ only. When written in the eigenbasis of the system Hamiltonian H_s, and assuming a thermal initial state of the bath so that the first term in Eq. (4.3) vanishes, we arrive at the standard Bloch-Redfield equation [167] of the form

$$\dot{\tilde{\rho}}_{\mathbf{m},\mathbf{n}}(t) = \sum_{\mathbf{m}',\mathbf{n}'} R_{\mathbf{mn},\mathbf{m}'\mathbf{n}'} \, \tilde{\rho}_{\mathbf{m}',\mathbf{n}'}(t) \,, \tag{4.11}$$

with the so-called Redfield tensor R. This Markovian equation of motion with its static decay rates leads typically to exponential decay laws, which for a two-level system can be quantified by T_1 and T_2 times. They are defined as the inverse of the exponential decay rates. The T_1 time characterizes the relaxation of the system, i.e. the change in the diagonal elements of the reduced density matrix, whereas the T_2 time characterizes the dephasing, that is the decay of the non-diagonal matrix elements. The Markovian description is in line with Fermi's golden rule which entails that relaxation rates depend on the spectral density of the environment at the transition frequency of interest. In quantum optics, where the bath is the electromagnetic field that causes pure relaxation, the Bloch-Redfield equation has proven its use since many decades. However, we will see later in Chap. 7 that it violates causality when applied to the reduced dynamics of a spatially extended quantum system.

4.2 When second order is exact

Let us give our attention again to the non-Markovian Born master equation (4.3). The pure phase-noise model considered in the first section provides an ideal testing candidate for the master equation, since it is then possible to compare its results with an exact analytical solution. We expect that the master equation (4.3) provides better results for weaker coupling of the system and the heat bath, since it is based on a perturbative expansion. However, we now show that within the time-local master equation approach even the exact result of the phase noise model can be obtained already in second order of the system-bath coupling [168]. To ease the presentation, we will concentrate on an interaction Hamiltonian of the form $H_{\mathrm{sb}} = \hbar X \xi$ for the rest of this section, i.e. in Eq. (3.2) we choose $N = 1$. However, the statements hold true for the general case as well.

4.2.1 Comparison with the exact solution

It is convenient to expand the master equation (4.3) into the eigenbasis of the system-bath interaction. We then obtain for a matrix element $\langle m|\tilde{\rho}|n\rangle = \tilde{\rho}_{m,n}$ the differential equation

$$\begin{aligned}\dot{\tilde{\rho}}_{m,n}(t) = \Big[&- \mathrm{i}(\chi_m - \chi_n)\langle\tilde{\xi}(t)\rangle_{\mathrm{b}} - (\chi_m - \chi_n)^2 \int_0^t \mathrm{d}\tau\, \mathcal{S}(t, t-\tau) \\ &- \mathrm{i}(\chi_m^2 - \chi_n^2) \int_0^t \mathrm{d}\tau\, \mathcal{A}(t, t-\tau) \Big] \tilde{\rho}_{mn}(t)\,,\end{aligned} \tag{4.12}$$

where we have set the initial time $t_0 = 0$. The expectation value of the bath coordinate $\tilde{\xi}$ and the correlation functions $\mathcal{S}$ and $\mathcal{A}$ are obtained from Eqs. (4.7)–(4.9) by setting $\mathbf{x}_\nu = \mathbf{x}_{\nu\nu'} = 0$.

To compare the master equation (4.12) with the exact solution (3.14), we compute the time-derivative of the latter. We find the relations

$$\dot{\varphi}_{m,n}(t) = (\chi_m - \chi_n)\langle\xi(t)\rangle_{\mathrm{b}}\,, \tag{4.13}$$

$$\dot{\phi}_{m,n}(t) = -(\chi_m^2 - \chi_n^2) \int_0^t \mathrm{d}\tau\, \mathcal{A}(t, t-\tau)\,, \tag{4.14}$$

$$\dot{\Lambda}_{m,n}(t) = (\chi_m - \chi_n)^2 \int_0^t \mathrm{d}\tau\, \mathcal{S}(t, t-\tau)\,, \tag{4.15}$$

which reveal the surprising fact that the exact solution obeys the quantum master equation (4.12). Or put differently, for pure phase noise the exact result can be obtained within second-order perturbation theory from the master equation (4.12). In turn, from the exact relations (4.13)-(4.15) one can get information about the spectral properties of the bath by comparing our results with the experimentally observed dephasing at short times. For large times t, this master equation becomes the standard Markovian Bloch-Redfield equation. Thus, the latter contains the exact long-time limit of the rates (4.13)–(4.15). Moreover, for our model the Redfield equation is of Lindblad form, i.e. although it will not yield the exact result for short times, the complete positivity of the reduced density operator is conserved [188, 189].

4.2.2 Time ordered cumulants and Gaussian bath initial state

We have seen that for pure dephasing, the time-local master equation (4.1) derived within second order perturbation theory provides the exact time evolution of the reduced density matrix. This implies that in the expansion of the Liouvillian $\mathcal{K}(t)$, all higher order contributions vanish, which on the one hand nicely simplifies practical calculations. On the other hand, it poses the question whether we face a coincidence or whether there is any profound reason for the equivalence. In order to underline the latter point of view, we now demonstrate that for phase noise, the time-ordered cumulant in the ℓth order generator (4.2) is proportional to the usual classical cumulant of the initial bath state. Consequently, we can argue that for the Gaussian initial state (3.6), the series $\mathcal{K}(t) = \sum_\ell \mathcal{K}_\ell(t)$ terminates after $\ell = 2$, which implies that the second-order time-local master equation (4.12) is exact.

We start out by defining averages with respect to the P-function as

$$\langle \cdots \rangle_P = \int \cdots \prod_{\mathbf{k}} P(\beta_{\mathbf{k}}, \beta_{\mathbf{k}}^*) \mathrm{d}^2\beta_{\mathbf{k}} \,. \tag{4.16}$$

With this notation, the exact solution (3.10) reads

$$\tilde{\rho}_{m,n}(t) = \left\langle \exp\left\{ \int_0^t \mathrm{d}t' \, f_{mn}(t') \right\} \right\rangle_P \tilde{\rho}_{m,n}(0) \,, \tag{4.17}$$

with the complex valued function

$$f_{mn}(t) = \mathrm{i}\phi_{m,n}(t) - \sum_k \left\{ (\chi_m - \chi_n)^2 \frac{|y_{\mathbf{k}}(t)|^2}{2} - (\chi_m - \chi_n)[y_{\mathbf{k}}(t)\beta_{\mathbf{k}}^* - y_{\mathbf{k}}^*(t)\beta_{\mathbf{k}}] \right\}. \tag{4.18}$$

The average in Eq. (4.17) is obtained from a distribution function for the c-numbers β_k. Thus, it can be formally considered as the averaged solution of a stochastic differential equation that obeys a time-local differential equation of the form (4.1), but with the generator $\mathcal{K}$ now being a c-number, not an operator. Thus, we can adapt the line of argumentation given by van Kampen for classical Gaussian stochastic processes [174]: Differentiating the Taylor expansion of Eq. (4.17), we find

$$\begin{aligned} \dot{\tilde{\rho}}_{m,n}(t) = \Bigg[& \langle f_{mn}(t) \rangle_P + \int_0^t \mathrm{d}t_1 \langle f_{mn}(t) f_{mn}(t_1) \rangle_P \\ & + \int_0^t \mathrm{d}t_1 \int_0^{t_1} \mathrm{d}t_2 \, \langle f_{mn}(t) f_{mn}(t_1) f_{mn}(t_2) \rangle_P + \ldots \Bigg] \tilde{\rho}_{m,n}(0). \end{aligned} \tag{4.19}$$

A time-local equation of motion for $\tilde{\rho}_{m,n}(t)$ can be obtained by inserting $\tilde{\rho}_{m,n}(0)$ from Eq. (4.17), which yields [174]

$$\begin{aligned} \dot{\tilde{\rho}}_{m,n}(t) = & \sum_{\ell=1}^{\infty} \int_0^t \mathrm{d}t_1 \int_0^{t_1} \mathrm{d}t_2 \ldots \int_0^{t_{\ell-2}} \mathrm{d}t_{\ell-1} \\ & \times \langle\langle f_{mn}(t) f_{mn}(t_1) \ldots f_{mn}(t_{\ell-1}) \rangle\rangle_P \, \tilde{\rho}_{m,n}(t) \,, \end{aligned} \tag{4.20}$$

where $\langle\langle \ldots \rangle\rangle_P$ denotes the cumulants with respect to the P-function. Note that for the cumulants of a classical process, time-ordering is not relevant [174]. Thus the only difference of this expansion and the one in Eq. (4.2) for the quantum master equation is that the latter contains time-ordered cumulants.

For a Gaussian P-function, all cumulants of β_k and β_k^* beyond second order vanish [190]. Since $f_{mn}(t)$ is linear in these variables, the same is true for the cumulants in Eq. (4.20) and, consequently, only the terms with $\ell = 1, 2$ contribute to this expansion. Evaluating the expansion coefficients explicitly, one finds that they are identical to those of the second-order time-local master equation (4.20).

We find that the equivalence of the second-order master equation and the exact solution is based on two requirements: First, the coupling operator X needs to be diagonal in the eigenbasis of the system, i.e. its interaction-picture representation is time-independent, $\widetilde{X}(t) = X$, so that it can be effectively treated as a c-number. Hence the quantum mechanical time-ordering affects only the bath coordinate $\tilde{\xi}(t)$ for which we can express multi-time expectation values as cumulants of the P-function. In that way, we can circumvent the tedious task of normal-ordering the operators b_k and $b_k^\dagger$. With this precondition, secondly, the Gaussian initial state of the bath ensures that the cumulant expansion terminates after the second order and agrees with the expansion of the master equation (4.1). For any non-Gaussian state infinitely many higher-order cumulants are non-zero, both in the classical case [191–193] and in the quantum mechanical case [194–196]. Consequently, the expansion of the Liouvillian is of infinite order and any truncation represents an approximation. If one of these conditions, pure phase noise and a Gaussian initial state, is violated, there might still exist an exact solution, but it can no longer be obtained within second-order perturbation theory, as for example is the case for the dissipative harmonic oscillator [142, 144].

Let us finally stress that the second-order Nakajima-Zwanzig master equation [182, 183], which we did not consider here, can be expressed in terms of cumulants (the so-called partial cumulants) as well [197, 198]. Note that the ordered and the partial cumulants up to second order coincide, see App. C. However, the Nakajima-Zwanzig equation is an integro-differential equation for the reduced density matrix, i.e. the past system dynamics enter the master equation via a memory kernel. Since it is not in time local form it cannot yield the exact result for the model discussed here [199]. Thus, phase noise constitutes an example for which the time-local approach is more accurate than the time-nonlocal one when comparing their perturbation expansions up to the same order. This outcome is in agreement with some recent findings for harmonic oscillator baths [200, 201] and for spin baths [202, 203]. Nevertheless, the quality of each of the approaches seems to be model dependent [197, 204–206]. The second-order time-local master equation employed in this work agrees with the exact solution at any time. In particular in the long-time limit, it becomes Markovian and identical to the standard Bloch-Redfield master equation, which for pure phase noise is of Lindblad form. This also explains the previously observed "excellent agreement" [207] between the exact dynamics and results obtained within Bloch-Redfield theory.

4.3 Conclusion

Quantum systems under the influence of pure phase noise represent an important special case of dissipative quantum mechanics owing to the existence of an exact solution. Moreover, on short time scales, on which the coherent system dynamics cannot manifest itself, the behavior of the phase noise model is even generic [152]. Despite the exact solubility of the phase noise problem, it is often convenient to study the reduced dynamics within a master equation approach based on second-order perturbation theory in the system-bath coupling. For a general Gaussian initial bath state, of which the thermal Gibbs state is a special case, we have demonstrated that the coherence decay is determined by the symmetric bath correlation function, while the anti-symmetric correlation function gives rise to a time-dependent phase shift. For the pure-phase noise model, the (time-nonlocal) second-order Nakajima-Zwanzig constitutes an approximation of the the reduced dynamics. For the time-local version of such a master equation, by contrast, we have found that it provides the exact solution. After noticing that this facilitates practical calculations, one might wonder why and when this equivalence holds true. By mapping the initial bath density operator to a P-function, we showed that a formal expansion of the time-local master equation for phase noise is in fact an ordinary cumulant expansion. Consequently, for a Gaussian initial bath state, all terms beyond the second order vanish, so that the master equation becomes exact. Thus for a bosonic heat bath, there are two conditions for the exact agreement: First, the system-bath coupling must commute with the system Hamiltonian constituting the case of pure phase noise and, second, the initial state of the bath must correspond to a Gaussian P-function.

5

Fast initial decoherence

As a first application of the analytical results obtained in Chap. 3 we discuss the exact pure dephasing of a single qubit $N = 1$. For various spectral densities of the environment the different stages are identified during which the single qubit coherence decays, and it is shown that only for an ohmic spectral density and for long times, the coherence decay settles exponential, i.e. can be described by a constant rate $1/T_2$. By contrast, the dynamics during short and intermediate times generally follows algebraic decay laws. They lead to a fast initial loss of the coherence which in a purely exponential description of the dynamics would show up as a reduced visibility of the coherent qubit oscillations. We derive analytical expressions quantifying the amount of this reduced contrast and analyze its dependence on temperature and qubit-bath coupling strength.

5.1 Single qubit dephasing

As discussed in Chap. 3 we choose at time $t = 0$ an initial condition of the Feynman-Vernon type, i.e. the bath is initially not correlated with the qubit and in thermal equilibrium at a temperature T. To ease the notation, we again use the cutoff frequency ω_c of the spectral density (3.24) of the bath to introduce the scaled time $\tau = \omega_\mathrm{c} t$ and the scaled temperature $\theta = k_\mathrm{B} T/\hbar\omega_\mathrm{c}$. In the eigenbasis $\{|0\rangle, |1\rangle\}$ of the qubit in which the Pauli-matrix σ_z is diagonal, $\sigma_z |n\rangle = (-1)^n |n\rangle$, the qubit Hamiltonian reads

$$H_\mathrm{s} = \frac{\hbar\Omega}{2}\sigma_z\,, \tag{5.1}$$

with $\hbar\Omega$ being the level splitting. In this basis, the reduced density matrix takes the form

$$\tilde{\rho}(\tau) = \begin{pmatrix} \tilde{\rho}_{0,0}(0) & \tilde{\rho}_{0,1}(0)c(\tau) \\ \tilde{\rho}_{1,0}(0)c(\tau) & \tilde{\rho}_{1,1}(0) \end{pmatrix}, \tag{5.2}$$

where have already used that for pure dephasing the populations $\tilde{\rho}_{n,n} = \langle n|\tilde{\rho}|n\rangle$ do not change in time. The non-diagonal elements $\tilde{\rho}_{n,m}$ evolve according to Eq. (3.14). Their amplitude is determined by the decoherence function

$$c(\tau) = \mathrm{e}^{-\Lambda_{0,1}(\tau)} \tag{5.3}$$

with the damping amplitude (3.22). Note that the decoherence function is independent of the Lamb-shift (3.19) since this shift results from an effective qubit-qubit interaction,

i.e. it contributes only when at least two qubits are present. The discussion of the single-qubit decoherence simplifies further since it does not involve transit times, i.e. in Eq. (3.25) we can set $\tau_{11} = 0$ so that we obtain the explicit expression

$$\begin{aligned}\Lambda_{0,1}(\tau) = 8\alpha(-\theta)^{s-1}\Big[F^{(s-1)}\big(\theta\big) - \mathrm{Re}\, F^{(s-1)}\big(\theta[1+\mathrm{i}\tau]\big)\Big] \\ + 4\alpha\Gamma(s-1)\left(\frac{\cos\big[(s-1)\arctan\big(\tau\big)\big]}{[1+\tau^2]^{\frac{s-1}{2}}} - 1\right),\end{aligned} \tag{5.4}$$

which contains the full information about the time-dependent loss of coherence of a single qubit subject to pure dephasing. Note that this exact result simply scales linearly with the qubit-bath coupling strength α.

To quantify the coherence of the qubit, one typically refers to a basis-independent measure as for example the purity $P = \mathrm{tr}\,\tilde{\rho}^2$. However, for phase noise the single-qubit matrix (5.2) depends on time only by the decoherence function $c(\tau)$ and, thus, it is sufficient to focus on this quantity in the following. To begin with, for extremely short times $\tau \ll 1$, i.e. $t \ll 1/\omega_\mathrm{c}$, we can use the expansion $F^{(s-1)}(\theta) - \mathrm{Re}\, F^{(s-1)}(\theta[1+\mathrm{i}\tau]) \approx \tau^2\theta^2\Psi_s(\theta)/2$. The expansion of the terms in round brackets of the second line in Eq. (5.4) reads $\tau^2 s(1-s)/2$, so that in total we find

$$\Lambda_{0,1}(\tau) \approx \alpha f(\theta)\tau^2\,, \tag{5.5}$$

i.e. the damping amplitude initially depends quadratically on time and vanishes for $\tau \to 0$, in agreement with the initial condition $c(0) = 1$. The prefactor reads $f(\theta) = 4(-\theta)^{s+1}\Psi_s(\theta) - 2s!$ and for low temperatures it depends only weakly on the temperature, $f(\theta) \approx \mathrm{const} + O(\theta^2)$. The quadratic time dependence in Eq. (5.5) reveals the presence of a quantum Zeno regime [208, 209], namely the inhibition of the coherence decay by repeated projective measurements: By measuring the qubit n-times during the time $\tau = n\Delta\tau$ and projecting it back to its initial state, the coherence after time τ is $c^n(\Delta\tau) \approx [1 - \Lambda_{01}(\Delta\tau)]^n \approx 1 - \alpha f(\theta)\tau^2/n$. Thus, the coherence can be kept stable by sufficiently frequent measurements $n \to \infty$. This limit corresponds to the application of an error correcting code with a correction rate $n\omega_\mathrm{c}$ large enough so that after each correction step the "no-error" syndrom is detected. A number of quantum codes utilizing this error prevention in the Zeno limit have been proposed [210–213], and their relations to other approaches for error suppression like bang-bang control or dynamical decoupling was explored [214, 215]. Recently, the performance of continuous quantum error correction was studied and it was found that the suppression of decoherence for noise sources featuring a quantum Zeno regime is enhanced as compared to Markovian models leading to a pure exponential decay of the coherence [216].

5.1.1 Ohmic spectral density

Let us first study the decoherence for an ohmic spectral density (3.24) for which the corresponding damping amplitude is obtained by taking in Eq. (5.4) the limit $s \to 1$,

$$\Lambda_{0,1}(\tau) = 8\alpha\left[\log\frac{\Gamma(\theta)}{|\Gamma(\theta[1+\mathrm{i}\tau])|} - \frac{1}{4}\log(1+\tau^2)\right]. \tag{5.6}$$

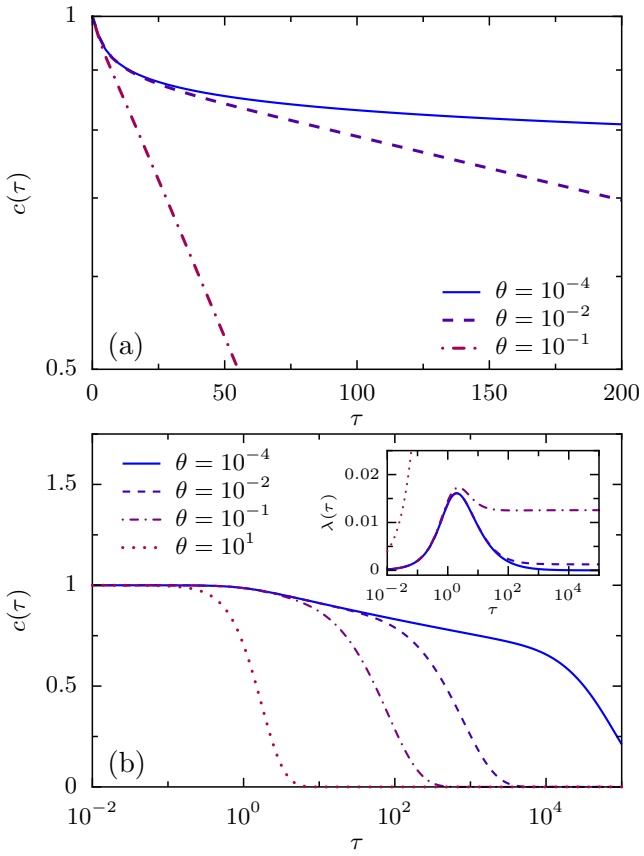

Figure 5.1: Loss of coherence of a single qubit subject to pure phase noise for an ohmic spectral density $s = 1$ and different temperatures θ, (a) on a linear timescale with coupling strength $\alpha = 0.05$ and (b) on a logarithmic timescale with coupling strength $\alpha = 0.01$. The insets shows the corresponding damping rate $\lambda(\tau) = \Lambda(\tau)/\tau$.

Figure 5.1a shows the resulting time evolution of the decoherence function $c(\tau)$ for different temperatures $\theta = k_\mathrm{B}T/\hbar\omega_\mathrm{c}$ on a logarithmic y-axis. As expected, decoherence is faster for higher temperatures. The exact coherence loss is not purely exponential: At short times and in particular for low temperatures it features a fast non-exponential decay which settles exponential only for larger times.

In Fig. 5.1b the time evolution of the decoherence function $c(\tau)$ is plotted on a logarithmic time scale which enables the identification of three stages in the single-qubit time evolution [6,164]: Very shortly after the preparation, i.e. for times $\tau \lesssim \min\{1, \theta^{-1}\}$, the fluctuations of the bosonic field are not yet effective, leading to a "quiet regime" in which essentially no single-qubit decoherence takes place. Then, for low temperatures $\theta < 1$, there is an intermediate stage, $1 \lesssim \tau \lesssim 1/\theta$, where the main origin of single-qubit decoherence is quantum vacuum fluctuations. They lead to a fast loss of the coherence. Finally for times larger than the thermal coherence time, $\tau \gtrsim 1/\theta$, thermal fluctuations dominate the coherence loss, leading to the above mentioned exponential decay. To analyse this behaviour more quantitatively, we consider the damping *rate* $\lambda(\tau)$ defined by $c(\tau) = \exp[-\tau\lambda(\tau)]$,

$$\lambda(\tau) = \frac{\Lambda_{0,1}(\tau)}{\tau}\,. \tag{5.7}$$

Expanding Eq. (5.6) for times $\tau \gtrsim \max\{1, \theta^{-1}\}$, we find at long times

$$\lambda(\tau) = 4\pi\alpha\theta - \frac{8\alpha\theta}{\tau}\log\tau + \lambda_1(\alpha,\theta)\frac{1}{\tau} + O\left(\tau^{-3}\right)\,, \tag{5.8}$$

with the prefactor

$$\lambda_1(\alpha,\theta) = 4\alpha\log\frac{\Gamma^2(\theta)}{2\pi\theta^{2\theta-1}}\,. \tag{5.9}$$

The rate $\lambda(\tau)$ is plotted in the inset of Fig. 5.1b on a logarithmic time axis. During an initial time interval it starts to increase rapidely but for larger times $\tau \gtrsim 1/\theta$ saturates to a constant value which is given by the first term of the expansion (5.8), i.e. by $\lambda(\infty) = 4\pi\alpha\theta$. We found in the previous chapter that for pure dephasing, a Markovian description of the reduced dynamics yields the exact time evolution for long times. The decay rate $1/T_2$ obtained from the Bloch-Redfield approach (4.11) reads

$$\frac{1}{T_2} = \lim_{\omega\to 0} J(\omega)\coth\left(\frac{\omega}{2\theta}\right) \tag{5.10}$$

so that $1/T_2 = 4\pi\alpha\theta$ for an ohmic spectral density, which indeed coincides with the exact rate in the limit $\tau \to \infty$. Thus, for long times the quantum coherence decays exponentially and the exponent $-\lambda(\tau)\tau$ diverges, leading to a complete dephasing $c(\infty) = 0$. In Fig. 5.2 the exact decoherence at a fixed temperature $\theta = 10^{-3}$ is opposed to a pure exponential coherence decay with rate $1/T_2$. We find that the exact coherence loss is for all times larger than what the exponential decay predicts. In fact, for $\theta \lesssim$ the difference arises by the intermediate decoherence stage when mainly vacuum fluctuations affect the qubit. The coherence loss during this regime is determined by the prefactor (5.9) of the third term in the expansion (5.8) and reads

$$v_1(\alpha,\theta) = \mathrm{e}^{-\lambda_1(\alpha,\theta)} = \left(\frac{2\pi\theta^{2\theta-1}}{\Gamma^2(\theta)}\right)^{4\alpha}\,. \tag{5.11}$$

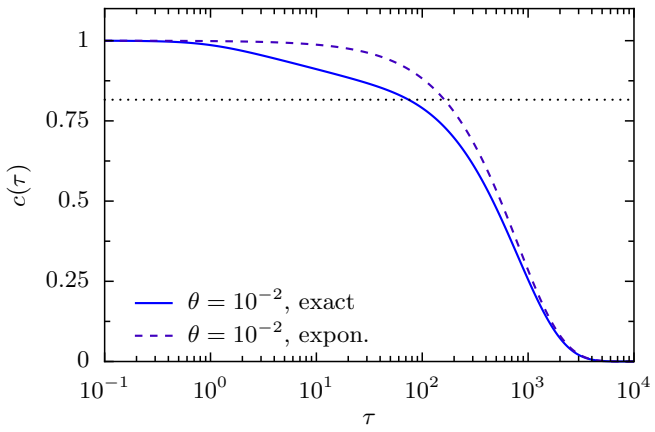

Figure 5.2: Dephasing of a single qubit coupled to an ohmic environment with temperature $\theta = 10^{-3}$ and $\alpha = 0.01$. The exact dynamics (solid line) is compared with a purely exponential decay (dotted line) with rate $1/T_2 = 4\pi\alpha\theta$. The dotted horizontal line indicates corresponding reduced visibility (5.11), see text.

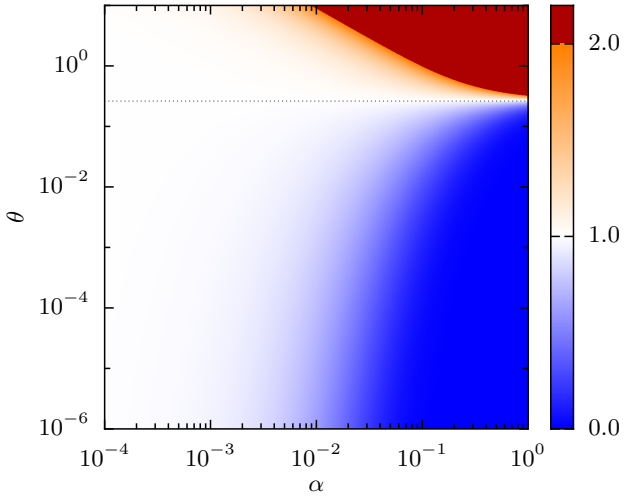

Figure 5.3: Values of the correction factor $v_1(\alpha, \theta)$ given in Eq. (5.11), color-coded according to the sidebar. The dotted horizontal line indicates the critical temperature θ_*.

Note that the second term in Eq. (5.8) is already two orders of magnitude less than the first for times $\tau \gtrsim 10^3$ and thus, for not too large temperatures, can safely be neglected in the long-time limit.

The factor (5.11) describes how much a purely exponential decay law deviates from the exact coherence at long times. In other words, when extrapolated back to the initial time $\tau = 0$, the exponential amplitude decay of coherent qubit oscillations exhibits a reduced visibility of which Eq. (5.11) is a quantifier. For the parameters in Fig. 5.2 it assumes a value of 0.816 and is indicated by the horizonal dotted line. Note that for an ohmic environment the amount of the reduced visibility depends on the duration of the vacuum-fluctuation dominated regime which, in turn, is longer for lower temperatures. This fact is nicely reflected by the temperature-dependence in Eq. (5.11).

Fig. 5.3 shows the value of the visibility (5.11) for a wide range of temperatures θ and coupling strengths α. Interestingly, there is one particular temperature θ_* for which the correction factor equals unity, irrespective of the coupling strength α. Using Eq. (5.11), we find $\theta_* \approx 0.262$, i.e. $T_*/\omega_c \approx 1.99 \times 10^{-12}\mathrm{K\,s}$. Thus, at this moderate temperature T_* a Markovian master equation performs best, but dephasing rates $\propto T_*$ are already high. Note that for larger temperatures the factor (5.11) assumes rather large values; in this temperature regime, the second term in Eq. (5.8) becomes more important and

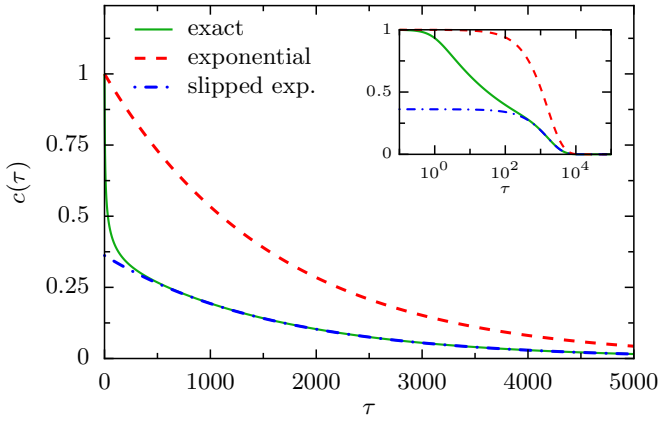

Figure 5.4: Comparison of the exact decoherence $c_1(\tau)$ for an ohmic bath (solid lines), the exponential coherence decay $\exp(-\tau/T_2)$ (dashed lines) and the latter with the correction factor v_1 taken into account (dashed dotted lines). The coupling strength $\alpha = 0.05$ and the temperature $\theta = 10^{-3}$ leading to a slip factor $v_1 \approx 0.36$.

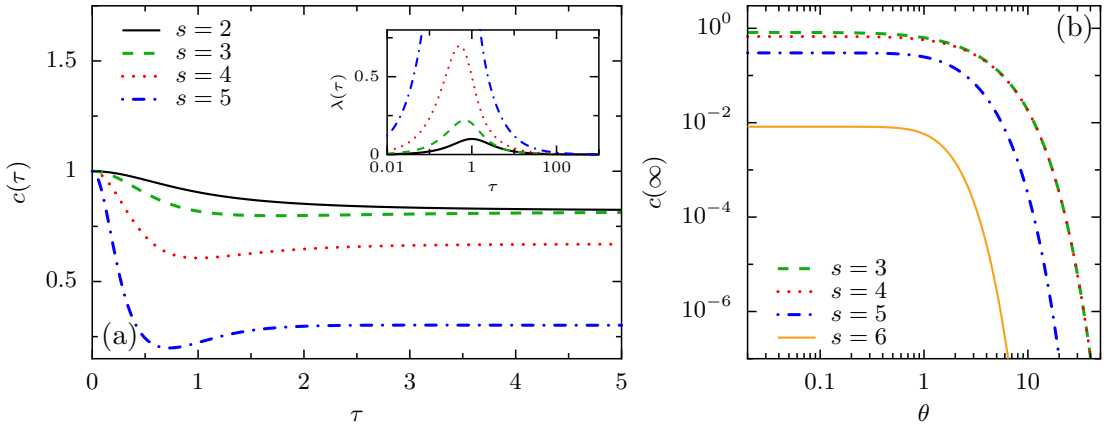

Figure 5.5: Pure dephasing of a single qubit for super-ohmic environments with qubit-bath coupling strength $\alpha = 0.01$. Tablet (a) shows the time evolution of the decoherence function $c(\tau)$ for spectral densities with $s = 2, 3, 4$, and 5 at a fixed temperature $\theta = 0.01$; the inset depicts the dynamics of the corresponding daming rates on a logarithmic time scale. In tablet (b), the dependence of the final stable coherence $c(\infty)$ on the temperature is shown for different spectral densities $s = 3, 4, 5$, and 6. Note that the case $s = 2$ is not shown since the final coherence vanishes.

has to be taken into account.

For most experiments in quantum information processing the system is cooled to low temperatures to obtain lower dephasing rates. If the short-time dynamics is not resolved and thus one gets stuck with a characterization of the decoherence by a time T_2, it is inevitable that visibilities $v_1(\alpha, \theta) < 1$ must be taken into account. A typical example is shown in Fig. 5.4 for a low temperature $\theta = 10^{-3}$, and a small coupling strength $\alpha = 0.05$. The corresponding visibility (5.11) takes the value $v_1 \approx 0.36$. Assuming a qubit frequency of $\Omega = 10^{-2}\omega_c$, Fig. 5.4 shows that the coherence abruptly decays to a value 0.36 already during the first three coherent oscillations of the qubit. Only then the typical exponential decay, i.e. the $1/T_2$-process sets in.

5.1.2 Super-ohmic spectral densities

Let us now discuss pure dephasing caused by baths with super-ohmic spectral densities proportional to $\omega^s e^{-\omega/\omega_c}$. Figure 5.5a shows the exact time evolution of the decoherence

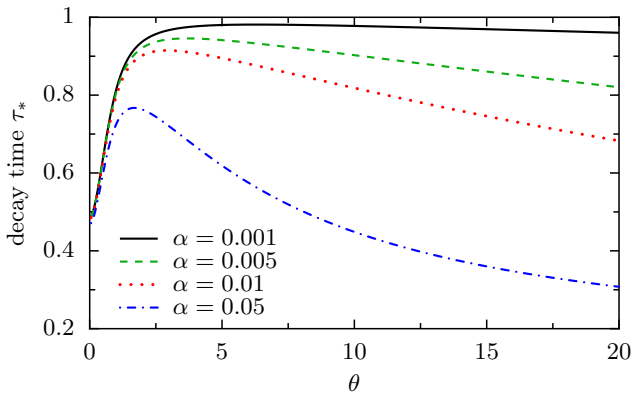

Figure 5.6: Initial decay time τ_* of the single-qubit coherence for a super-ohmic spectral density $\propto \omega^3$. The data shows the dependence on temperature for different coupling strengths α.

function $c(\tau) = \exp[-\Lambda_{0,1}(\tau)]$ for different $s = 2, 3, \ldots$ at a temperature $\theta = 10^{-2}$. The damping $\Lambda_{0,1}(\tau)$ is given in Eq. (5.4). During a short time scale $\tau \approx 1$, the coherence drops suddenly to a value which is less for larger s. For $s = 2$, the coherence keeps on decaying but as shown below, the decay never becomes exponential. For $s \geq 3$, the coherence decay simply stops at long times, i.e. the decoherence is incomplete.

From the exact damping amplitude (5.4) we find the rate (5.7) for long times $\tau \gg 1$:

$$\lambda(\tau) = 0 + \delta_{s,2}\frac{8\alpha\theta}{\tau}\log(\tau) + \lambda_s(\alpha,\theta)\frac{1}{\tau} + O(\tau^{-2}) \tag{5.12}$$

$$\text{with } \lambda_s(\alpha,\theta) = 8\alpha\left[(-\theta)^{s-1}\left[\Psi_{s-2}(\theta) - \delta_{s,2}\log(\theta)\right] - \frac{(s-2)!}{2}\right]. \tag{5.13}$$

In fact, the vanishing of the first (constant) term in the expansion leads to the important conclusion that super-ohmic baths do not give rise to exponentially decaying coherences. In other words, the T_2 time scale for pure dephasing diverges. The appearance of the Kronecker-delta in Eq. (5.12) indicates that $s = 2$ is a particular case: The second term of Eq. (5.12) for long times leads to an algebraic decay $c(\tau) \propto \tau^{-8\alpha\theta}$. So although for $s = 2$ we found $T_2 = \infty$, the dephasing will finally be complete, i.e. $c(\infty) = 0$.

For $s = 3, 4, \ldots$ the situation is different. The damping rate (5.12) vanishes as τ^{-1}, and hence the coherence saturates. The coherence loss v_s equals the final stable value $c(\infty)$ and is determined by the prefactor (5.12) in the expansion (5.13), i.e.

$$c(\infty) = v_s(\alpha,\theta) = \mathrm{e}^{-\lambda_s(\alpha,\theta)}\,. \tag{5.14}$$

Figure 5.5b shows the dependence of the stable coherence on the temperature for different spectral densities. For low temperatures $\theta \lesssim 1$ it depends only weakly on temperature and after an expansion we find its value

$$v_s(\alpha,\theta) \approx \exp\left\{8\alpha\left(\frac{(s-2)!}{2} + (-1)^s\left[\frac{\Psi_0(2-s)}{\Gamma(2-s)} - \frac{\theta\gamma_\mathrm{E}}{\Gamma(3-s)} + \frac{\pi^2\theta^2}{6\Gamma(4-s)}\right]\right)\right\}, \tag{5.15}$$

where $\gamma_\mathrm{E} \approx 0.5772$ is the Euler–Mascheroni constant. Note that the effective cutoff frequency of the bosonic modes is typically determined by the characteristic size a of the quantum dot so that the low temperature regime is given by $T \lesssim \hbar c/ak_\mathrm{B}$.

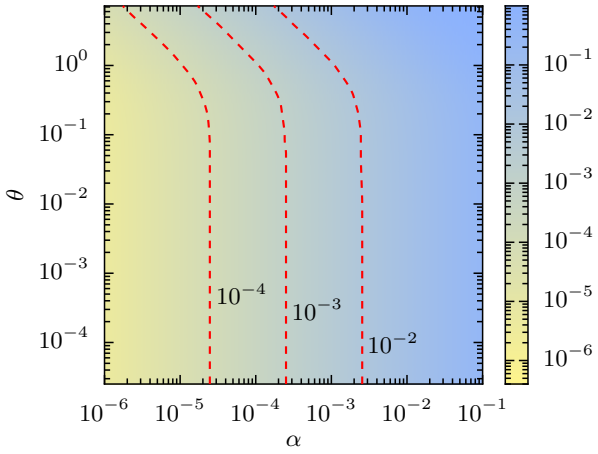

Figure 5.7: Deviation $p = 1 - v_3(\alpha, \theta)$ from the perfect visibility of single-qubit coherence for a super-ohmic spectral density $s = 3$, color-coded according to the sidebar. The red dashed lines mark the boundaries for which $p = 10^{-4}, 10^{-3}$, and 10^{-2}, respectively.

The fact that the third term of the expansion (5.12) determines the final coherence just means that in the independent-boson model the state of the qubit dephases only during a short time. Figure 5.5b reveals that the coherence for super-ohmic baths with $s = 3, 4, \ldots$ drops to its final value during a time of the order of the inverse of the cutoff frequency. As a measure of this time scale, we define the critical time τ_* at which the coherence has dropped to half of its initial value.

For $s = 3$ and different coupling strengths α, the temperature dependence of the critical time is depicted in Fig. 5.6. It exhibits a weak but non-monotonous dependence on temperature: For low temperatures the decay time increases for increasing temperature, in agreement with the findings of Ref. [217] where the polarization of the optical response in self-assembled GaAs quantum dots was studied theoretically. For the same system, the non-monotonous behaviour of the coherence decay was also measured experimentally [218]. The confinenment of the charge carriers in the quantum dots used in this experiment was $a \approx 3$nm for the growth direction axis, and approx. 13nm for the lateral directions. With a sound velocity of $c = 3.3 \times 10^3$m/s for accoustic longitudinal phonons, we identify the inverse of the confinement a with our cutoff frequency, $\omega_c = c/a$. The measured maximum of the decay time τ^* is at a temperature $T \approx 18$K which relates to $\theta = ak_BT/\hbar c \approx 2$. This is in good agreement with the curve in Fig. 5.6 for a coupling $\alpha = 0.05$. The corresponding decay time $t_* = \tau_*/\omega_c \approx 1$ps fits well with measured data of Ref. [218].

An environment with a spectral density $J(\omega) \propto \omega^3$ is an important case of our general formulas. Using expression (5.14) with $s = 3$, we identify in Fig. 5.7 the temperatures θ and coupling strengths α that support different upper bounds for the deviation $p = 1 - v_3(\alpha, \theta)$ from the perfect visibility. From Eq. (5.14) we find that at low temperatures and for a given tolerable error p, the condition $p < 1 - \exp[-4\alpha(1 + \pi^2\theta^2/3)]$ must be fulfilled. If in addition the qubit-environment coupling is weak, we are surely in the limit $\alpha\theta^2 \ll 1$. Then the visibility is limited solely by the intrinsic coupling strength and the above condition reduces to $\alpha < -\log(1-p)/4$. For example, if we can tolerate an upper bound $p = 10^{-4}$ of the error, we have to demand small coupling strengths $\alpha < 2.5 \times 10^{-5}$.

6

Pure dephasing of spatially separated qubits

We now focus on the influences of phase noise on a spatially extended N-qubit register. The analytical expressions obtained in Chap. 3 allow us to study the consequences of finite spatial qubit separations in an exact manner, for all temperatures and qubit-bath coupling strengths. By varying the qubit-qubit distance from zero to infinity, the results will interpolate between the two limiting cases of collective and independent noise.

We first focus on the entanglement of two qubits ($N = 2$) prepared in particular Bell states which for vanishing qubit separation are known as robust and fragile entangled states. We discuss how the entanglement changes upon increasing their separation and find for a wide range of physical parameters, that the dynamics shows highly non-Markovian features [159]. We also study the robustness of the two-qubit decoherence-free subspace with respect to physical parameters such as temperature and qubit-bath coupling strength. Moreover, we clarify the relation between two-qubit entanglement and the dynamics of single-qubit coherence which we already discussed in some detail in the previous chapter. As a generalization of the robust entangled Bell state we then investigate the time evolution of N qubits in a linear arrangement prepared in the so-called W state. Explicit expressions for the coherence loss are presented and the scaling of decoherence as a function of the number of qubits and their spatial separations is studied [160].

In the following, we consider a system Hamiltonian of the form

$$H_{\mathrm{s}} = \frac{\hbar}{2} \sum_{\nu=1}^{N} \Omega_{\nu} \sigma_{\nu z} \,, \tag{6.1}$$

and the interaction (3.2) with the qubit coupling operators $X_{\nu z} = \sigma_{\nu z}$. Here, $\sigma_{\nu z}$ is a Pauli matrix for qubit ν and $\hbar\Omega_{\nu}$ is its level splitting. Since we will not address the coherent control of individual qubits explicitly, the specific choice for the energy splittings is not of major relevance. Note that there is no direct interaction between the qubits. However, a direct qubit-qubit interaction of Ising-type $\sum_{\nu\nu'} J_{\nu\nu'} \sigma_{\nu z} \sigma_{\nu' z}$ or, more generally, any qubit Hamiltonian that commutes with Eq. (6.1) can be added leaving the results of this chapter unchanged. We will consider the elements $\tilde{\rho}_{\mathbf{m},\mathbf{n}} = \langle \mathbf{m}|\tilde{\rho}|\mathbf{n}\rangle$ of the qubits' density matrix in the computational basis

$$|\mathbf{n}\rangle = |n_1, n_2, \ldots, n_N\rangle, \quad \text{where } \sigma_{\nu z} |\mathbf{n}\rangle = (-1)^{n_{\nu}} |\mathbf{n}\rangle \,, \tag{6.2}$$

with $n_\nu = 0, 1$, i.e. we set $\chi_{\nu,m_\nu} = (-1)^{m_\nu}$ in the damping (3.22) and the phase (3.19) of the exact solution (3.14).

6.1 Robust and fragile entangled qubit pairs

Yu and Eberly [153] studied the entanglement dynamics for two qubits coupled to the same heat bath at *identical* positions, in particular for a preparation of the maximally entangled Bell states

$$|\psi_{\text{robust}}\rangle = |\psi_-\rangle = \frac{|01\rangle + |10\rangle}{\sqrt{2}}\,, \qquad |\psi_{\text{fragile}}\rangle = |\psi_+\rangle = \frac{|00\rangle + |11\rangle}{\sqrt{2}}\,, \tag{6.3}$$

where $|\mathbf{n}\rangle = |n_1, n_2, \ldots, n_N\rangle$ denotes the N qubit state with $n_\nu = 0, 1$ [cf. Eq. (6.2)]. The notation $|\psi_\pm\rangle$ has been introduced for writing equations more efficiently. In Ref. [153] it was found, that the "robust state" lives in a decoherence-free subspace and consequently its entanglement is preserved. Indeed, when both qubits couple via a collective coordinate $X = \sigma_{1z} + \sigma_{2z}$ to the same bath coordinate, the states $|01\rangle$ and $|01\rangle$ are eigenstates of X to the *same* eigenvalue. Hence, they fullfill the condition for a decoherence-free subspace. By contrast, the states $|00\rangle$ and $|11\rangle$ are eigenstates to different eigenvalues and thus superpositions of them like the "fragile state" aquire relative phase shifts and decohere. In the following we will consider the robust and fragile initial states (6.3) and employ the model dicussed in Chap. 3 which takes a finite qubit separation into account, i.e. the two qubits couple at positions $\mathbf{x}_1$ and $\mathbf{x}_2$ to the bath, respectively. We have already found the exact solution (3.14) for the reduced density matrix $\tilde{\rho}(t)$ of the qubits. Here, the tilde again denotes the interaction picture representation.

Two-qubit entanglement can be measured by the concurrence C defined by Wooters [219]:

$$C[\tilde{\rho}] = \max\{0, \sqrt{\lambda_1} - \sqrt{\lambda_2} - \sqrt{\lambda_3} - \sqrt{\lambda_4}\}\,. \tag{6.4}$$

Here, λ_i denotes the eigenvalues of the matrix $\tilde{\rho}\sigma_{1y}\sigma_{2y}\tilde{\rho}^*\sigma_{1y}\sigma_{2y}$ in decreasing order, and $\tilde{\rho}^*$ is the complex conjugate of the reduced density matrix $\tilde{\rho}$. For maximally entangled states, one finds $C = 1$, while C vanishes for incoherent mixtures of product states. It was noticed [153] that for phase noise and two qubits with vanishing separation initially in either of the states (6.3), the concurrence is given by the absolute values of particular density matrix elements $\tilde{\rho}_{\mathbf{m},\mathbf{n}} = \langle\mathbf{m}|\tilde{\rho}|\mathbf{n}\rangle$, namely $C_- = 2|\tilde{\rho}_{01,10}|$ and $C_+ = 2|\tilde{\rho}_{00,11}|$, respectively. These relations hold for spatially separated qubits as well [159]. Since all quantities considered in the following are given by absolute values of single density matrix elements, the phases $\phi_{\mathbf{m},\mathbf{n}}$ in the exact solution (3.14) do not contribute, i.e. $|\tilde{\rho}_{\mathbf{m},\mathbf{n}}(t)| = \exp[-\Lambda_{\mathbf{m},\mathbf{n}}(t)]$, with the time-dependent damping $\Lambda_{\mathbf{m},\mathbf{n}}(t)$ given in Eq. (3.15). The respective concurrences $C_\pm(t)$ for the robust and fragile entangled states thus read

$$C_\pm(t) = \mathrm{e}^{-\Lambda_\pm(t)}\,, \tag{6.5}$$

with $\Lambda_+ = \Lambda_{00,11}$ and $\Lambda_- = \Lambda_{01,10}$. For accoustic bosons, we find from Eq. (3.22) the damping

$$\Lambda_\pm^{(d)}(t) = 8\int_0^\infty \mathrm{d}\omega\, J(\omega)\left[1 \pm G^{(d)}(\omega t_{12})\right]\frac{1-\cos(\omega t)}{\omega^2}\coth\left(\frac{\hbar\omega}{2k_\mathrm{B}T}\right)\,, \tag{6.6}$$

where the index d denotes the dimension of the environment and $t_{12} = |\mathbf{x}_1 - \mathbf{x}_2|/c$ is the transit time of a field distortion from one qubit to the other. In the following we will consider the qubits embedded in both an one-dimensional environment ($d = 1$) and a three-dimensional environment ($d = 3$). Quasi one-dimensional geometries may, for example, be realized by carbon nanotubes or linear ion traps. They represent configurations in which the requirements of qubit protection and adressability are well-balanced, and where we expect the effects of spatial noise correlations to be most overt. In this case, the spectral density $J(\omega)$ is typically of the ohmic type [97]. For the three-dimensional environment, we consider a super-ohmic spectral density proportional to ω^3 for low frequencies. Thus, we identify $s = d$ in the spectral density (3.24) and write

$$J(\omega) = J^{(d)}(\omega) = \alpha\,\omega \left(\frac{\omega}{\omega_\mathrm{c}}\right)^{d-1} \mathrm{e}^{-\omega/\omega_\mathrm{c}}\,, \tag{6.7}$$

Below, we will compare the concurrence of a qubit pair with the single-qubit coherence $|\rho_{0,1}(t)/\rho_{0,1}(0)| = \exp\{-\Lambda_{0,1}^{(d)}(t)\}$, which we define for $N=1$, i.e. when only one qubit is present. The corresponding damping rate $\Lambda_{0,1}^{(d)}$ was discussed in detail in the preceeding section [cf. Eq. (5.4) with $s \to d$] and is formally given by the rhs of Eq. (6.6) but with the replacement $1 \pm G^{(d)} \to \frac{1}{2}$. Thus it is the geometrical factor $G^{(d)}$ given in Eq. (3.21) which determines the difference between single-qubit decoherence and entanglement decay of a qubit pair. In particular, the dimension dependence of $G^{(d)}$ will turn out to be crucial but has been ignored in prior studies [154]. Since the geometrical factor $G^{(3)}(x)$ vanishes for large arguments, we find for qubits coupled to a three-dimensional bath in the remote limit $t_{12} \to \infty$ for both concurrences the relation $C_\pm^{(3)}(t) = \exp[-2\Lambda_{0,1}^{(3)}(t)]$. This was also obtained for a model consisting of independent baths [157].

An intriguing corollary to Eq. (6.5) is the exact relation

$$C_+^{(d)}(t)\, C_-^{(d)}(t) = \exp[-4\Lambda_{0,1}^{(d)}(t)]\,, \tag{6.8}$$

which for arbitrary separation links the concurrences to the single-qubit coherence. It implies that if one of the concurrences vanishes, the single-qubit coherence must vanish as well. A finite single-qubit coherence, in turn, requires non-vanishing concurrences. In Sect. (5.1) we found that for a super-ohmic environment with a spectral density $J^{(3)}$, the single-qubit coherence indeed saturates for long times to a finite value. We thus expect that the decay of two-qubit concurrences in a three-dimensional environment for both the robust and the fragile states is incomplete. In fact, below we show that for physically relevant qubit separations, a distinction of robust and fragile states is meaningful only for one-dimensional geometries.

In order to evaluate the concurrences (6.5), we again introduce the scaled time $\tau = \omega_\mathrm{c} t$ and transit time $\tau_{12} = \omega_\mathrm{c} x_{12}/c$, and the scaled temperature $\theta = k_\mathrm{B} T/\hbar\omega_\mathrm{c}$. We then find from Eq. (3.25) for the one-dimensional environment the concurrence

$$C_\pm^{(1)}(\tau) = \mathrm{e}^{-2\Lambda_{0,1}^{(1)}(\tau)} \left| \frac{\Gamma(\theta[1 - \mathrm{i}(\tau_{12} - \tau)])\Gamma(\theta[1 - \mathrm{i}(\tau_{12} + \tau)])}{\Gamma^2(\theta[1 - \mathrm{i}\tau_{12}])} \right|^{\pm 8\alpha} \left| 1 + \frac{\tau^2}{(1 - \mathrm{i}\tau_{12})^2} \right|^{\pm 4\alpha} \tag{6.9}$$

with the single-qubit coherence

$$\mathrm{e}^{-\Lambda_{0,1}^{(1)}(\tau)} = \left| \frac{\Gamma(\theta[1 + \mathrm{i}\tau])\Gamma(\theta[1 - \mathrm{i}\tau])}{\Gamma^2(\theta)} \right|^{4\alpha} \left(1 + \tau^2\right)^{2\alpha}\,, \tag{6.10}$$

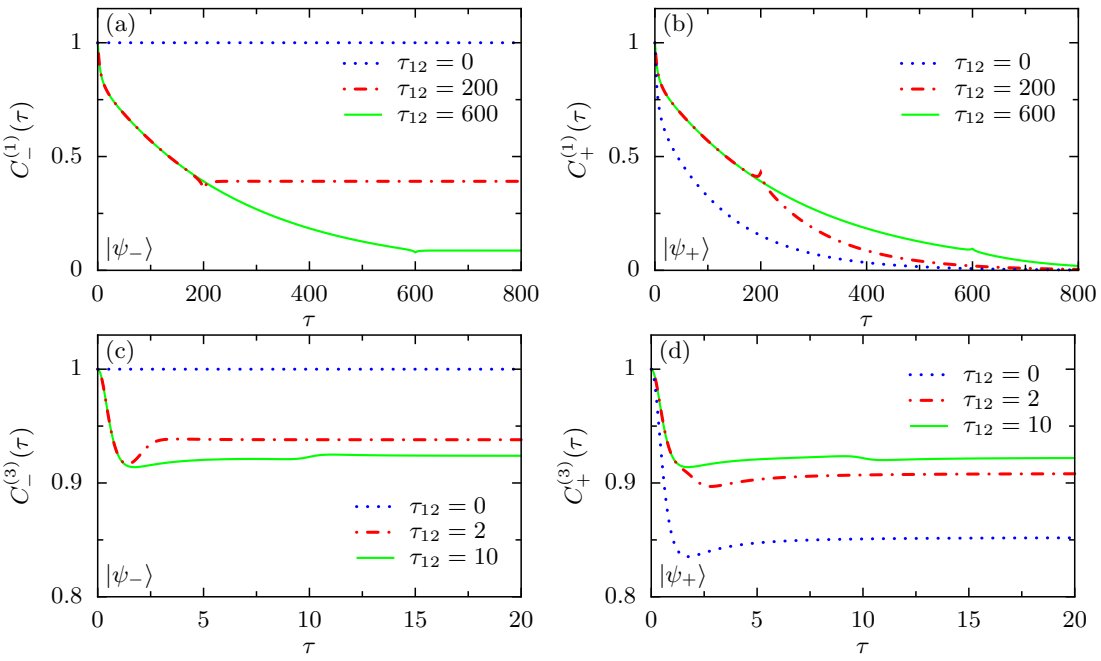

Figure 6.1: Time evolution of the concurrence for the robust (left) and the fragile (right) Bell state for various spatial separations $c\tau_{12}/\omega_c$. The qubits couple with a strength $\alpha = 0.01$ to a one-dimensional (a,b) and a three-dimensional bath (c,d) at temperature $\theta = k_B T/\hbar\omega_c = 0.015$. For qubit frequencies $\Omega = 0.1\omega_c$, the time range in the upper (lower) plots corresponds to 13 (0.3) coherent oscillations.

where Γ is the Euler Gamma function. The corresponding expressions for a three-dimensional environment read

$$C_\pm^{(3)}(\tau) = \mathrm{e}^{-2\Lambda_{0,1}^{(3)}(\tau)} \exp\left\{ \pm 8\alpha \left(\frac{\theta}{\tau_{12}} \mathrm{Im}\big[2\Psi_0(\theta[1-\mathrm{i}\tau_{12}]) - \Psi_0(\theta[1-\mathrm{i}(\tau-\tau_{12})]) \right.\right.$$
$$\left.\left. - \Psi_0(\theta[1-\mathrm{i}(\tau+\tau_{12})]) \big] + \frac{\tau^2(\tau^2-\tau_{12}^2+3)}{(1+\tau_{12}^2)(\tau^4 - 2\tau^2\left[\tau_{12}^2-1\right] + \left[1+\tau_{12}^2\right]^2)} \right) \right\}, \tag{6.11}$$

$$\mathrm{e}^{-\Lambda_{0,1}^{(3)}(\tau)} = \exp\left\{ -4\alpha \left(2\theta^2\, \mathrm{Re}\big[\Psi_1(\theta) - \Psi_1(\theta[1-\mathrm{i}\tau]) \big] - \frac{\tau^2(\tau^2+3)}{(1+\tau^2)^2} \right) \right\}, \tag{6.12}$$

where Ψ_0 and Ψ_1 are Di-Gamma and Tri-Gamma functions, respectively. The importance of Eqs. (6.9) and (6.11) lies in the fact that they explicitly yield the concurrences at all times for arbitrary spatial separations τ_{12}, from a perfect decoherence-free subspace ($\tau_{12} = 0$) to uncorrelated noise ($\tau_{12} \to \infty$). In both expressions, the respective single-qubit coherences (6.10) and (6.12) appear.

6.1.1 Robust Bell state

Let us first focus on the entanglement of a qubit pair that starts out in the robust state $|\psi_-\rangle$ and couples to a one-dimensional heat bath. Figure 6.1a depicts the time-evolution of the concurrence for a temperature $k_B T$ well below the cutoff energy scale $\hbar\omega_c$. For

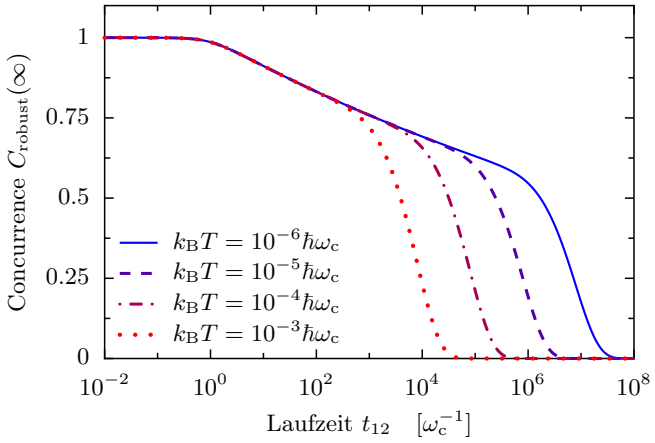

Figure 6.2: Final value (6.13) of the concurrence for the robust state $|\psi_-\rangle$ coupled to the one-dimensional environment, as a function of the spatial separation $x_{12} = c\tau_{12}/\omega_{\mathrm{c}}$ for various temperatures. The coupling strength is $\alpha = 0.005$.

vanishing separation, $\tau_{12} = 0$, the concurrence $C_-^{(1)}(\tau)$ remains at its initial value 1. This reflects the fact that then $|\psi_-\rangle$ lives in a decoherence-free subspace and, consequently, is robust. For $\tau_{12} > 0$, we find that the concurrence initially decays until the transit time τ_{12} is reached. At time $\tau = \tau_{12}$, the decay comes to a standstill and the concurrence remains at the finite value

$$C_-^{(1)}(\tau \to \infty) = (1+\tau_{12}^2)^{4\alpha} \left| \frac{\Gamma(\theta[1-\mathrm{i}\tau_{12}])}{\Gamma(\theta)} \right|^{16\alpha}, \tag{6.13}$$

which becomes $(1+\tau_{12}^2)^{-4\alpha}$ for $\theta \to 0$. Figure 6.2 shows this final concurrence as a function of the transit time τ_{12} for various temperatures $\theta = k_{\mathrm{B}}T/\hbar\omega_{\mathrm{c}}$. As for the dynamics of the single-qubit coherence (see Fig. 5.1), three regimes can be identified: For very small separations $x_{12} < c/\omega_{\mathrm{c}}$, the concurrence remains at $C = 1$, while for $c/\omega_{\mathrm{c}} < x_{12} < \hbar c/k_{\mathrm{B}}T$, the entanglement is no longer perfect, but still at an appreciably large value. For large separations, $x_{12} > \hbar c/k_{\mathrm{B}}T$, the concurrence essentially decays to zero. The latter limit is a prerequisite for the application of quantum error-correction schemes that assume that the qubits experience uncorrelated noise.

The time evolution in Fig. 6.1a allows the interpretation that before the transit time is reached, uncorrelated noise affects the qubits and entails an entanglement decay. After the transit time, the noise at the two positions is sufficiently correlated to establish a decoherence-free subspace. In the remote limit $\tau_{12} \to \infty$, the concurrence of the robust state finally vanishes and, thus, the residual entanglement for finite τ_{12} can be attributed to spatial bath correlations. We emphasize that for a one-dimensional bath, this scenario holds true for all temperatures.

An intuitive physical picture for the observed entanglement dynamics is that at long times, decoherence is governed by the low-frequency modes of the bath. Owing to their large wavelengths, these modes act effectively as a collective bath coordinate which leaves the entanglement robust. In higher dimensions, the role of the low-frequency modes is suppressed and, thus, the long-time behaviour may be significantly different [6].

Figure 6.1c reveals that for a three-dimensional bath, in general the concurrence (6.11) decays and saturates at a finite value which stays larger for closer qubits. In the experimentally relevant limit of low temperatures and $\tau_{12}\theta^2 \lesssim 1$, the final concurrence

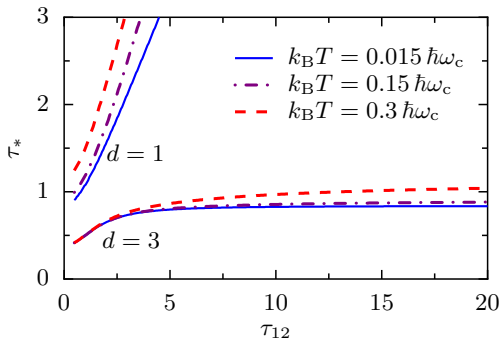

Figure 6.3: Duration τ_* of the concurrence decay of the robust Bell state $|\psi_-\rangle$ as a function of the transit time τ_{12} for one- and three-dimensional baths. The dissipation strength is $\alpha = 0.01$.

emerges as

$$C_-^{(3)}(\tau \to \infty) = \exp\left\{-8\alpha\left(1 - \frac{1}{1+\tau_{12}^2} + \frac{\pi^4\tau_{12}^2\theta^4}{45}\right)\right\}. \tag{6.14}$$

However, the saturation generally occurs already at a time $\tau \ll \tau_{12}$, i.e. long before a field distortion can have propagated from one qubit to the other. Cooperative effects are though still visible by a small stepwise increase of the concurrence at the transit time, see the solid line in Fig. 6.1c at time $\tau \approx \tau_{12}$. In Ref. [154] a pronounced peak instead of a monotonous step was found for the same model. However, the dimension dependence of the geometrical factor was ignored in this work and the one-dimensional expression (3.21a) was used instead of the correct three-dimensional form (3.21c).

We numerically estimate the duration τ_* of the concurrence decay by the time at which 90% of the decay has happened. Figure 6.3 shows that $\tau_* \approx 1$. In particular, τ_* is independent of the spatial separation τ_{12}, unless the qubits are very close. Hence the saturation of $C_-^{(3)}(\tau)$ cannot be explained as a delayed build-up of a decoherence-free subspace. Instead, a single-qubit mechanism is at work, since at times $\tau < \tau_{12}$, the qubits experience effectively *uncorrelated* noise. This conjecture is supported by the resemblance of $C_-^{(3)}(\tau)$ to the single-qubit coherence $\exp[-\Lambda_{0,1}^{(3)}(\tau)]$ shown in Fig. 5.5. A second difference to the one-dimensional case concerns the remote limit of the qubits: For $\tau_{12} \to \infty$, the stationary value is still finite. In this limit, $G^{(3)}$ in Eq. (6.6) is negligible and the concurrence is given by the square of the finite single-qubit coherence.

The concurrence (6.14) depends only quadratically on τ_{12} and, thus, is rather robust against variations of the separation, provided the separation is small. Such robustness was predicted [220] and confirmed experimentally [221] for symmetry-breaking perturbations. Interestingly, Eq. (6.14) shows that the concurrence is robust against temperature variations as well, about which the theory in Ref. [220] makes no predictions.

6.1.2 Fragile Bell state

If the qubits are initially in the fragile state $|\psi_+\rangle$, a one-dimensional bath causes an entanglement decay that becomes faster once the transit time is reached; see Fig. 6.1b. As for the robust state $|\psi_-\rangle$, cooperative effects only set in after a time τ_{12}. Whether the qubits are spatially separated or not, for a one-dimensional environment their concurrence $C_+^{(1)}(\tau)$ ultimately decays to zero. By contrast, for the three-dimensional case, the concurrence (6.11) for the fragile state shown in Fig. 6.1d decays, but the final

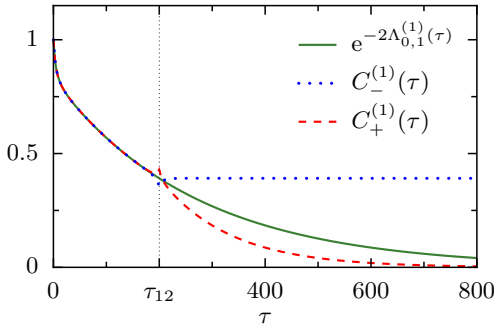

Figure 6.4: Comparison of the *squared* single-qubit decoherence (solid line) and the decay of concurrence for the robust (dotted lines) and fragile (dahsed line) state for the one-dimensional environment. The vertical dotted line indicates the transit-time $\tau_{12} = 200$ and the other parameters are choosen as in Fig. 6.1.

value $C^{(3)}_{+}(\tau \to \infty)$ is nonzero, in contrast to earlier statements [153, 156]. For low temperatures such that $\theta \lesssim 1, \tau_{12}^{-1/2}$, the long-time limit is given by

$$C^{(3)}_{+}(\tau \to \infty) = \exp\left\{-8\alpha\left(1 + \frac{1}{1+\tau_{12}^2} + \frac{2\pi^2\theta^2}{3}\right)\right\}. \tag{6.15}$$

This asymptotic value can be increased by reducing the temperature and by increasing the qubit separation. For a separation $\tau_{12} \gtrsim 1$, $C^{(3)}_{+}(\infty) = C^{(3)}_{-}(\infty)$, i.e. the concurrence of both the "robust" and the "fragile" state become identical [cf. the solid lines in figs. 6.1c,d]. Hence, only for a one-dimensional environment where spatial correlations are overt for arbitrary qubit separations τ_{12} it is meaningful to distinguish between the robust and fragile entangled states.

6.1.3 Discussion

The explicit evaluation of the exact reduced dynamics of two qubits with a nondemolitian coupling to a bosonic heat bath made it possible to investigate the consequences of a spatial qubit separation. We focused on two Bell states whose entanglement for vanishing separation is either robust or fragile. The most significant consequence of a finite spatial separation is that the entanglement of the robust Bell state no longer remains robust: It decays initially, yet after a time $t^* = \tau_*/\omega_c$, it saturates. For a physical realization with a GaAs substrate, the sound velocity is $c \approx 3 \times 10^3\,\mathrm{ms}^{-1}$. Thus, for an order of magnitude estimate with a typical lateral confinement length a in gated quantum dots of several tens of nanometer, the effective cutoff frequencies of the phonon spectrum is $\omega_c = c/a \approx 10^{12}\,\mathrm{s}^{-1}$. This is an order of magnitude smaller than typical Debye frequencies $5 \times 10^{13}\,\mathrm{s}^{-1}$. Then a qubit separation $x_{12} = 100\,\mathrm{nm}$ corresponds to the transit time $\tau_{12} = t_{12}\omega_c = 10^2$. With a temperature $T = 10\,\mathrm{mK}$ we have $k_B T/\hbar\omega_c \approx 10^{-3}$. This implies that ω_c^{-1} is typically the smallest timescale of the problem, while the transit time is less than or, for higher temperatures or larger separations, of the same order as the thermal coherence time.

Indeed, it is interesting to find stable finite bipartite entanglement even at high temperatures in our macroscopic system-bath model, which resembles recent results for a quite different model [222]. The duration t^* of the entanglement decay depends sensitively on the dimension of the environment and its spectral density. In one dimension with an ohmic spectral density, it equals the transit time of the field from one qubit to the other. In Fig. 6.4 the entanglement dynamics of both the fragile and the robust

state is compared for a fixed transit time $t_{12}\omega_c = 200$ with the *square* of the single-qubit coherence (6.10), i.e. the first exponential in the expression for the concurrences (6.9). The curves nicely demonstrate that for times before the transit time, the entanglement decay is determined solely by single qubit decoherence. Although not obvious from the general expression of the concurrences, we conjecture that only the first exponential factor in Eq. (6.9) contributes until the transit time is reached. This again confirms the interpretation that for times less the transit time the dynamics shows up as if both qubits would couple to independent heat baths. For ohmic heat baths, the coherence of a single qubit decays and thus both the fragile and the robust state initially decohere. After the transit time, the dissipative dynamics of both qubits is no longer independent since spatial bath correlations are build up so that the picture of independent heat baths no longer holds true. For the one-dimensional environment, these correlations are perfect since the geometrical factor $G^{(1)}$ does not decay. After the transit time, a delayed decoherence-free subspace exists so that the entanglement decay of the "robust" state suddenly stops. Since the entanglement is no longer perfect, we may call it rather a "decoherence-poor" than a "decoherence-free" subspace.

In principle, the same interpretation is true for the three-dimensional environment with a super-ohmic spectral density: Spatial correlations set in at time τ_{12}, but their cooperative effects are small for transit times $\tau_{12} \gtrsim 1$ because of the τ_{12}^{-1} dependence of the geometrical factor $G^{(3)}$. Hence, the entanglement saturation is governed by a single-qubit effect and t^* is approximately given by the inverse of the cutoff frequency ω_c. Although not visible in the figures shown here, a decoherence-poor subspace caused solely by spatial correlations exists also for the three-dimensional case, but only for very short transit times $\tau_{12} < 1$, i.e. distances $x_{12} < c/\omega_c$. For substrate phonons of a semiconductor quantum dot qubit, the cutoff frequency typically is determined by the dot size. Hence, such short qubit separations are unphysical since they are smaller than the size of a single dot. However, the cutoff of the phonon spectrum is ultimatly limited by the Debye temperature of the substrate, so that one might find appropriate parameter regimes for very small quantum dots.

For the fragile Bell state, a three-dimensional environment in combination with a finite qubit separation prevents the entanglement from decaying entirely. If the qubits are sufficiently well separated, i.e. for $x_{12} \gtrsim c/\omega_c$, the entanglement of the "fragile" and the "robust" Bell state even assumes practically the same final value. In the above example, this is already the case if the qubit-qubit distance is larger than $1\,\mu$m, which is realistic for solid state qubits. For typical parameters, the concurrence initially drops to and then remains at values of the order 0.9 already long before a first coherent oscillation is performed. Thus, uncorrelated phase noise creates decoherence-poor subspaces, which might be used for quantum information processing when complemented with quantum error-correction protocols.

6.2 Incomplete pure dephasing of a qubit register

The results of the last section show that not all qubit states are equally sensitive to the influence of an environment. Depending on the symmetries of the qubit-environment coupling, there can exist decoherence-free subspaces of the qubit Hilbert space that

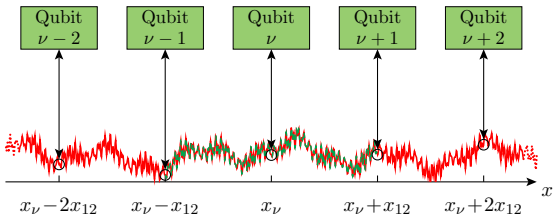

Figure 6.5: Schematic representation of N qubits labeled by numbers ν in a linear arrangement. The qubits (green boxes) are equally spaced with a distance x_{12} and interact via a coupling to the substrate phonon field (red line). The dashed green line indicates the noise correlations of qubit ν with its neighbours $\nu-1$ and $\nu+1$ at time $t=t_{12}$.

are effectively decoupled from the environment. A perfect decoherence-free subspace requires the presence of perfectly correlated noise, which can be fullfilled if the distance of the qubits vanishes. However, for two spatially separated qubits we found above that entanglement is no longer perfectly stable but undergoes an initial decay. This puts limitations on the applicability of the concept of decoherence-free subspaces, since at best decoherence-poor subspaces emerge instead.

We now turn to the effects of phase noise on the N-qubit generalization of the robust entangled state, namely the so-called W state [223]. It is a coherent superposition of all states with exactly one qubit in state 1 while all the others are in state 0,

$$|W_N\rangle = \frac{1}{\sqrt{N}}\big(\,|100\ldots0\rangle + |010\ldots0\rangle + \ldots + |000\ldots1\rangle\,\big). \tag{6.16}$$

Note that for two qubits ($N=2$), the state $|W_2\rangle$ equals the robust Bell state $|\psi_-\rangle$ discussed above.

The motivation to focus on the initial states (6.16) is twofold: First, W states play an important role in several protocols for quantum information processing, for example quantum teleportation [224, 225], superdense coding [225] and quantum games [226], so that their sensitivity to an environment is relevant in itself. In quantum optics, the W states have already been realized, first with three [227–229] and recently even with eight qubits [48]. Proposals exist to produce W states in atomic gases [230] and in solid-state environments [231–234]. Thus, understanding the scaling of multi-qubit decoherence is experimentally relevant, as many groups take the challenge of implementing more complex qubit architectures with solid-state devices.

Second, it is important to understand the scalability of the present few-qubit setups, because decoherence is expected to become more pronounced as the number of qubits increases. Among all fully entangled N-qubit states the W states are special in that they maintain their N-qubit entanglement under collective dephasing (i.e. for vanishing qubit separations). Now if already the W states start to loose their entanglement due to a finite spatial separation of the qubits, then this is a strong indication that for other fully entangled N-qubit states, the situation would be worse. Or, to put it simply, a good way to give the most optimistic estimate about N-qubit decoherence is by focusing on the W states. Below we find explicit expressions for their coherence loss which shows how decoherence scales as a function of the number of qubits, and demonstrates the

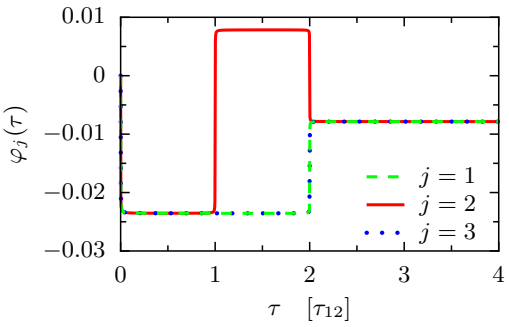

Figure 6.6: Time-dependent frequency shifts (6.19) for three qubits $N = 3$. The time axis is in units of the nearest-neighbour transit time $\tau_{12} = 2\times10^3$. The coupling strength $\alpha = 0.005$.

consequences of spatial qubit separations. Note that the stability of the W states with respect to the system size N has been studied previously [235–237], however only for local decoherence models where the qubits couple to effectively independent heat baths.

For the geometry of the qubits we consider a linear arrangement with equal nearest-neighbor separations $x_{\nu,\nu+1} = x_1 - x_2$ sketched in Fig. 6.5. Then the transit time between qubits ν and ν' becomes $t_{\nu\nu'} = |x_{\nu\nu'}|/c = |\nu - \nu'|t_{12}$. To elaborate on the impact of spatially correlated noise, we assume the chain of qubits to be embedded in a medium with a channel structure, i.e. we treat the bosonic field as effectively one-dimensional and as in the section above, assume that the spectral density is of the ohmic type, $J(\omega) = \alpha\,\omega e^{-\omega/\omega_c}$.

The fact that no bit flips occur under pure dephasing is reflected in the structure of the exact solution which we obtained in Sec. 3.1 [cf. Eq. (3.14)]: The matrix elements $\tilde{\rho}_{\mathbf{m},\mathbf{n}}$ of the reduced N-qubit density operator $\tilde{\rho}$ that are initially zero remain zero for all times, so that for the state $|W_N\rangle$, the dissipative quantum dynamics is restricted to the states

$$|j\rangle = |00\ldots1_j\ldots0\rangle, \quad j = 1, 2, \ldots, N. \tag{6.17}$$

Thus, the W state takes the form $|W_N\rangle = \sum_j |j\rangle/\sqrt{N}$, and at most N^2 out of 2^{2N} density matrix elements are nonvanishing. Initially they are all equal, i.e. $\langle j|\tilde{\rho}(0)|j'\rangle = \tilde{\rho}_{jj'}(0) = 1/N$. From the Hamiltonian (6.1) of the N-qubit register directly follows, that the states $|j\rangle$ possess the eigenenergies $\hbar\omega_j = \frac{\hbar}{2}\sum_{\nu=1}^{N}\Omega_\nu - \hbar\Omega_j$ and a back-transformation of the coherence $\tilde{\rho}_{jj'}(t)$ to the Schrödinger picture provides the phase factor $\exp[i(\omega_j - \omega_{j'})t]$.

6.2.1 Frequency shifts and damping factors

To begin our discussions of the decoherence of the W state, let us consider the Lamb-shifts (3.19) that appear in the exact solution of the reduced dynamics. Recall that they can be interpreted as a result from an effective coherent interaction of the qubits mediated by the vacuum fluctuations of the bosonic field. On the one hand they are not present when looking at a single-qubit system. On the other hand they did not contribute in our study of two qubits in the previous section, since the concurrences for the Bell states only involve absolute values of single density matrix elements. However, for the N-qubit W states which we are discussing now, the Lamb-shifts become important and result in a frequency shift $\delta\Omega_j$ which we obtain in the following way: Upon noticing that one can separate the phases (3.19) into terms that depend on only j or j',

we write $\phi_{jj'}(t) = \phi_j(t) - \phi_{j'}(t)$. Each $\phi_j(t)$ turns out to consist of a finite contribution and a contribution that grows linearly in time, i.e. $\phi_j(t) = \varphi_j(t) - \delta\Omega_j\, t$. The linear contribution leads to a static frequency shift. For the ohmic spectral density, we obtain

$$\delta\Omega_j = -\alpha \sum_{\nu,\nu'=1}^{N} (-1)^{\delta_{j\nu}+\delta_{j\nu'}} \frac{1}{1+\tau_{\nu\nu'}^2}\,, \tag{6.18}$$

$$\varphi_j(\tau) = -\frac{\alpha}{2} \sum_{\nu,\nu'=1}^{N} (-1)^{\delta_{j\nu}+\delta_{j\nu'}} \sum_{\pm} \arctan[\tau \pm \tau_{\nu\nu'}]\,, \tag{6.19}$$

where again the scaled time $\tau = t\omega_\mathrm{c}$ and the scaled transit times $\tau_{\nu\nu'} = \omega_\mathrm{c} t_{\nu\nu'}$ are used. Thus the effective energy splitting of qubit j becomes $\hbar(\Omega_j + \delta\Omega_j)$. Note that both $\delta\Omega_j$ and $\varphi_j(\tau)$ depend on the transit times $t_{\nu\nu'}$ and the system size N but not on the temperature. $\delta\Omega_j$ arises from an induced static exchange interaction and its onset is described by $\varphi_j(\tau)$ [162]. Figure 6.6 shows that the onset takes place until the transit time between the two outmost qubits of the chain is reached, i.e. during times $\tau \leq \tau_{1N}$. Later on the onset functions $\varphi_j(\tau)$ become static and equal for all qubits j, hence their pairwise differences vanish. Note that the dominant contribution to the static shift $\delta\Omega_j$ stems from the diagonal terms $\nu = \nu'$ in Eq. (6.18), whereas the non-diagonal terms are suppressed by a factor $\tau_{\nu\nu'}^2$, respectively.

We henceforth work in the interaction picture with respect to the renormalized qubit energies so that the density matrix element $\tilde{\rho}_{jj'}$ reads

$$\tilde{\rho}_{jj'}(\tau) = \frac{1}{N} e^{-\Lambda_{jj'}(\tau) + i\varphi_{jj'}(\tau)}\,, \tag{6.20}$$

with the damping given in Eq. (3.22). The time-dependent phases $\varphi_{jj'}(\tau) = \varphi_j(\tau) - \varphi_{j'}(\tau)$ contribute only for times $\tau < \tau_{1N}$ until the Lamb-shifts are static, see above. Thus, they influence the decoherence process only during an initial stage.

The coherence loss is given by the damping factors $\exp[-\Lambda_{jj'}(\tau)]$. For two qubits, the state $|W_2\rangle$ equals the robust Bell state $|\psi_-\rangle$ discussed in Sect. 6.1, and, thus, the damping factor $\exp[-\Lambda_{12}(\tau)]$ reduces to the robust concurrence C_- given in Eq. (6.9). Since the general W state (6.16) for N qubits involves only pairwise qubit-qubit coherences $\tilde{\rho}_{jj'}$, the corresponding damping factors $\exp[-\Lambda_{jj'}(\tau)]$ are straightforwardly obtained by replacing τ_{12} with $\tau_{jj'}$ in Eq. (6.9). We find

$$\begin{aligned} \mathrm{e}^{-\Lambda_{jj'}(t)} = \mathrm{e}^{-2\Lambda_{0,1}(\tau)} &\left| \frac{\Gamma(\theta[1-\mathrm{i}(\tau_{jj'}-\tau)])\Gamma(\theta[1-\mathrm{i}(\tau_{jj'}+\tau)])}{\Gamma^2(\theta[1-\mathrm{i}\tau_{jj'}])} \right|^{\pm 8\alpha} \\ &\times \left| 1 + \frac{\tau^2}{(1-\mathrm{i}\tau_{jj'})^2} \right|^{\pm 4\alpha}\,, \end{aligned} \tag{6.21}$$

where the first exponential is the single-qubit coherence given in Eq. (6.10).

6.2.2 N-qubit fidelity

With the exact dynamics known, the only remaining question is how to quantify the entanglement. If there were no interaction with the environment, then the qubits would

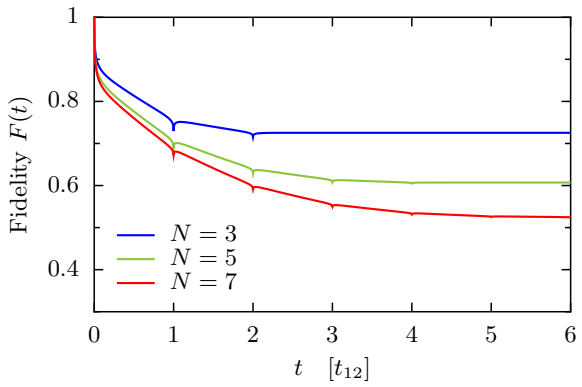

Figure 6.7: Exact time evolution of the fidelity F for $N = 3$, $N = 5$, and $N = 7$ qubits at a temperature $\theta = 10^{-4}$. The time axes is in units of the transit time between nearest-neighbor qubits $\tau_{12} = 2 \times 10^3$, and the qubit-field coupling strength $\alpha = 0.005$.

remain in their pure entangled W state (6.16), which in density-matrix notation reads $\rho(0) = |W_N\rangle\langle W_N|$. After the dissipative time evolution, the qubit state deviates from this "ideal" output state $\tilde{\rho}_{\text{ideal}}(t) = \rho(0)$. The question is how much. A proper measure for this quantity is the fidelity [238] $F(t) = \text{tr}\{\rho(t)\rho_{\text{ideal}}(t)\}$. In our case it reads

$$F(t) = \text{tr}\left\{\rho(0)\tilde{\rho}(t)\right\} = \langle W_N|\tilde{\rho}(t)|W_N\rangle. \tag{6.22}$$

In general, the fidelity is bounded by $0 \leq F \leq 1$, where $F = 1$ corresponds to a pure state [1]. For qubits subject to pure dephasing, the somewhat more strict condition $\sum_j \rho_{jj}^2(0) \leq F \leq 1$ applies, because the populations do not change. In particular the inequalities $1/N \leq F \leq 1$ will hold for the initial state $|W_N\rangle$, as illustrated below. To give another argument why fidelity makes a good measure of entanglement for our particular purpose, we emphasize that for two qubits prepared in the state $|W_2\rangle$, it directly relates to the concurrence via the relation $C(t) = 2F(t) - 1$.

We note in passing that for other initial states that are *not* pure N-qubit entangled states, one should be careful to use fidelity as an entanglement measure, for example because it may remain constant while the system undergoes nontrivial dynamics [72]. Finding other entanglement measures for three or more qubits is an active field of research [38,223,239,240]. Their numerical evaluation can be rather involved, especially for larger systems. These issues need not concern us here, since we start with an N-qubit entangled pure state for which the fidelity is a good measure of entanglement. It has the additional advantage that it is easily evaluated analytically for larger systems as well.

For the robust state (6.16), the fidelity becomes

$$F(t) = \frac{1}{N}\sum_{j,j'=1}^{N} \tilde{\rho}_{jj'}(t), \tag{6.23}$$

where the coherences $\tilde{\rho}_{jj'}$ are given in Eq. (6.20). The time evolution of the fidelity for $N = 3$, $N = 5$, and for $N = 7$ qubits is shown in Fig. 6.7. We find that whenever a transit time is reached, i.e. at times $\tau = \tau_{jj'}$ the fidelity decay is slowed down. This resembles the behavior of the concurrence for two qubits shown in Fig. 6.1a. For a larger number of qubits, the fidelity saturates at a lower value. In order to gain a more quantitative understanding of the fidelity saturation, we focus on the final fidelity $F(\infty)$. In the zero-temperature limit, which provides a lower bound for the coherence loss, we find from

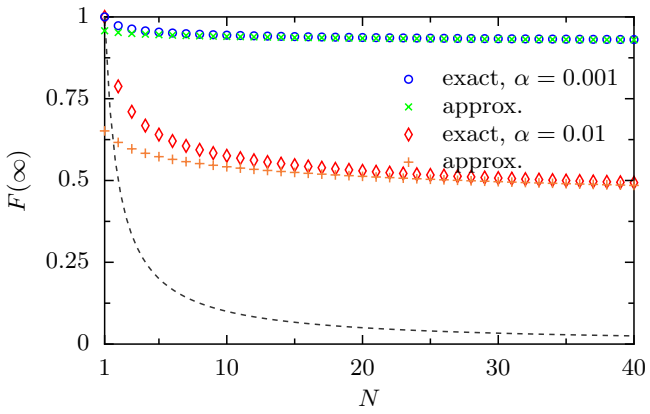

Figure 6.8: Final fidelity (6.24) as a function of the number N of qubits at zero temperature for two coupling strengths $\alpha = 0.001$ (blue circles) and $\alpha = 0.01$ (red diamonds). The nearest-neighbor transit time is again $\tau_{12} = 2 \times 10^3$. The crosses (orange) and plus signs (green) mark the approximative result (6.26), respectively. The dashed line indicates the lower bound $1/N$ of the fidelity.

Eqs. (6.20) and (6.21) the density matrix elements $\tilde{\rho}_{jj'}(\infty) = [1 + \tau_{12}^2 (j - j')^2]^{-4\alpha}/N$. Hence the fidelity (6.23) saturates to

$$F(\infty) = \frac{1}{N}\left[1 + 2\sum_{q=1}^{N-1} \frac{1 - q/N}{(1 + q^2\tau_{12}^2)^{4\alpha}}\right]. \tag{6.24}$$

Although we start out with a "robust" entangled state, this final fidelity $F(\infty)$ can be as low as $1/N$, which marks the large-distance limit $\tau_{12} = x_{12}\omega_c/c \to \infty$. More generally, we find that for zero temperature, the final fidelity decreases with increasing cutoff frequency ω_c, increasing spatial separation, and for a larger qubit-bath coupling strength α.

An intriguing aspect of the fidelity is its scaling behavior as a function of the system size N. Will $F(\infty)$ decay to zero for larger arrays of qubits, or converge to a finite value? For large N we can neglect the term $1/N$ in Eq. (6.24) and replace the sum over q by an integration over the continuous variable $x = q/N$. Then we obtain

$$\begin{aligned} F(\infty) &\simeq 2\int_0^1 \mathrm{d}x\, \frac{1 - x}{(1 + N^2\tau_{12}^2 x^2)^{4\alpha}} \\ &= 2\,{}_2F_1\left(\frac{1}{2}, 4\alpha, \frac{3}{2}, -N^2\tau_{12}^2\right) + \frac{1 - (1 + N^2\tau_{12}^2)^{1-4\alpha}}{N^2\tau_{12}^2(1 - 4\alpha)}\,, \end{aligned} \tag{6.25}$$

where the evaluation of the integral yields Gauss' hypergeometric function ${}_2F_1$. The expression (6.25) is valid for a general coupling constant α, but beyond weak coupling its value is rather small. We will now approximate Eq. (6.25) for $\alpha \ll 1$. Furthermore, in a solid state environment typically many cutoff wavelengths $2\pi c/\omega_c$ will fit between two neighboring qubits, so that $\omega_c t_{12} \gg 1$, as we argued above in the discussion on page 55. Since we already assumed $N \gg 1$ to arrive at the integral (6.25), we are surely in the limit $N\omega_c t_{12} \gg 1$. Then we can approximate the hypergeometric function by its asymptotic expansion for large fourth argument. We finally obtain

$$F(\infty) \simeq \left[\frac{\Gamma(\frac{1}{2} - 4\alpha)}{\Gamma(\frac{3}{2} - 4\alpha)} - \frac{1}{1 - 4\alpha}\right] \frac{1}{(N\tau_{12})^{8\alpha}}\,. \tag{6.26}$$

Hereby we found the important result that although the final fidelity is smaller for larger systems, the scaling is only algebraic in N. This stability under dephasing is a property

of the initial N-qubit W state (6.16). Clearly, for nonvanishing transit time this state lives in a decoherence-poor rather than in a decoherence-free subspace. Equation (6.26) shows that at zero temperature, the final fidelity is determined by two dimensionless numbers, the one number being α and the other the ratio between the array length Nct_{12} and the cutoff wavelength $2\pi c/\omega_{\mathrm{c}}$.

In Fig. 6.8, we compare for two values of α the exact expression (6.24) for the final fidelity as a function of N with the weak-coupling approximate result (6.26). Clearly, for state-of-the-art well-isolated qubits with typically $\alpha = 0.001$, the agreement is excellent already for $N \gtrsim 5$, while for $\alpha = 0.01$ convergence is reached for $N \gtrsim 10$. The figure clearly shows that in the weak coupling limit $\alpha \ll 1$, the final fidelity $F(\infty)$ in (6.26) is almost independent of the length of the array. For $\alpha < 0.005$ the factor in square brackets in Eq. (6.26) is less than 1.05, so that the large-N expression for the final fidelity could be further simplified as $F(\infty) \simeq (N\tau_{12})^{-8\alpha}$.

The above estimates were derived in the limit of strictly zero temperature, so that the question arises up to which temperature they still represent a reasonably good approximation. A closer inspection of the exact result (6.21) reveals that this is certainly the case if the condition

$$\frac{\hbar c}{k_{\mathrm{B}}T} \gg Nct_{12} \tag{6.27}$$

holds, i.e. if the thermal coherence length of the bath is much larger than the length of the array. Assuming $T = 10\,\mathrm{mK}$, the thermal coherence length is $2.3\,\mu\mathrm{m}$. This value corresponds to an array length of 24 qubits with a nearest-neighbor distance $x_{12} = ct_{12} = 100\,\mathrm{nm}$. The final fidelity that we obtain for $T = 0$ in Eq. (6.26) can therefore be considered as an upper bound for what could be realized in state-of-the-art quantum information processing experiments on arrays of qubits.

6.2.3 Discussion

Decoherence of an array of qubits can be a rather complex process that proceeds in several qualitative different stages, even in the case of pure phase noise which we investigated here: If the qubits are coupled to the bosonic field of the substrate vibrations, the dynamics during a first, very short period is essentially noiseless. In a second stage, the bosonic vacuum fluctuations are most relevant, while finally, thermal noise dominates. The spatial separation of the qubits brings in further time scales, namely the transit times of sound waves between the qubits.

Here, robust entangled N-qubit W states were considered which do not decohere for vanishing qubit separations. For finite separations we find instead that the qubits start to dephase. However, the dephasing slows down whenever the elapsed time reaches a transit time, until it eventually comes to a standstill. The final N-qubit quantum coherence increases with decreasing qubit-qubit separation, qubit-bath coupling strength, cutoff frequency, and temperature. By contrast, single qubits in the same one-dimensional environment would loose all quantum coherence for all finite values of these bath parameters. Note that the two-qubit W state is identical to the robust-entangled Bell state and the saturation of entanglement does not occur for fragile two-qubit states.

Cooperative effects can be advantageous or detrimental, depending on the specific protocol that one has in mind. For example, one may fight decoherence by creating

decoherence-free subspaces. To that end, one could bring the qubits close together and use the W states for quantum information processing because their entanglement is robust. Nevertheless, the qubits must be sufficiently well separated, either to enable their individual manipulation or because of their finite extensions. We found that this requirement prevents the realization of decoherence-free subspaces. Cooperative effects are still advantageous, since decoherence-poor subspaces are built up instead. Good results require the length of the array of qubits to be smaller than the thermal coherence length $\hbar c/k_{\mathrm{B}}T$.

Alternatively, one may wish to implement active quantum error-correction schemes, where logical qubits are redundantly encoded into several physical qubits. Here, by contrast, the cooperative effects are detrimental, since standard error-correction schemes [1, 241] and recent generalizations to non-Markovian baths [242, 243] will only work perfectly if the physical qubits couple to spatially uncorrelated baths. Neighboring physical qubits should then be separated by more than the thermal coherence length $\hbar c/k_{\mathrm{B}}T$. By reducing the temperature, single-qubit dephasing is suppressed, but the assumption of uncorrelated baths becomes worse. This suggests that there may be an optimal working temperature for quantum error correction, given a geometry of physical qubits.

Thus the calculations show how well decoherence-free subspaces or quantum error-correction protocols could be realized with linear arrays of qubits. The aforementioned conflicting requirements for both strategies seem to rule out the implementation of both strategies in one experiment.

7

Causal master equation

The exact solvability of the pure phase noise model allowed us in the last chapter to study the decoherence a spatially extended qubit register in an exact manner. Altough analytical expressions for the reduced dynamics can be obtained, they involve rather complex expressions and, thus, an intuitive picture of the observed behavior can be hard to find. For a better and more qualitative understanding, one may benefit from an approximate treatment in the spirit of a Bloch-Redfield master equation approach. As we have seen in Sect. 4.1.2, a cornerstone of the Bloch-Redfield theory is the underlying Markov-approximation, i.e. neglecting memory effects of the bath by assuming the bath correlation time to be the smallest time scale of the problem. In this way the Bloch-Redfield theory provides a direct access to the dephasing and damping rates.

The non-local interaction of separated qubits via the environment, however, introduces memory effects that arise when bath distortions can propagate from one qubit to another during a finite time. This timescale can be much larger than the intrinsic memory time of the bath. As will be detailed below, a direct application of the standard Bloch-Redfield theory to a spatially extended system of qubits leads to a violation of causality. A consequence of this deficiency is the prediction of spurious decoherence-free subspaces.

In this chapter, we adress this issue and identify why the standard Bloch-Redfield theory fails. We derive a causal master equation that on the one hand captures the main effects of the spatial separation while one the other hand still is intuitive [160]. Compared to other non-Markovian master equations whose coefficients in general possess a complex time-dependence, the causal master equation has the advantage of still allowing algebraic methods to be applied to the problem of decoherence [8, 9]. This can lead to additional insight in cases in which tracing out the bath degrees of freedom reveals symmetries that are obeyed by the dissipative central system, but not by the system-bath Hamiltonian. In particular, the causal master equation allows a separation of the reduced dynamics into time regimes for which different strategies of error correction can be adapted. Moreover, the causal master-equation approach is applicable to problems that do not possess an exact solution.

Finally, we compare the results of the causal master equation for the pure phase noise model with the exact dynamics obtained above. This enables a better interpretation of the latter and at the same time a critical examination of the validity of the former. It is shown that not only retardation effects but also non-Markovian decoherence stemming from the short-time dynamics can be taken into account by using results for the reduced

visibility of single qubit coherences found in Sec. 5.1.

7.1 Spurious effects from Bloch-Redfield theory

The Bloch-Redfield equation (4.11) is based on a perturbative treatment of the qubit-environment coupling, followed by neglecting memory effects in the kernel of the resulting quantum master equation. Thereby one entirely ignores the dependence of the dynamical equations on the qubits' history and, thus, on the initial preparation. To learn about the consequences of a fully Markovian description for the reduced dynamics of a spatially extended system, let us again consider two separated qubits prepared in the robust Bell state $|\psi_-\rangle$ [cf. Eq. (6.3)]. We found that for pure phase noise, the concurrence of the qubits is for all times determined by the relevant non-diagonal element of the density matrix, i.e. $C(t) = 2|\tilde{\rho}_{01,10}(t)|$. By a straightforward calculation, one can show that the application of the Bloch-Redfield equation (4.11) to this matrix element yields $\dot{\tilde{\rho}}_{01,10} = 0$, for all dimensions and spectral densities of the environment, and in particular for all distances $\mathbf{x}_{12}$ of the qubits. In other words, in the Markovian description, on which the analysis of decoherence-free subspaces often relies [9,244,245], the dynamics shows up as if the qubit separation would vanish, and consequently the concurrence remains robust for all times. This is in clear contrast to the exact dynamics depicted in Fig. 6.1a,c, where the concurrence initially decays and only at later times, a decoherence-poor subspace is build up.

7.2 Taking causality into account

Taking the above considerations as a motivation, we now derive a generalization of the Bloch-Redfield master equation that is able to capture the retardation effects stemming from a finite field velocity. In doing so we pursue closely the standard approach that leads to a Markovian equation of motion. In this way, it can be identified where it fails and how to improve it accordingly.

Our starting point is the non-Markovian Born master equation (4.3) considered in Sec. 4.1.1. At the initial time $t = t_0$, we assume that the bath is in thermal equilibrium for which the master equation reduces to the form

$$\frac{\mathrm{d}}{\mathrm{d}t}\tilde{\rho}(t) = -\sum_{\nu,\nu'}\int_0^{t-t_0} \mathrm{d}t'\, \kappa_{\nu\nu'}(t,t')\tilde{\rho}(t)\,, \tag{7.1}$$

where $t \geq t_0$ and the super-operator

$$\begin{aligned}\kappa_{\nu\nu'}(t,t')[\ldots] = {}& \mathcal{S}_{\nu\nu'}(t')\big[\widetilde{X}_\nu(t), \big[\widetilde{X}_{\nu'}(t-t'), \ldots\big]\big] \\ & + \mathrm{i}\mathcal{A}_{\nu\nu'}(t')\big[\widetilde{X}_\nu(t)\big\{\widetilde{X}_{\nu'}(t-t'), \ldots\big\}\big]\,.\end{aligned} \tag{7.2}$$

The symmetric and anti-symmetric bath correlation functions $\mathcal{S}_{\nu\nu'}(t')$ and $\mathcal{A}_{\nu\nu'}(t')$ are given in Eqs. (4.8) and (4.9), respectively. By replacing summations over the wave vector $\mathbf{k}$ with frequency integrations over the spectral bath density $J(\omega)$, we find in the

continuum limit

$$\mathcal{S}_{\nu\nu'}(t') = \int_0^\infty \mathrm{d}\omega\, J(\omega) G^{(d)}(\omega t_{\nu\nu'}) \cos(\omega t') \coth\left(\frac{\hbar\omega}{2k_\mathrm{B}T}\right), \tag{7.3}$$

$$\mathcal{A}_{\nu\nu'}(t') = -\int_0^\infty \mathrm{d}\omega\, J(\omega) G^{(d)}(\omega t_{\nu\nu'}) \sin(\omega t'), \tag{7.4}$$

with the dimension-dependent geometrical factor (3.21).

To discuss the master equation (7.1) in more detail we first consider the local terms, i.e. those with $\nu = \nu'$, for which the transit time $t_{\nu\nu'}$ vanishes. Hence, the geometrical factor in the correlation functions equals unity, so that they reduce to the standard symmetric and anti-symmetric bath correlation functions $\mathcal{S}_{\nu\nu}(t') = \mathcal{S}(t')$ and $\mathcal{A}_{\nu\nu}(t) = \mathcal{A}(t')$, respectively, which are well known from local heat-bath models [97, 99–101, 169]. As detailed in App. B.2 we find for the spectral densities (3.24) the explicit expressions

$$\begin{aligned}\mathcal{S}(t') = \alpha\omega_\mathrm{c}^2\Gamma(s+1)\Bigg[&\frac{\cos[(s+1)\arctan(\omega_\mathrm{c}t')]}{(1+\omega_\mathrm{c}^2t'^2)^{\frac{s+1}{2}}} \\ &+ \left(\frac{2k_\mathrm{B}T}{\hbar\omega_\mathrm{c}}\right)^{s+1} \mathrm{Re}\,\zeta\Big(s+1, 1+\frac{k_\mathrm{B}T}{\hbar\omega_\mathrm{c}}[1+\mathrm{i}\omega_\mathrm{c}t']\Big)\Bigg],\end{aligned} \tag{7.5}$$

$$\mathcal{A}(t') = -\alpha\omega_\mathrm{c}^2\Gamma(s+1)\frac{\sin[(s+1)\arctan(\omega_\mathrm{c}t')]}{(1+\omega_\mathrm{c}^2t'^2)^{\frac{s+1}{2}}}. \tag{7.6}$$

Then one can introduce a Markov approximation in the usual way: If the standard correlation functions $\mathcal{S}(t')$ and $\mathcal{A}(t')$ contribute to the integral in Eq. (7.1) essentially only in a small time interval of size t_b around $t' = 0$, then for $t - t_0 \gg t_\mathrm{b}$, we can extend the t'-integration to infinity, i.e. we impose the approximation

$$\int_0^{t-t_0} \mathrm{d}t'\, \kappa_{\nu\nu}(t,t') \approx \int_0^\infty \mathrm{d}t'\, \kappa_{\nu\nu}(t,t'). \tag{7.7}$$

This expression implies a coarse-graining in time so that the resulting master equation is valid only for time steps larger than the bath correlation time t_b. In general, the bath correlation time depends on the properties of the spectral density $J(\omega)$ and the bath temperature. If the temperature is not too low and the spectral density is fairly smooth and decays sufficiently fast for $\omega \to 0$ and $\omega \to \infty$, as is the case here, then the correlation time is only weakly temperature dependent and reads $t_\mathrm{b} \approx 1/\omega_\mathrm{c}$ [246].

In the above treatment of the local terms, i.e. those with $\nu = \nu'$, we have followed the route towards a Markovian equation of motion. For the nonlocal terms, however, the arguments of the last paragraph are not valid any more. For $\nu \neq \nu'$, the geometrical factor in the correlation functions (7.3) and (7.4) becomes important. It turns out that the line of argumentation for the different dimensions d remains the same, although the explicit calculation for $d = 2, 3$ is more involved. Thus, to ease the following presentation, we restrict ourselves to a one dimensional environment $d = 1$ and use the corresponding geometrical factor (3.21a). By applying trigonometric addition formulas to the integral kernels of the correlation functions, one recognizes that it is possible to express them by

linear combinations of the standard correlators

$$\mathcal{S}_{\nu\nu'}(t') = \frac{1}{2}\left[\mathcal{S}(t'-t_{\nu\nu'}) + \mathcal{S}(t'+t_{\nu\nu'})\right] , \tag{7.8}$$

$$\mathcal{A}_{\nu\nu'}(t') = \frac{1}{2}\left[\mathcal{A}(t'-t_{\nu\nu'}) + \mathcal{A}(t'+t_{\nu\nu'})\right] . \tag{7.9}$$

Thus, the correlation functions $\mathcal{S}_{\nu\nu'}(t')$ and $\mathcal{A}_{\nu\nu'}(t')$ are generally not peaked at $t'=0$, but at $t'=\pm t_{\nu\nu'}$. It turns out that this is true for the higher-dimensional cases $d=2,3$ as well, although the relations (7.8) and (7.9) may look different.

A finite transit time $t_{\nu\nu'}$ for a realistic qubit separation typically exceeds the bath correlation time t_b. Then we have to distinguish the cases $t-t_0 < t_{\nu\nu'}$ and $t-t_0 > t_{\nu\nu'}$. In the former case, the peak of the correlation functions lies outside the integration interval so that the integral is small and, consequently, will be neglected. By contrast, in the latter case the peak fully contributes and the integral can again be extended to infinity. In summary, this amounts to the approximation

$$\int_0^{t-t_0} \mathrm{d}t'\, \kappa_{\nu\nu'}(t,t') \approx \Theta(t-t_0-t_{\nu\nu'}) \int_0^{\infty} \mathrm{d}t'\, \kappa_{\nu\nu'}(t,t') , \tag{7.10}$$

where $\Theta(t)$ is the Heaviside step function. For $\nu=\nu'$, this expression coincides with Eq. (7.7).

Inserting the approximation (7.10) into the weak-coupling master equation (7.1) and setting again the initial time $t_0=0$, we find as the main result of this section, the causal master equation (CME)

$$\frac{\mathrm{d}}{\mathrm{d}t}\tilde{\rho}(t) = \mathcal{G}(t)\tilde{\rho}(t) \tag{7.11}$$

with the time-dependent superoperator

$$\begin{aligned}\mathcal{G}(t)[\ldots] = -\sum_{\nu,\nu'=1}^{N} \Theta(t-t_{\nu\nu'}) \int_0^{\infty} \mathrm{d}t' \Big(&\mathcal{S}_{\nu\nu'}(t')\big[\widetilde{X}_\nu(t), \big[\widetilde{X}_{\nu'}(t-t'),\ldots\big]\big] \\ &+ \mathrm{i}\mathcal{A}_{\nu\nu'}(t')\big[\widetilde{X}_\nu(t), \big\{\widetilde{X}_{\nu'}(t-t'),\ldots\big\}\big]\Big) .\end{aligned} \tag{7.12}$$

The step functions ensure causality which requires that the cross terms can only be active after the propagation time between the respective qubits has passed. In the limit of vanishing separation, the causal master equation reduces to a standard Bloch-Redfield equation. Compared to the non-Markovian time-local master equation (7.1), the causal master equation is much simpler and faster to solve. Besides beeing more intuitive, it allows for analytical calculations and algebraic methods like a symmetry analysis to be applied to the problem [8, 9]. Below, we will demonstrate that the causal master equation indeed reproduces the effects of spatial bath correlations in the qubit register rather well, while a standard Bloch-Redfield approach clearly fails.

7.3 Incomplete pure dephasing revisited

Let us now apply the causal master equation to a qubit register subject to the dephasing induced by an ohmic environment, i.e. the problem defined in Sects. 6.1 and 6.2. The

qubit coupling operators $X_\nu = \sigma_{\nu z}$ commute with the system Hamiltonian (6.1), so that the interaction-picture operators stay time-independent, $\widetilde{X}_\nu(t) = \sigma_{\nu z}$. Then the time integration in the generator (7.12) of the causal master equation involves only the bath correlation functions and we obtain for the density matrix element $\tilde{\rho}_{\mathbf{m},\mathbf{n}}$ the equations of motion

$$\frac{\mathrm{d}}{\mathrm{d}t}\tilde{\rho}_{\mathbf{m},\mathbf{n}} = \left[-\Lambda^{\mathrm{CME}}_{\mathbf{m},\mathbf{n}}(t) + \mathrm{i}\phi^{\mathrm{CME}}_{\mathbf{m},\mathbf{n}}(t)\right]\tilde{\rho}_{\mathbf{m},\mathbf{n}}\,, \tag{7.13}$$

with the damping

$$\Lambda^{\mathrm{CME}}_{\mathbf{m},\mathbf{n}}(t) = \frac{\alpha\pi k_{\mathrm{B}}T}{\hbar}\sum_{\nu,\nu'=1}^{N}\Theta(t-t_{\nu\nu'})\left[(-1)^{m_\nu}-(-1)^{n_\nu}\right]\left[(-1)^{m_{\nu'}}-(-1)^{n_{\nu'}}\right], \tag{7.14}$$

and the phase shift

$$\phi^{\mathrm{CME}}_{\mathbf{m},\mathbf{n}}(t) = \sum_{\nu,\nu'=1}^{N}\Theta(t-t_{\nu\nu'})\frac{\alpha\omega_{\mathrm{c}}}{1+\omega_{\mathrm{c}}^2 t_{\nu\nu'}^2}\left[(-1)^{m_\nu+m_{\nu'}}-(-1)^{n_\nu+n_{\nu'}}\right]. \tag{7.15}$$

This master equation is non-Markovian due to the appearance of the step functions, which change the effective damping and phase shift whenever a transit time $t_{\nu\nu'}$ is reached. These stepwise time-dependent frequency shifts and decay rates are characteristic features of the causal master equation. We will see, that it is these steps that allow the causal master equation to follow more closely the time-dependent variations of shifts and decay rates of the exact dynamics than the standard Bloch-Redfield formalism manages to do with its static shifts and decay rates.

As in Sec. 6.1, we first consider as an initial state the robust Bell state $|\psi_-\rangle$ defined in Eq. (6.3). From the master equation (7.13), we find that the concurrence $C_{\mathrm{CME}} = 2|\tilde{\rho}_{01,10}|$ obeys

$$\frac{\mathrm{d}}{\mathrm{d}t}C_{\mathrm{CME}}(t) = -\frac{8\alpha\pi k_{\mathrm{B}}T}{\hbar}\left[1-\Theta(t-t_{12})\right]C_{\mathrm{CME}}(t)\,. \tag{7.16}$$

This differential equation is readily integrated to provide the solution

$$C_{\mathrm{CME}}(t) = \begin{cases} \mathrm{e}^{-8\alpha\pi k_{\mathrm{B}}Tt/\hbar}\,, & 0\le t<t_{12} \\ \mathrm{e}^{-8\alpha\pi k_{\mathrm{B}}Tt_{12}/\hbar} = \text{const.}\,, & t\ge t_{12}\,, \end{cases} \tag{7.17}$$

i.e. the concurrence decays exponentially until the transition time is reached and thereafter remains constant. This clear separation of two dynamical regimes facilitates an intuitive interpretation: For times $t < t_{12}$, the qubits have not "seen" each other so that we are in a regime of single-qubit decoherence. Indeed, during this first time interval the causal master equation (7.13) coincides with a standard Bloch-Redfield approach in which the qubits are coupled to truly independent heat baths. Consequently, the relative phase between the qubits is randomized and the concurrence decays. However, for $t > t_{12}$, both qubits experience perfectly correlated quantum noise and undergo collective decoherence. Thus, the concurrence decay comes to a standstill and a decoherence-poor subspace can emerge.

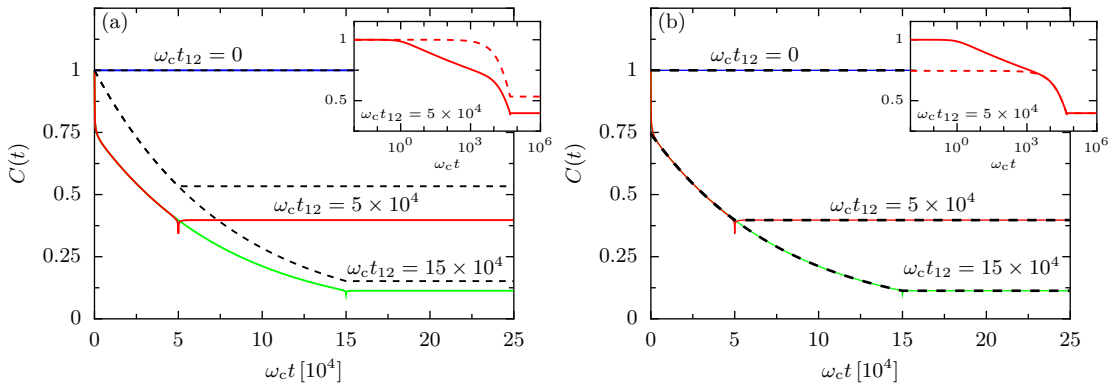

Figure 7.1: Time evolution of the concurrence C for two qubits initially prepared in the robust state $|\psi_-\rangle$ for various transit times t_{12}: In panel (a) the exact time evolution (solid lines) is compared to the results obtained from the causal master equation (7.17) (dashed). The temperature is $k_B T = 10^{-4}\hbar\omega_c$ and the coupling strength $\alpha = 0.005$. Inset: Blow-up on a logarithmic scale for the transit time $t_{12} = 5\times 10^4/\omega_c$. Panel (b) compares the exact and the master equation result (7.20) taking short-time decoherence into account.

This time evolution is compared to the exact solutions in Fig. 7.1a. We find that generally the causal master equation describes the slow decay of the concurrence and its saturation very well. The benefits of the causal master equation become obvious: Since the Bloch-Redfield treatment is recovered by setting the transit time $t_{12} = 0$, Eq. (7.16) reveals that $\mathrm{d}C_{\mathrm{BR}}/\mathrm{d}t = 0$ for all times, i.e. the concurrence remains at its initial value. This spurious robustness of the concurrence is, however, in clear contrast to the exact result.

At very short times, however, the causal master equation does not capture the initial slip of the concurrence. The reason for this is, that the dynamics on timescales that are comparable to the bath correlation time cannot be resolved in a coarse-grained time approximation underlying the causal master equation. The same generally holds true for Markovian quantum master equations, in particular for the standard Bloch-Redfield approach. As a consequence, the causal master equation overestimates at long times the final, stable concurrences of the respective decoherence-poor subspaces, i.e. provides an upper bound for the quality of robust entanglement. To overcome this quantitative failure, one has to take the short-time decoherence into account. In Sec. 5.1 we discussed the reduced visibility of a single qubit, and found explicit formulas for the coherence loss not captured by exponential decay laws [cf. Eqs. (5.11) and (5.14)]. If the transit times between the qubits are larger than the time scale t_* during which the fast initial decoherence takes place, each qubit experiences this coherence loss independently of the others. Then it is possible to directly incorporate the reduced visibility factors (5.11) for the ohmic and (5.14) for super-ohmic environments. For the ohmic case discussed here the visbility was found to read

$$v_1(\alpha,\theta) = \left(\frac{2\pi\theta^{2\theta-1}}{\Gamma^2(\theta)}\right)^{4\alpha}. \tag{7.18}$$

Thus, we apply the following correction scheme: For times $t < t_*$, the coherence of each qubit is reduced independently by a factor (7.18). This provides a new initial

condition at time t_* for the causal master equation, i.e. the initial qubit state $\tilde{\rho}(0)$ is first mapped to $\tilde{\rho}(t_*)$ according to

$$\tilde{\rho}_{\mathbf{m},\mathbf{n}}(t_*) = v_s^{H(\mathbf{m},\mathbf{n})}\tilde{\rho}_{\mathbf{m},\mathbf{n}}(0) \tag{7.19}$$

and for times $t > t_*$ evolves according to the causal master equation (7.13). Here $|\mathbf{n}\rangle$ is the eigenbasis of the system-bath coupling and $H(\mathbf{m},\mathbf{n}) = \sum_\nu |m_\nu - n_\nu|$ is the Hamming distance of the two binary strings $\mathbf{m}$ and $\mathbf{n}$. Its appearance in Eq. (7.19) ensures that a multi-qubit coherence is reduced according to the number of qubits contributing to it. Note that diagonal matrix elements are not changed since in the eigenbasis of the coupling, the short-time dynamics only influences the phase coherences.

For the matrix element $\tilde{\rho}_{01,10}$ which is relevant for the two-qubit robust Bell state discussed above we find $\tilde{\rho}_{01,10}(t_*) = v_1^2(\alpha,\theta)\tilde{\rho}_{01,10}(0)$, and the solution (7.17) of the causal master equation for the concurrence becomes

$$C_{\mathrm{CME}}(t) = \begin{cases} v_1^2(\alpha,\theta)\mathrm{e}^{-8\alpha\pi k_\mathrm{B}Tt/\hbar}\,, & t_* \le t < t_{12} \\ v_1^2(\alpha,\theta)\mathrm{e}^{-8\alpha\pi k_\mathrm{B}Tt_{12}/\hbar}\,, & t \ge t_{12}\,, \end{cases} \tag{7.20}$$

where t_* is the time scale of the coherence loss quantified by the visibility factor (7.18). In Sect. 5.1 we found for the ohmic model $t_* = \min\{1/\omega_\mathrm{c}, \hbar/k_\mathrm{B}T\}$. Figure 7.1b shows that with the short-time decoherence taken into account, the causal master equation does not only render the stepwise change of the decoherence rates, but also agrees quantitatively with the exact result.

For a more detailed investigation of the quality of the corrected causal master equation, we compare the final values of the concurrence, $\lim_{t\to\infty} C(t)$. Figure 7.2 depicts the difference of the exact solution and the causal master equation result (7.20), $\delta C = C(\infty) - C_{\mathrm{CME}}(\infty)$, as a function of transit time and temperature. It demonstrates that the final value obtained from the causal master equation agrees perfectly with the exact result unless the transit times are smaller than the time scale t_* of the short-time decoherence. In fact, for those qubit separations the initial loss of decoherence is stopped by spatial correlations already before it completes. Hence, the visibility prefactor (7.18) overestimates the initial loss of coherence in this parameter regime, i.e. the difference δC of the concurrences is positive.

Let us finally apply the master equation (7.11) also to the case of a linear N-qubit arrangement with equal nearest-neighbor spacings x_{12} as discussed in Sec. 6.2.2. We again consider the initial preparation in the robust state (6.16) using the shorthand notation (6.17). To calculate the fidelity F defined in Eq. (6.23), we need to compute the values of the density matrix elements $\tilde{\rho}_{jj'}$. Unlike for the two-qubit concurrence, phase shifts now also play a role. The time-dependent phase shift $\phi_{jj'}^{\mathrm{CME}}(t)$ [see Eq. (7.15)] can be written as the difference of two terms, one of them only depending on j and the other only on j'. Both terms describe stepwise time-dependent frequency shifts of the corresponding qubits. Interestingly, after the longest transit time $t > t_{1N}$, these shifts in the causal master equation become static and $\phi_{jj'}^{\mathrm{CME}}(t)$ agrees with the exact result (6.18) of Sect. 6.2.2, i.e. $\phi_{jj'}^{\mathrm{CME}}(t) = \delta\Omega_j - \delta\Omega_{j'}$. For an unambiguous comparison of fidelities in the exact and in the causal master-equation formalism, it is an important result that we can work in the same interaction picture with the same renormalized

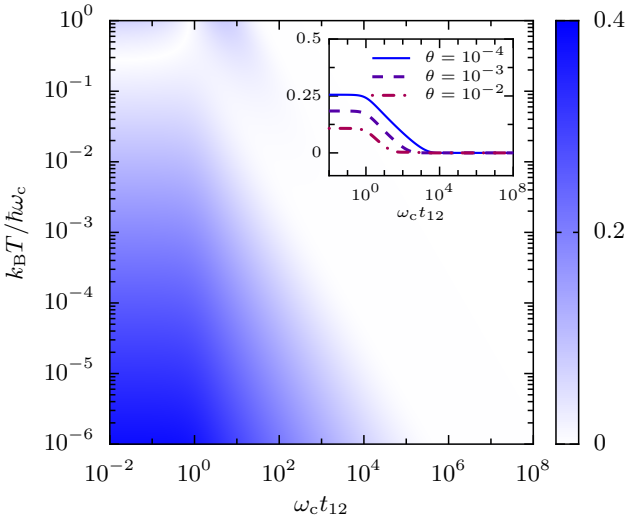

Figure 7.2: Difference between the exact result and the causal master equation result (7.17) for the final value of the concurrence, $\delta C = C(\infty) - C_\mathrm{CME}(\infty)$, for the robust entangled 2-qubit state $|\psi_-\rangle$. The coupling strength is $\alpha = 0.005$. The inset depicts δC for the fixed temperatures $\theta = k_\mathrm{B}T/\hbar\omega_\mathrm{c} = 10^{-4}$ (solid), $\theta = 10^{-3}$ (dashed) and $\theta = 10^{-2}$ (dash-dotted), respectively.

qubit frequencies $\Omega_j \to \Omega_j + \delta\Omega_j$. It remains to be discussed what is the effect of the stepwise frequency shifts in the causal master equation for times $t < t_{1N}$. It is the non-diagonal terms $\nu \neq \nu'$ in Eq. (7.15) that make up the difference between the frequency shifts at time $t = 0$ and the exact static renormalization at times $t > t_{1N}$. However, this difference is very small due to large factors $\omega_\mathrm{c}^2 t_{\nu\nu'}^2 \gg 1$ in the denominator of Eq. (7.15), and can safely be neglected in the following.

From the causal master equation (7.13) we then obtain

$$\frac{\mathrm{d}}{\mathrm{d}t}\tilde{\rho}_{jj'}(t) = -\frac{8\alpha\pi k_\mathrm{B}T}{\hbar}[1 - \Theta(t - t_{jj'})]\tilde{\rho}_{jj'}(t)\,. \tag{7.21}$$

Interestingly enough, in the present case only two types of terms of the master equation (7.13) contribute: the local terms with $\nu = \nu'$ and those with $|\nu - \nu'| = |j - j'|$. As a consequence, the decay rate of $\rho_{jj'}(t)$ changes only at the transit time $t_{jj'}$.

In order to evaluate the fidelity (6.23), we integrate Eq. (7.21) and sum over all density matrix elements $\tilde{\rho}_{jj'}(t)$ so that we obtain

$$F_\mathrm{CME}(t) = \frac{1}{N^2}\sum_{j,j'=1}^{N}\left[\Theta(t_{jj'} - t)\mathrm{e}^{-8\alpha\pi k_\mathrm{B}Tt/\hbar} + \Theta(t - t_{jj'})\mathrm{e}^{-8\alpha\pi k_\mathrm{B}Tt_{jj'}/\hbar}\right]. \tag{7.22}$$

For vanishing qubit separation, the master equation predicts $F_\mathrm{CME}(t) = 1$, i.e. a decoherence-free behavior. For $x_{12} > 0$, however, all coherences $\tilde{\rho}_{jj'}$ initially decay and so does the fidelity. When the smallest transit time t_{12} is reached, a perfect correlation between nearest neighbors is built up and the coherences $\tilde{\rho}_{j,j+1}$ saturate. Since these $N-1$ coherences are no longer time-dependent, the fidelity decay is reduced accordingly. This process continues until ultimately all transition times have passed, i.e. until $t = t_{1N}$, and the fidelity decay comes to a standstill.

In Fig. 7.3, we compare this behavior to the exact solution. For very low temperatures [panel (a)], we observe that the master equation reproduces the reduction of the fidelity decay whenever a transit time is reached. The relative difference between the exact result and the causal master equation is of the order of 10% as in Fig. 7.1a for the case

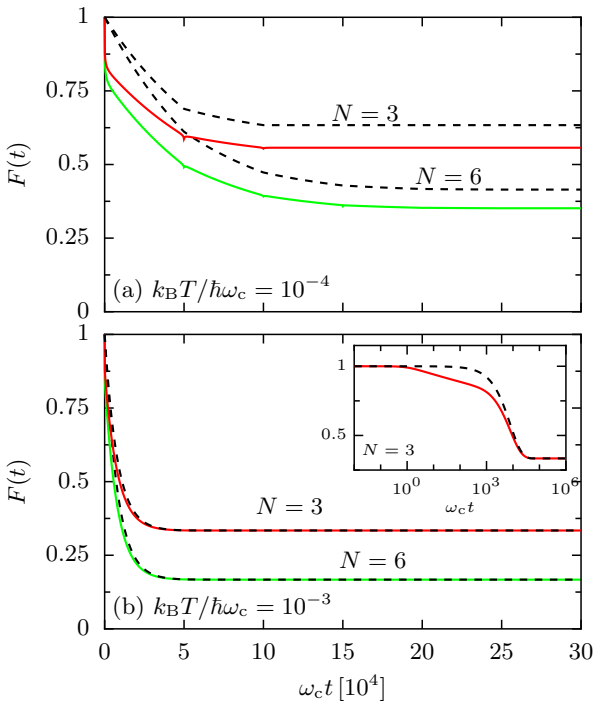

Figure 7.3: Exact time evolution of the fidelity $F(t)$ (solid lines) and result (7.22) obtained from the causal master equation (dashed lines) for $N = 3$ and $N = 6$ qubits, respectively. The temperatures are $k_BT = 10^{-4}/\hbar\omega_c$ (a) and $k_BT = 10^{-3}/\hbar\omega_c$ (b). The transit time between nearest-neighbor qubits is $t_{12} = 5 \times 10^4/\omega_c$ and the qubit-field coupling strength $\alpha = 0.005$. The inset in panel (b) shows the data for $N = 3$ on a logarithmic time axis.

of two qubits, but can be corrected by applying the scheme (7.19) discussed above (not shown). If the temperature becomes larger [panel (b)] such that the nearest neighbor separation exceeds the thermal coherence length, the fidelity decay is determined by thermal noise. In that case, F already saturates to a rather small value before the first transit time is reached. The inset of Fig. 7.3b shows that then even the uncorrected causal master equation agrees quantitatively.

7.4 Conclusions

We have shown that the common Bloch-Redfield master equation cannot account for the intrinsically non-Markovian effects stemming from spatial bath correlations. For a qubit register, the Bloch-Redfield approach predicts spurious decoherence-free subspaces, which in fact are at best decoherence-poor.

In order to capture delocalization effects with a master equation, we have derived a modified Bloch-Redfield approach that ensures causality for the qubit-qubit interaction mediated by the substrate. A characteristic feature of the proposed causal master equation is that it selects the Bloch-Redfield kernel depending on the time elapsed since the preparation. This means that the time evolution is governed by a time-dependent Liouville operator which renders the dynamics non-Markovian. Besides being a proper tool for studying retardation effects in models that do not possess an exact solution, the causal master equation describes the time evolution in an intuitive and concise manner. Thereby, it enables decoherence studies with algebraic methods which possibly will provide suggestions for coherence stabilization. The causal master equation proved to be reliable for all those parameter sets for which the standard Bloch-Redfield theory for a

single qubit is reliable. This is the case for sufficiently high temperatures or small enough coupling strengths such that initial-slip effects are small. However, we have shown that when adequate corrections for the short-time dynamics are taken into account as well, i.e. when the reduced visibility factors of Sect. 5.1 are considered, the master equation approach is applicable to much wider parameter regimes and agrees quantitatively well with the exact solution that can be obtained for pure phase-noise models.

8

Spatially separated qubits subject to bit-flip noise

Already over 50 years ago, Dicke pointed out that the radiative decay in an ensemble of gas atoms can exhibit collective effects [247]: Although the atoms may not couple directly to each other, they interact with a common radiation field so that they cannot be considered independently. For a system of two identical two-level atoms the consequence is that when separated by distances smaller than their characteristic wavelength, the decay rate due to spontaneous emission is enhanced or suppressed, depending on whether the initial state is symmetric or anti-symmetric with respect to atom exchange, i.e. one finds superradiance and subradiance, respectively. Cooperative radiation of atoms is a well studied subject in quantum optics [110, 248], and only recently it was demonstrated experimentally for a lateral arrangement of quantum dots that superradiant behavior can also be found in a solid state system [249].

Collective effects by electromagnetic interaction in three dimensions typically disappear very fast as soon as the Dicke limit is left, i.e. whenever the (real or artificial) atoms are not co-located [110]. Recently it was found that for relaxation caused by a homogeneous isotropic Markovian and three-dimensional reservoir, there is no multi-particle decoherence-free subspace outside the Dicke limit [245]. The situation may be different for one-dimensional structures for which we showed in the previous chapters that at least for pure dephasing, spatial correlations are more overt although decoherence-poor subspaces emerge if qubits are separated. For solid-state qubits, phonons in the substrate are an important source of decoherence. As bosonic excitations, lattice vibrations are also candidates for the realization of mechanical counterparts of quantum optical phenomena [250]. The technical improvements during the last years made it possible to fabricate nanodevices as for example quantum wires and carbon nanotubes whose electronic, but also vibrational properties differ drastically from bulk material [251–254]. It is thus an interesting question how spatial correlations influence the entanglement properties of solid-state qubits in such quasi one-dimensional geometries.

In contrast to pure dephasing, including bit-flip noise usually renders the qubit-environment model no longer exactly solvable. Therefore one has to resort to approximation schemes like, e.g, a master-equation approach. The causal master equation derived in Chap. 7 is applicable to such problems, in particular because it captures the effects of spatial noise correlations very well. We now employ this approach to study the dis-

sipative entanglement dynamics of two spatially separated qubits in a one-dimensional bosonic environment. As in our discussion of pure dephasing, our focus here is on two entangled Bell states, one that is relaxation-free, i.e. robust under collective bit-flip noise, whereas the other is not. Note that in quantum optics it is typically assumed that atoms couple to a single field mode or a continuum initially in its vacuum state [110, 255–259]. This is well justified since the thermal energy is in most cases negligible as compared to optical transition frequencies. By contrast, we here focus on the solid state and allow for a thermal initial state of the phonon bath. We find that at distinct qubit separations, noise correlations can considerably suppress the decoherence also at temperatures as large as the corresponding qubit energy splittings.

8.1 Model

As in Chap. 6, we consider a qubit register with Hamiltonian (6.1). We focus on two qubits in the following, so that in the energy eigenbasis $|\mathbf{n}\rangle = |n_1 n_2\rangle$ the system Hamiltonian simplifies to

$$H_\mathrm{s} = \frac{\hbar\Omega_1}{2}\sigma_{1z} + \frac{\hbar\Omega_2}{2}\sigma_{2z}\,, \tag{8.1}$$

where again $\sigma_{\nu z}$ is a Pauli-matrix for qubit $\nu = 1, 2$, $\hbar\Omega_\nu$ is the respective level splitting, and the basis states obey $\sigma_{z\nu}|\mathbf{n}\rangle = (-1)^\nu |\mathbf{n}\rangle$, $n_\nu = 0, 1$. For bit-flip noise, the qubits couple via operators X_ν to the bath that do not commute with H_s. In this way bath fluctuations eventually can flip the eigenstates of the qubits and, thus, lead to relaxation. We here choose an interaction of the form

$$H_\mathrm{sb} = \hbar\sigma_{1x}\xi_1 + \hbar\sigma_{2x}\xi_2\,, \tag{8.2}$$

i.e. we set the coupling operators $X_\nu = \sigma_{\nu x}$. In the interaction representation with respect to H_s they are time-dependent and read $\widetilde{X}_\nu(t) = \sigma_{x\nu}\cos(\Omega_\nu t) - \sigma_{y\nu}\sin(\Omega_\nu t)$. The bath coordinate ξ_ν is given in Eq. (3.3) and depends on qubit ν through its position $\mathbf{x}_\nu$. For collective decoherence, i.e. for vanishing distance of the qubits, we have $\xi_1 = \xi_2 = \xi$ and as in the case of pure dephasing one expects to find also here a robust two-qubit state which does not suffer from decoherence. Such a state must obey the condition (1.2), i.e. is an eigenstate of the collective coupling coordinate $\sigma_{1x} + \sigma_{2x}$. We here consider the maximally entangled singlet state

$$|\mathrm{S}\rangle = \frac{1}{\sqrt{2}}(|01\rangle - |10\rangle)\,, \tag{8.3}$$

which is an eigenstate with eigenvalue 0 and, moreover, a stationary state of H_s. In the language of quantum optics, this Bell state is the anti-symmetric, subradiant Dicke state [110]. As an example for a fragile state, we consider the symmetric (superradiant) superposition, i.e. the maximally entangled triplet state

$$|T\rangle = \frac{1}{\sqrt{2}}(|01\rangle + |10\rangle)\,. \tag{8.4}$$

Note that also $(|00\rangle + |11\rangle)/\sqrt{2}$ is an eigenstate of the collective coupling operator and one might expect that like the singlet state it is robust under bit-flip noise for vanishing

qubit separation. However, the coherent dynamics of the qubit register according to the Hamiltonian H_s maps this state into parts of the qubit Hilbert space that are affected by the noise. Indeed, for two equal qubits $\Omega_1 = \Omega_2$ the superposition $(|00\rangle + |11\rangle)/\sqrt{2}$ acquires a relative phase $\exp(-2\mathrm{i}\hbar\Omega t)$ and evolves to states which are not decoherence-free.

8.2 Causal master equation in energy eigenbasis

Since the bit-flip model does not allow for an exact solution, we employ the causal master equation (7.11) for weak qubit-bath coupling. It is convenient to express the causal master equation in the eigenbasis $|\mathbf{n}\rangle$ of the system defined by $H_\mathrm{s}|\mathbf{n}\rangle = E_\mathbf{n}|\mathbf{n}\rangle$. For the two qubits with Hamiltonian (8.1) we find the energies $E_{00} = -E_{11} = \hbar(\Omega_1 + \Omega_2)/2$ and $E_{01} = -E_{10} = \hbar(\Omega_1 - \Omega_2)/2$. With the transition frequencies $\hbar\omega_\mathbf{mn} = E_\mathbf{m} - E_\mathbf{n}$ the causal master equation (7.11) can be written in the form

$$\frac{\mathrm{d}}{\mathrm{d}t}\tilde{\rho}_{\mathbf{m},\mathbf{n}}(t) = -\sum_{\mathbf{ll}'}\sum_{\nu\nu'=1}^{2}\Theta(t-t_{\nu\nu'})R_{\mathbf{mnll}',\nu\nu'}\,\mathrm{e}^{\mathrm{i}(\omega_\mathbf{mn}-\omega_{\mathbf{ll}'})t}\tilde{\rho}_{\mathbf{l},\mathbf{l}'}(t)\,, \tag{8.5}$$

with the generalized Redfield tensor

$$R_{\mathbf{mnll}',\nu\nu'} = -\delta_{\mathbf{l}'\mathbf{n}}\sum_\mathbf{k}\Gamma_{\mathbf{mkkl},\nu\nu'} + \Gamma_{\mathbf{l}'\mathbf{nml},\nu\nu'} - \delta_{\mathbf{lm}}\sum_\mathbf{k}\Gamma^*_{\mathbf{nkkl}',\nu'\nu} + \Gamma^*_{\mathbf{lmnl}',\nu'\nu}\,, \tag{8.6}$$

$$\Gamma_{\mathbf{mkln},\nu\nu'} = \langle\mathbf{m}|X_\nu|\mathbf{k}\rangle\,\langle\mathbf{l}|X_{\nu'}|\mathbf{n}\rangle\,L_{\nu\nu'}(\omega_\mathbf{ln})\,. \tag{8.7}$$

The functions $L_{\nu\nu'}$

$$L_{\nu\nu'}(\omega) = \int_0^\infty \mathrm{d}t\,[\mathcal{S}_{\nu\nu'}(t) + \mathrm{i}\mathcal{A}_{\nu\nu'}(t)]\mathrm{e}^{-\mathrm{i}\omega t} \tag{8.8}$$

are given by a Laplace transform of the bath correlation functions (7.3) and (7.4) evaluated at the corresponding transition frequencies $\omega_\mathbf{ln}$. They depend on the details of the qubit-bath coupling as well as the pairwise qubit-qubit separations $\mathbf{x}_{12} = \mathbf{x}_1 - \mathbf{x}_2$. For vanishing distance of the qubits, the functions $L_{\nu\nu'}$ are all equal, and the master equation (8.5) reduces to the standard Bloch-Redfield form.

The oscillating exponential factor on the right hand side of Eq. (8.5) stems from the time dependence of the coupling operators X_ν in interaction representation. In a secular approximation one would neglect these oscillating terms keeping only those with $\mathbf{m} = \mathbf{n}$ and $\mathbf{l} = \mathbf{l}'$, or $\mathbf{m} = \mathbf{l}$ and $\mathbf{n} = \mathbf{l}'$ for which the phase in the exponent necessarily vanishes [167]. In the presence of degeneracies in the spectrum of H_s one should be more careful [260, 261], since there can be more terms with vanishing phases. Below, we will not use the secular approximation unless explicitly noted. If so, only those terms are neglected for which the total phase $\omega_\mathbf{mn} - \omega_{\mathbf{ll}'}$ is finite, irrespective of the indices $\mathbf{m}, \mathbf{n}, \mathbf{l}$, and $\mathbf{l}'$.

With the coupling operators $X_\nu = \sigma_{\nu x}$, most of the elements in the tensor (8.7) vanish. To be definite, one finds

$$\langle\mathbf{m}|X_\nu|\mathbf{k}\rangle\,\langle\mathbf{l}|X_{\nu'}|\mathbf{n}\rangle = (1-\delta_{m_\nu k_\nu})\delta_{m_{\bar{\nu}}k_{\bar{\nu}}}(1-\delta_{l_\nu n_\nu})\delta_{l_{\bar{\nu}}n_{\bar{\nu}}}\,, \tag{8.9}$$

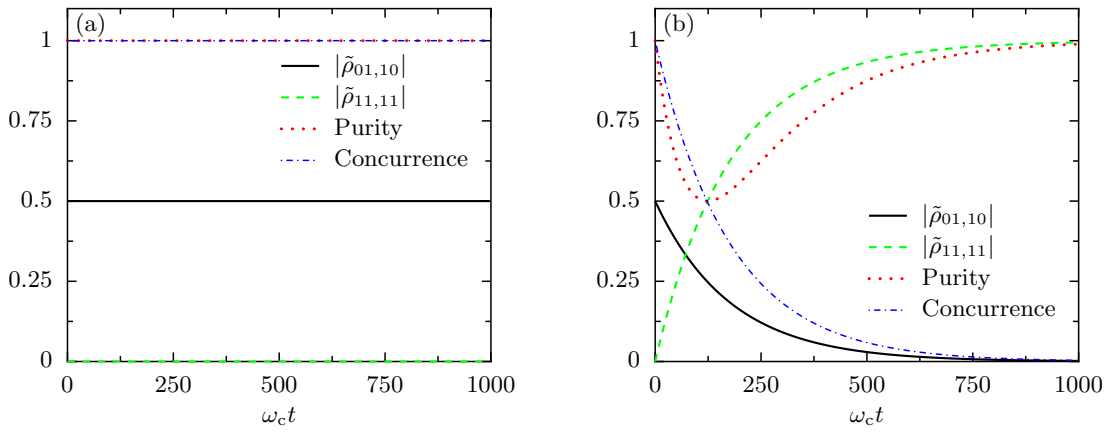

Figure 8.1: Reduced dynamics for two qubits initially prepared in the robust Bell state $|\psi_a\rangle$ and subject to collective relaxation. The temperature $k_B T = 10^{-3}\hbar\omega_c$ and the coupling strength $\alpha = 0.005$. The level splittings are (a) $\Omega_1 = \Omega_2 = 0.1\omega_c$ and (b) $\Omega_1 = 0.08\omega_c$ and $\Omega_2 = 0.12\omega_c$ The data in panel (b) is obtained by using the secular approximation.

where $\bar{\nu} = 2$ if $\nu = 1$, and $\bar{\nu} = 1$ if $\nu = 2$. In particular, Eq. (8.7) vanishes for terms with $\mathbf{m} = \mathbf{k}$ or $\mathbf{l} = \mathbf{n}$, and only those terms contribute for which the function $L_{\nu\nu'}(\omega)$ is evaluated at the frequencies $\omega = 0, \pm\Omega_1, \pm\Omega_2$. Nevertheless, in contrast to the pure dephasing model where one obtains independent equations of motion for each reduced density matrix element [cf. Eq. (3.14)], the master equation (8.5) constitutes a set of coupled differential equations with time-dependent coefficients.

8.3 Super- and subradiance at a distance

Let us start with a discussion of numerical results. To this end, the set of differential equations is integrated by an explicit Runge-Kutta method [262]. We first focus on the limiting case of a vanishing qubit separation, i.e. both qubits undergo collective amplitude damping. Figure 8.1a shows the reduced dynamics for two qubits with equal frequencies $\Omega_\nu = \Omega = 0.1\hbar\omega_c$ at a low temperature $k_B T = 10^{-2}\hbar\Omega$. It confirms that the singlet state $|S\rangle$ is indeed a robust state. In particular the amplitude of the coherence $\tilde{\rho}_{01,10}$ does not change in time and remains at its initial value 0.5. Likewise, there is no energy exchange with the environment which can already be seen by the fact that the ground state $|11\rangle$ of the qubits remains unpopulated, i.e. $\tilde{\rho}_{11,11}(t) = 0$. As a consequence, the purity $P(t) = \mathrm{tr}\,\tilde{\rho}^2(t)$ of the reduced density matrix stays constant as well as the bipartite entanglement of both qubits which we measure by the concurrence $C(t)$ defined in Eq. (6.4).

The situation is different if the qubits are not equal. An example is shown in Fig. 8.1b for the same parameters as in panel (a), but for a detuning of the qubit frequencies of $\Omega_2 - \Omega_1 = 0.4\omega_c$. Then the eigenenergies E_{01} and E_{10} of the qubit Hamiltonian are not equal anymore and a superposition of the states $|01\rangle$ and $|10\rangle$ undergoes a coherent evolution. This renders the initial singlet state to be no longer stationary, i.e. it gets

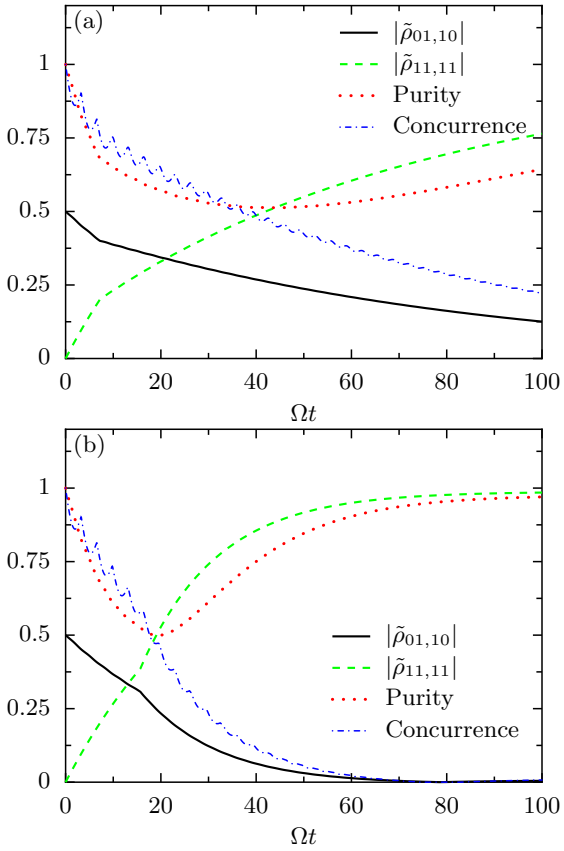

Figure 8.2: Reduced dynamics of two equal qubits with $\Omega = 10^{-2}\omega_c$ initially prepared in the singlet state $|S\rangle$, for two different qubit separations (a) $x_{12} = 6.9c/\Omega$, and (b) $x_{12} = 15.7c/\Omega$. The temperature $k_B T = 10^{-1}\hbar\Omega$ and the coupling strength $\alpha = 0.005$.

affected by the noise and the coherence $\tilde{\rho}_{01,10}$ decays. As a consequence, the reduced density operator no longer represents a pure but rather a mixed state and the purity decays. However, for longer times the purity starts to increase again. This can be explained by the fact that due to relaxation, the two-qubit ground state $\tilde{\rho}_{11,11}$ gets populated so that for low temperatures and at long times, the qubit system reaches a thermal equilibrium with a dominant population of the ground state. Hence the final state is nearly pure. The coherence decay is responsible for the initial loss of the purity, whereas for larger times the relaxation to the ground state takes over. This is nicely reflected by the fact that the purity starts to change its slope just after the time at which the amplitude of the coherence $\tilde{\rho}_{01,10}$ and the population $\tilde{\rho}_{11,11}$ cross.

We now turn to the interesting question to which extend relaxation paired with a finite qubit separation influences the entanglement decay of the qubits. Figure 8.2 shows the reduced dynamics of two qubits with equal frequencies $\Omega_\nu = \Omega = 0.01\omega_c$ again for the robust initial preparation but for a finite qubit separation. The respective transit times are (a) $t_{12} = x_{12}/c = 6.9/\Omega$, and (b) $t_{12} = 15.7/\Omega$, i.e. the transit time in both cases is larger than the coherent oscillation period $2\pi/\Omega$. In other words, the separations are outside the Dicke limit so that for the case of a three dimensional environment, collective effects would hardly be observed [110]. For the one-dimensional geometry which we discuss here, Fig. 8.2a shows that at time $t = t_{12}$ the decay of the coherence $\tilde{\rho}_{01,10}$ is significantly slowed down, paired with a slowdown of the decay to the ground state. As a consequence, the initial decay of the purity and of the concurrence is decreased,

as one would expect for a robust entangled state. The concurrence additionally shows characteristic fast oscillations. They stem from the counter-rotating terms in the qubit-bath coupling (8.2), i.e. the energy non-conserving terms $\sigma_\nu^+ b_{\mathbf{k}}^\dagger$ and $\sigma_\nu^- b_{\mathbf{k}}$. Figure 8.2b shows that also at a larger distance the reduced dynamics is changed when the transit time is passed. However, the robust state now behaves more like a fragile one: The entanglement decay is enhanced when both qubits "see" each other, accompanied with an enhanced relaxation to the ground state.

Thus, cooperative effects in the presence of relaxation are quite different from what we found for pure dephasing: The entanglement decay of a robust entangled state does in general not stop when spatial noise correlations are build up. In fact, for the same initial preparation cooperative effects can slow down or enhance the decay of the entanglement. In order to see this more clearly, we show in Fig. 8.3a the time evolution of the concurrence for a broad range of transit times t_{12}, from $t_{12} = 0$ to a transit time that corresponds to six coherent oscillation periods, i.e. to $t_{12} = 6 \times 2\pi/\Omega$. The temperature was chosen to be an order of magnitude less than the level splitting $\hbar\Omega$. We observe that for all finite distances of the qubits, i.e. for all $t_{12} > 0$, the entanglement initially decays. When the distance is a multiple of the resonant wavelength $\lambda = 2\pi c/\Omega$, however, the entanglement decay stops at the transit time $t_{12} = x_{12}/c$. The concurrence still shows small oscillations that stem from the counter-rotating terms in the coupling, as mentioned above. For all other qubit separations, the entanglement decays to zero in the limit $t \to \infty$. Thus, the entanglement dynamics of the robust entangled singlet state shows both a robust and a fragile behavior which alternates periodically by increasing the qubit separation. The final stable value for resonant qubit distances $x_{12} = n\lambda$ decreases for increasing $n = 0, 1, 2, \ldots$. This is a consequence of causality reflected by the unit step functions in the causal master equation (8.5), i.e. both qubits initially decay independently until the transit time t_{12} is reached.

In Fig. 8.3b the concurrence dynamics is depicted for the same parameters as in panel (a), however at a temperature that is an order of magnitude larger, $k_\mathrm{B}T = \hbar\Omega$. One observes that even at this high temperature, there is finite stable entanglement when the qubits are separated by at most two resonant wavelengths $n = 1, 2$, although the respective final value of the concurrence decreases. Note also that at this high temperature, the robust entanglement is much more sensitive to a deviation of the qubit distance from the exact resonance condition. For a distance of the qubits larger than two resonant wavelengths, and also for smaller separations for which the resonance condition is not met, we see that the entanglement decays to zero already during a finite time. This abrupt disappearance of the entanglement was originally predicted for two qubits that independently undergo spontaneous emission and termed entanglement sudden death [263]. Only recently, entanglement sudden death was also measured experimentally in an optical setup [264, 265] and this phenomenon was shown to exist for qubits coupled to a common environment as well, both for pure bit-flip noise as well as pure phase noise [266, 267]. Whether one can observe entanglement sudden death depends typically much on the particular choice of the initial preparation. However, recently it was found that when each qubit is subject to independent thermal noise and relaxes to its equilibrium state asymptotically, the entanglement between them always vanishes in a finite time irrespective of the initial states of the qubits [268, 269]. Our discussion shows that spatial noise correlations present in a common heat bath can force or suppress entanglement

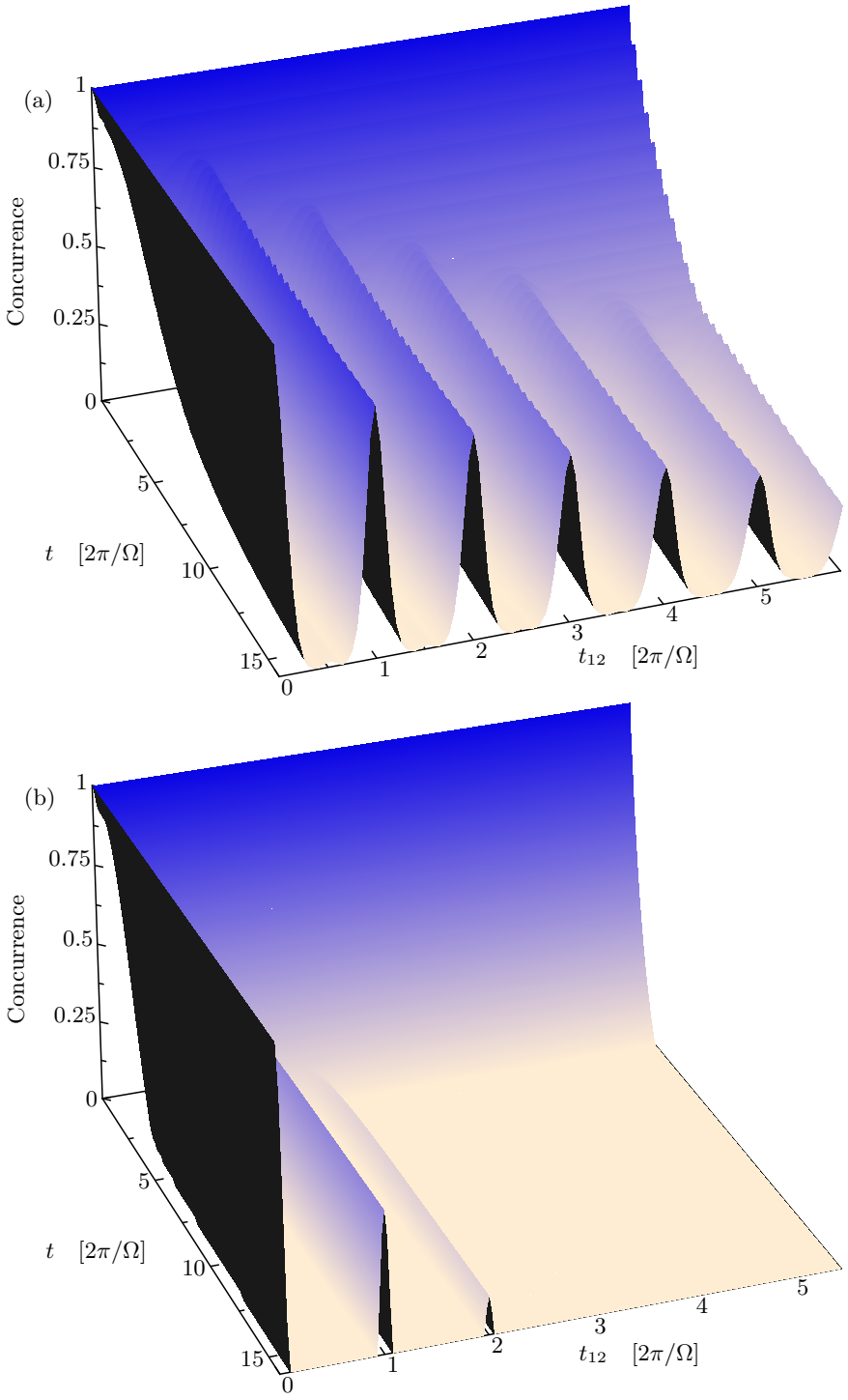

Figure 8.3: Time evolution of the concurrence $C(t)$ of two qubits with equal level splitting $\Omega = 10^{-2}\omega_c$ initially prepared in the robust singlet state $|S\rangle$ for various qubit separations $x_{12} = ct_{12}$. The time axes are scaled with respect to the oscillation period $2\pi/\Omega$ and the qubit-bath coupling strength $\alpha = 0.005$. The temperature is (a) $k_B T = 10^{-1}\hbar\Omega$ and (b) $k_B T = \hbar\Omega$.

sudden death, depending on the qubit separation.

Before we proceed our discussion, we briefly test whether the frequently employed secular approximation changes any of the findings discussed above. Figure 8.4a shows the concurrence dynamics for the same parameters as in Fig. 8.3a, but within the secular approximation. One observes that within this approximation the dynamics is described very well, in particular it also shows the characteristic periodic dependence of the robust and fragile behavior. However, the fast concurrence oscillations shown in Fig. 8.3a are not present. To compare the data more quantitatively, the difference δC of the concurrence without and within the secular approximation is plotted in Fig. 8.4b. It shows that both results deviate in particular for small times and for resonant transit times. The average difference is about 0.05 for our choice of parameters.

To gain a better understanding of the above results, let us examine the causal master equation (8.5) analytically. The real part of the Redfield tensor (8.6) is responsible for the relaxation and dephasing rates, whereas the imaginary part provides an environment induced shift of the transition frequencies $\omega_{\mathbf{mn}}$ [260, 270]. Since the matrix elements of the coupling operators $\sigma_{\nu x}$ are real-valued, the real part of the rates (8.7) are determined solely by the functions (8.8). After a lengthy but straightforward calculation one obtains for the one-dimensional environment

$$\operatorname{Re} L_{\nu\nu'}(\omega) = \begin{cases} \frac{J(|\omega|)}{2}\pi\cos(\omega t_{\nu\nu'})\left[\coth\left(\frac{\hbar|\omega|}{2k_{\mathrm{B}}T}\right) - \operatorname{sign}\omega\right] & \text{if } \omega \neq 0, \\ \lim_{\omega\to 0}\frac{J(\omega)}{2}\pi\coth\left(\frac{\hbar\omega}{2k_{\mathrm{B}}T}\right) & \text{if } \omega = 0. \end{cases} \tag{8.10}$$

Thus, for rates that involve finite transition frequencies ω, i.e. for the exchange of quanta with energy $\hbar\omega$ between the qubit system and the environment, the rates show an oscillatory dependence on the transit time $t_{\nu\nu'}$. In particular for equal qubit frequencies $\Omega_\nu = \Omega$ and at resonant qubit distances where $\Omega t_{\nu\nu'}$ is a multiple of 2π, the values of $\operatorname{Re} L_{\nu\nu'}(\omega = \Omega)$ are equal for all ν and ν'. Note that this is trivially the case when the functions $L_{\nu\nu'}$ are evaluated at zero frequency $\omega = 0$. Thus, for times $t \geq t_{12}$ at which both the local terms ($\nu = \nu'$) as well as the non-local terms ($\nu \neq \nu'$) contribute to the causal master equation (8.5), the damping rates of the density matrix elements at resonant qubit distances coincide with the rates obtained for vanishing separation. For the singlet state this means that it shows a robust behavior at resonant distances, in line with our findings above.

The argumentation of the last paragraph does not rely on the particular choice of the initial state. Thus, one expects that quite generally the entanglement decay of qubits placed at resonant distances is for times larger than the transit time, $t > t_{12}$, the same as for vanishing qubit separation, irrespective of the initial preparation. As an example, the time evolution of the concurrence for the qubits prepared in the maximally entangled triplet state $|\mathrm{T}\rangle$ is depicted in Figure 8.5. If the qubits are co-located, the symmetric preparation is known to show a enhanced decay of the populations, i.e. superradiance [110]. We here find that the collective decay of the qubits leads to a sudden death of their entanglement. The same happens not only when the distance of the qubits vanishes but also when their distance is a multiple of the resonance wavelength. Similar to the singlet state, the behavior of the triplet periodically changes with increasing separation from fragile to robust. In particular when the qubit-qubit distance is an odd multiple of the half resonance wavelength, the entanglement saturates to finite value.

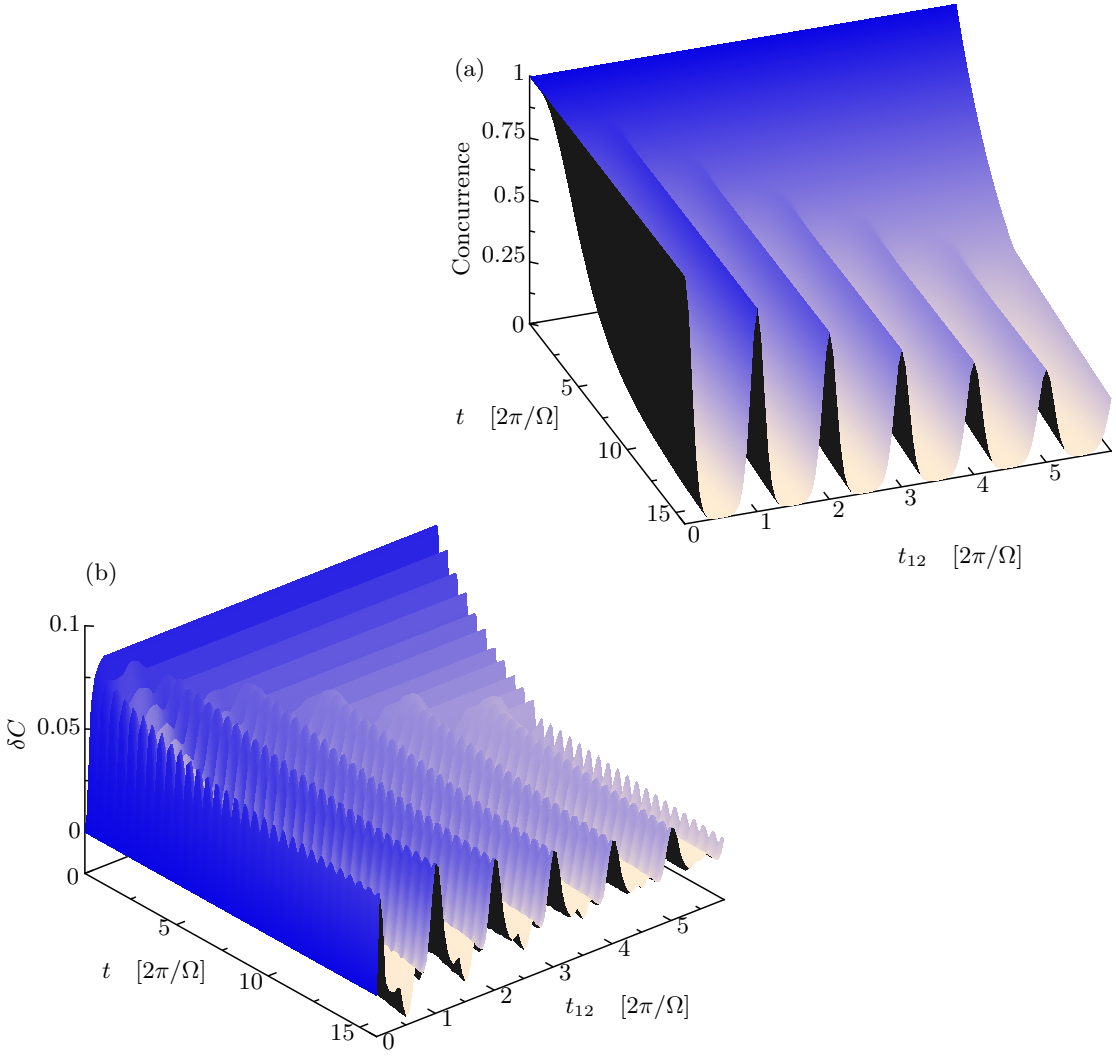

Figure 8.4: (a) Concurrence dynamics for the same parameters and initially preparation as in Fig. 8.3a, but within secular approximation. Panel (b) depicts the difference δC of the concurrences without [Fig. 8.3a] and within the secular approximation [panel (a)].

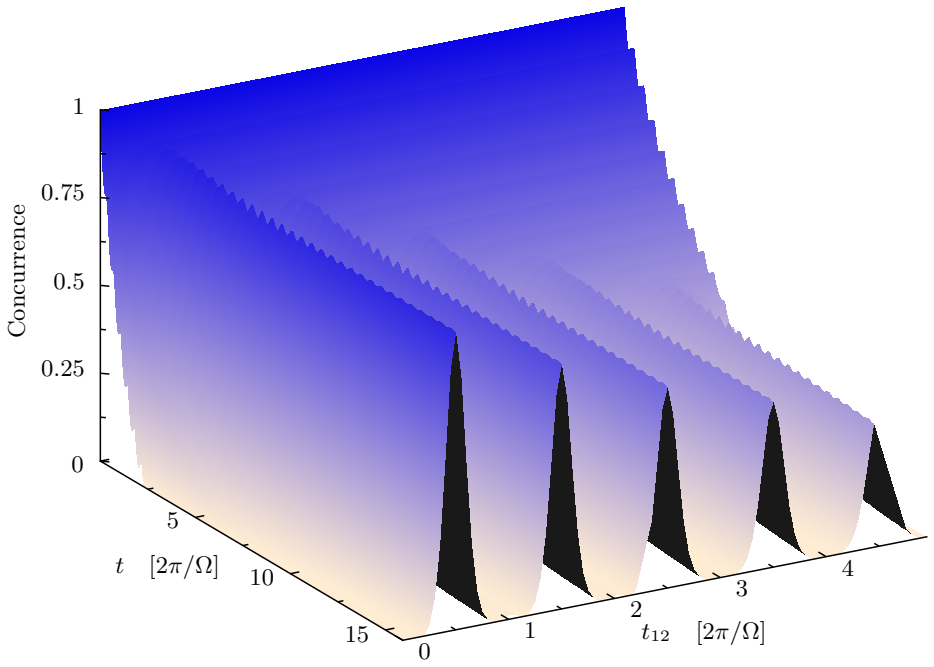

Figure 8.5: Concurrence dynamics for two qubits prepared in the fragile triplet state $|\mathrm{T}\rangle$ for various qubit separations $x_{12} = ct_{12}$. The parameters are the same as in Fig. 8.3a.

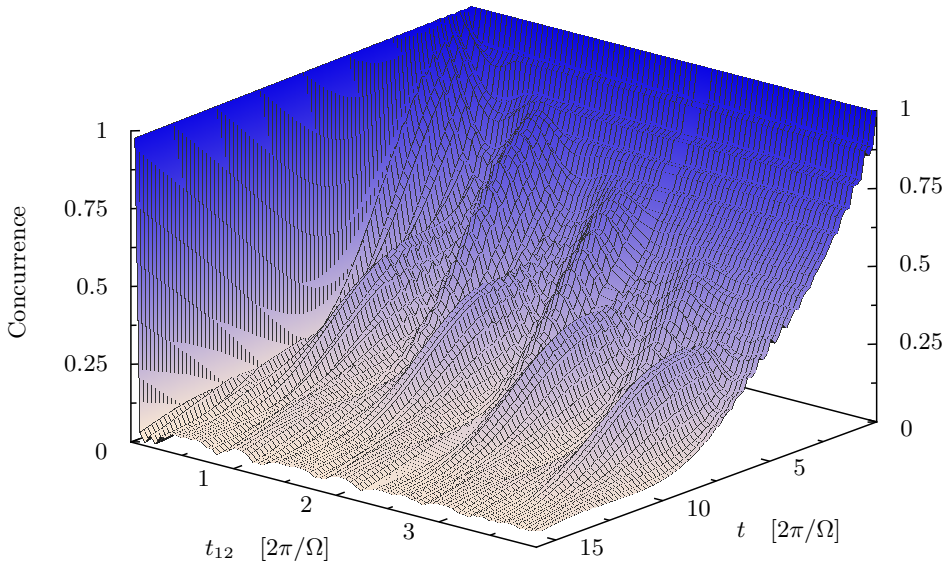

Figure 8.6: Concurrence dynamics of two qubits for various qubit distances $x_{12} = ct_{12}$. The respective level splittings are $\hbar\Omega_1 = 0.95\hbar\Omega$ and $\hbar\Omega_2 = 1.05\hbar\Omega$, with $\Omega = 10^{-2}\omega_c$ The temperature $k_B T = 10^{-1}\hbar\Omega$ and the qubit-bath coupling strength $\alpha = 0.005$.

The observed robust entanglement of qubits prepared in the singlet and the triplet state depends not only on the assumption that the qubits are placed exactly at the respective resonant distances, but also on the assumption that their level splittings are equal. As shown above, the entanglement no longer is perfectly stable if the distance deviates from the resonance conditions, and for a fixed threshold of the entanglement, the admissible tolerance depends on the temperature of the bath. The question arises how robust the collective entanglement effects are under variations of the level splittings, in particular when the qubits are not co-located. For the singlet state $|\mathrm{S}\rangle$ this situation is depicted in Fig. 8.6 for qubit frequencies $\Omega_1 = (1+\delta)\Omega$ and $\Omega_2 = (1-\delta)\Omega$ with the common frequency $\Omega = 10^{-2}\omega_\mathrm{c}$ and a relative deviation of $\delta = 0.05$. It shows that the singlet state no longer possesses stable final concurrence even for a vanishing qubit separation $t_{12} = 0$. Nevertheless, the entanglement decays only very slowly. For our choice of parameters, the concurrence at time $t = 15 \times 2\pi/\Omega$ is still at a considerable large value of $C \approx 0.98$. By contrast, if the distance is finite, the entanglement becomes quite fragile. At the resonant distances with transit times $t_{12} = n\,2\pi/\Omega$, the loss of entanglement is decreased when spatial correlations start to build up, but the entanglement continues decaying for longer times. Thus, when the level splittings of the qubits are detuned, their entanglement is not as robust as for vanishing separation.

8.4 Conclusion

We considered the dissipative entanglement dynamics of two qubits subject to thermal ohmic noise in a one-dimensional environment. Similar to subradiance and superradiance known from quantum optics, the entanglement of two equal qubits initially prepared in the singlet (triplet) state is robust (fragile) if the distance between them vanishes. In contrast to pure dephasing of qubits, the entanglement of the robust initial preparation in general decays to zero if the distance of the qubits becomes finite. However, for both the robust as well as the fragile initial state, there are distinguished qubit distances for which the entanglement saturates to a finite value. For the singlet state this is the case when both qubits are separated by any multiple of the resonance wavelength $2\pi c/\Omega$, whereas for the triplet state, the distance has to be an odd multiple of the half resonance wavelength. By increasing the qubit-qubit separation, we found that the entanglement dynamics periodically alternates between a robust and fragile behavior. This is the case for both initial states and even for large distances. It is interesting to find at resonant distances a considerable suppression of decoherence also for temperatures comparable to the qubit energy splitting, although the robustness is for higher temperatures much more sensitive to deviations from the resonance condition. An interesting application of these results could be the protection of qubits from phonon decoherence in quasi one-dimensional systems like quantum dot structures in carbon-nanotubes [83, 271]

9

Summary and Conclusion

We investigated the decoherence of a qubit register caused by spatially correlated quantum noise and developed theoretical tools to describe the associated reduced qubit dynamics. A main focus was put on the consequences for the qubit entanglement and the register fidelity. We modeled the environment as a bosonic field and allowed for a non-local qubit-field coupling to take the effects from a finite propagation time of field distortions between separated qubits into account. A natural realization of this model is the coupling of quantum dot spin and charge qubits to the phonon field of the underlying substrate. Nevertheless, we tried to keep the discussion general enough to study the generic effects of spatial noise correlations.

One part of the work concentrates on the case where the bath fluctuations induce pure dephasing of the qubit states. This allowed us to study the reduced qubit dynamics in an exact manner and to benchmark the validity of perturbative master equation approaches for weak qubit-bath coupling that are typically applied to the problem of decoherence. It turned out that the time-local version of such master equations yields the exact result for the reduced dynamics, even though it is based on a second-order perturbation theory. Since in the long-time limit it corresponds to the Markovian Bloch-Redfield theory, the latter predicts the exact long-time decay rates. For a bosonic heat bath, two conditions are necessary for the exact agreement: First, the system-bath coupling must commute with the system Hamiltonian constituting the case of pure phase noise and, second, the initial state of the bath must correspond to a Gaussian P-function. By contrast, the expansion of the time-nonlocal (Nakajima-Zwanzig) master equation, although often believed to be more accurate than the time-local version, represents an approximation when truncated at any finite order.

We showed that the frequency integrals which are of central importance for pure dephasing can be solved explicitly. By using these explicit expressions we analyzed in detail the coherence decay of a single qubit which frequently is quantified by a single exponential decay rate given by the inverse of the dephasing time T_2. We found that only for an ohmic spectral density of the environment the dephasing time is finite, i.e. after a transient time the coherence decays exponentially. For super-ohmic spectral densities the rate vanishes. Still for short times, non-Markovian errors lead to algebraic decay laws and fast initial loss of coherence. This behavior is not captured by a pure exponential description of the dynamics and shows up as a reduced visibility of the coherent qubit oscillations. The corresponding time scale depends on the spectral density of the

environment, and for an ohmic density also on the temperature. The amount of this reduced visibility has been quantified by explicit expressions. For typical temperatures below the corresponding cutoff frequency of the spectral density, they show for ohmic environments a quite strong dependence on the temperature. By contrast for super-ohmic environments, a further lowering of the temperature does not lead to a substantial suppression of the fast initial decoherence, i.e. it is determined solely by the microscopic qubit-bath coupling strength. One should note that these results are expected to be valid also in the presence of bit-flip noise, since on short time scales on which the coherent system dynamics cannot manifest itself, the behavior of the phase noise model is generic. Future work may employ our expressions of the reduced visibility to examine whether quantum error correction can overcome the fast initial coherence loss or to identify for concrete qubit realizations the parameter regimes in which unavoidable single-qubit errors hinder the feasibility of fault-tolerant quantum computing.

For the entanglement dynamics of two qubits, we found that robust entangled initial preparations, i.e. decoherence-free states of the two-qubit Hilbert space, are no longer perfectly robust if the qubit distance becomes finite. However, the entanglement of those states saturates at a finite value and a decoherence-poor subspace is built up. The duration of the initial entanglement decay depends sensitively on the dimension of the environment and its spectral density. In one dimension with an ohmic spectral density, it equals the transit time of a field distortion from one qubit to the other. In this case we found that perfect spatial correlations can emerge. By contrast, for a three-dimensional geometry with its super-ohmic spectral density, the two-qubit entanglement saturates during a time given by the inverse of the cutoff frequency. In this case a finite stable entanglement in the presence of dephasing is generally not due to spatial correlations. It rather is determined by single-qubit dynamics. As a consequence it turned out that for typical qubit separations a distinction between robust and fragile entangled states is only meaningful for one-dimensional geometries.

By studying the fidelity dynamics of a qubit register prepared in a robust W state, it turned out that the dephasing slows down whenever the elapsed time reaches a transit time between two qubits of the chain. When the transit time across the whole array is reached, the decay comes to a standstill. Single qubits in the same environment, by contrast, would loose all quantum coherence. This demonstrates that perfect noise correlations can be present also for large qubit registers when embedded in a one-dimensional environment. Although the fidelity for preserving the initial register state is smaller for larger systems, the scaling is only algebraic in the system size. This stability under dephasing is a property of the initial N-qubit W state.

To obtain a tool that allows to study approaches for coherence stabilization of spatially extended systems with algebraic methods, we derived a modified Bloch-Redfield approach that ensures causality for the qubit-qubit interaction mediated by the substrate. In contrast to the standard Bloch-Redfield theory which predicts spurious decoherence-free subspaces for a spatially extended qubit register, our causal master equation selects the Bloch-Redfield kernel depending on the time elapsed since the initial preparation. It describes the dynamics in a concise manner and allows for an intuitive interpretation.

Finally, we investigated the entanglement dynamics of two separated qubits in a one-dimensional geometry subject to bit-flip noise. For two equal qubits, collective effects similar to superradiance and subradiance were found. However, they are not limited to

the Dicke-limit but emerge as the qubits collectively exchange bosons via a thermal environment provided that their separation is a multiple of the half resonance wavelength. Depending on this distance, both the anti-symmetric (robust) and the symmetric (fragile) initial preparations exhibit robust and fragile behavior that interchanges periodically by increasing the separation. With increasing temperature of the environment, the maximal resonant distance at which a robust behavior is visible decreases, and collective effects become more sensitive to deviations from the resonance condition. Nevertheless, even at temperatures as high as the qubit energy splitting, finite stable entanglement can emerge for qubit distances of at most two resonance wavelengths. Whereas equal qubit frequencies proved to be crucial to observe collective effects of separated qubits, a small detuning leaves subradiant behavior nearly unchanged if the qubits are co-located.

The influence of noise is typically considered as purely detrimental, but quasi one-dimensional nanodevices open up possibilities where it may also be used and tailored to keep entanglement alive. Based on our results one should explore optimal geometric configurations for qubit realizations. We have seen that both perfectly uncorrelated as well as perfectly correlated noise can be present in one experiment. Decoherence-free subspace encoding is efficient for the former case whereas quantum error correction is efficient for the latter case. These conflicting requirements seem to rule out the simultaneous implementation of both strategies, e.g. by a static concatenation of both codes forming clusters of qubits. However, we identified time regimes in which either limit is realized. This suggests the possibility of time-dependent error correction protocols that dynamically adapt the appropriate error detection and recovery operation. The development of such protocols represents an intriguing line of future research.

A

Exact reduced dynamics

We here outline the derivation of the exact reduced dynamics of a spatially extended quantum system subject to pure phase noise caused by a bosonic heat bath.

A.1 Preconditions

We consider a general quantum system described by a Hamiltonian H_s that consists of $\nu = 1, 2, \ldots, N$ parts. Each part couples via a hermitian operator X_ν at a position $\mathbf{x}_\nu$ to a bosonic field. The total Hamiltonian of system and bath is given in Eq. (2.20), the coupling is bi-linear and reads

$$H_\mathrm{sb} = \sum_{\nu=1}^{N} X_\nu \xi_\nu \,, \tag{A.1}$$

with bath coordinates

$$\xi_\nu = \xi(\mathbf{x}_\nu) = \sum_{\mathbf{k}\kappa} g_{\mathbf{k}\kappa} b_{\mathbf{k}\kappa} \mathrm{e}^{\mathrm{i}\mathbf{k}\cdot\mathbf{x}_\nu} + g^*_{\mathbf{k}\kappa} b^\dagger_{\mathbf{k}\kappa} \mathrm{e}^{-\mathrm{i}\mathbf{k}\cdot\mathbf{x}_\nu} \,. \tag{A.2}$$

To ease the notation, we suppress the explicit summation over the branch index κ in the following. The total Hilbert space $\mathcal{H}_\mathrm{s}$ of the system is assumed to be a product space

$$\mathcal{H}_\mathrm{s} = \mathcal{H}_{\mathrm{s},1} \otimes \mathcal{H}_{\mathrm{s},1} \otimes \ldots \otimes \mathcal{H}_{\mathrm{s},N} \tag{A.3}$$

and the coupling operator X_ν acts on the subspace $\mathcal{H}_{\mathrm{s},\nu}$ for part ν, only. Thus, the operators X_ν pairwise commute with each other. Furthermore, for pure phase noise we require that the interaction H_sb commutes with the system Hamiltonian,

$$[H_\mathrm{sb}, H_\mathrm{s}] = 0 \,. \tag{A.4}$$

For this reason, the system Hamiltonian H_s and the set of coupling operators X_ν possess a complete set of common eigenstates, i.e. the product eigenbasis $|\mathbf{n}\rangle = |n_1, n_2, \ldots, n_N\rangle$ of the coupling operators which is defined by $X_\nu |\mathbf{n}\rangle = \chi_{\nu,n_\nu} |\mathbf{n}\rangle$ where χ_{ν,n_ν} is the n_ν-th eigenvalue of the operator X_ν.

The dynamics for the total density operator $R(t)$ of the system plus the bath is governed by the Liouville-von Neumann equation

$$\mathrm{i}\hbar\frac{\mathrm{d}}{\mathrm{d}t}\widetilde{R}(t) = \left[\widetilde{H}_{\mathrm{sb}}(t), \widetilde{R}(t)\right]. \tag{A.5}$$

The tilde denotes the interaction-picture representation with respect to $H_0 = H_\mathrm{s} + H_\mathrm{b}$, i.e. $\tilde{A}(t) = U_0^\dagger(t) A U_0(t)$, where $U_0(t) = \exp\{-\mathrm{i}H_0 t/\hbar\}$. In particular, one finds that the interaction-picture qubit operators remain time-independent, $\tilde{X}_\nu(t) = X_\nu$. For the bosonic annihilation and creation operators we obtain $\tilde{b}_\mathbf{k} = b_\mathbf{k}\exp(-\mathrm{i}\omega_\mathbf{k} t)$ and $\tilde{b}_\mathbf{k}^\dagger = b_\mathbf{k}^\dagger \exp(\mathrm{i}\omega_\mathbf{k} t)$, respectively.

We choose an initial condition of the Feynman-Vernon type, i.e. one for which the total density operator at time $t = 0$ can be factorized into a system and a bath contribution ρ and ρ_b, respectively,

$$\widetilde{R}(0) = R(0) = \rho(0) \otimes \rho_\mathrm{b}(0). \tag{A.6}$$

The bath itself is frequently assumed to be initially at thermal equilibrium. However, if the initial expectation value of the coupling operators X_ν does not vanish, the coupling (A.1) entails a force on the bath oscillators. Then the natural initial state $\rho_\mathrm{b} = \rho_\mathrm{b}(0)$ of the bath is rather a displaced thermal state which falls in the class of non-squeezed Gaussian states. A convenient basis for these states is provided by the coherent states $\{|\beta_\mathbf{k}\rangle\}$ defined by the eigenvalue equation $b_\mathbf{k}|\beta_\mathbf{k}\rangle = \beta_\mathbf{k}|\beta_\mathbf{k}\rangle$. Owing to the over-completeness of this basis, any hermitian operator can be written in a diagonal form, which assigns to each operator a P-function [101, 165]. In particular, the bath density operator can be written as

$$\rho_\mathrm{b} = \int \prod_\mathbf{k} \mathrm{d}^2\beta_\mathbf{k}\, P_\mathbf{k}(\beta_\mathbf{k}, \beta_\mathbf{k}^*) |\beta_\mathbf{k}\rangle\langle\beta_\mathbf{k}|\,, \tag{A.7}$$

where $\mathrm{d}^2\beta_\mathbf{k}$ denotes integration over the complex plane for each mode vector $\mathbf{k}$. Henceforth, we assume that the P-function of each $\mathbf{k}$ is a Gauss function, such that

$$P_\mathbf{k}(\beta_\mathbf{k}, \beta_\mathbf{k}^*) = \frac{1}{\pi n_\mathbf{k}} \exp\left(\frac{-(\beta_\mathbf{k} - \bar{\beta}_\mathbf{k})(\beta_\mathbf{k} - \bar{\beta}_\mathbf{k})^*}{n_\mathbf{k}}\right). \tag{A.8}$$

As a central property of a Gaussian state, all expectation values are fully determined by $\bar{\beta}_\mathbf{k} = \langle b_\mathbf{k}\rangle_\mathrm{b}$ and $n_\mathbf{k} = \langle b_\mathbf{k}^\dagger b_\mathbf{k}\rangle_\mathrm{b} - |\langle b_\mathbf{k}\rangle_\mathrm{b}|^2$, where

$$\langle \ldots \rangle_\mathrm{b} = \mathrm{tr}_\mathrm{b}(\rho_\mathrm{b} \ldots) \tag{A.9}$$

denotes the expectation value with respect to the bath state ρ_b. An important particular case is the canonical ensemble of the bath at temperature T such that $\rho_\mathrm{b} \propto \exp(-H_\mathrm{b}/k_\mathrm{B}T)$, which corresponds to $\langle b_k\rangle_\mathrm{b} = 0$ and $2n_k = \coth(\hbar\omega_k/2k_\mathrm{B}T) - 1$.

A.2 Derivation of the exact solution

We are exclusively interested in the reduced dynamics, i.e. the time evolution of the reduced density operator $\tilde{\rho}(t) = \langle \tilde{R}(t)\rangle_\mathrm{b}$. In what follows, we will consider the matrix elements $\tilde{\rho}_{\mathbf{m},\mathbf{n}} = \langle \mathbf{m}|\tilde{\rho}|\mathbf{n}\rangle$ in the product eigenbasis described above.

The formal solution $\tilde{\rho}(t) = \mathrm{tr_b}[U(t)R(0)U^\dagger(t)]$ of the Liouville-von-Neumann equation (A.5), is generated by the propagator

$$U(t) = \mathcal{T} \exp\left(\frac{1}{\mathrm{i}\hbar}\int_0^t \mathrm{d}s\, \widetilde{H}_{\mathrm{sb}}(s)\right), \tag{A.10}$$

where $\mathcal{T}$ denotes the time-ordering operator.

In a first step, we write the coupling Hamiltonian in the form $\widetilde{H}_{\mathrm{sb}}(t) = \widetilde{V}(t) + \widetilde{V}^\dagger(t)$ with the interaction

$$\widetilde{V}(t) = \hbar \sum_\nu X_\nu \sum_{\mathbf{k}} g_{\mathbf{k}} b_{\mathbf{k}} \mathrm{e}^{\mathrm{i}(\mathbf{k}\cdot\mathbf{x}_\nu - \omega_{\mathbf{k}} t)}, \tag{A.11}$$

and find $[\widetilde{V}(t), \widetilde{V}^\dagger(t')] = f(t-t')$, where

$$f(t) = \hbar^2 \sum_{\mathbf{k}} \sum_{\nu\nu'} |g_k|^2 X_\nu X_{\nu'} \mathrm{e}^{\mathrm{i}(\mathbf{k}\cdot\mathbf{x}_{\nu\nu'} - \omega_{\mathbf{k}} t)}. \tag{A.12}$$

Since $[\widetilde{V}(t), \widetilde{V}(t')] = [\widetilde{V}^\dagger(t), \widetilde{V}^\dagger(t')] = 0$ and $[f(t), \widetilde{V}(t')] = [f(t), \widetilde{V}^\dagger(t')] = 0$ for all times t and t', we can use the Baker-Campbell-Hausdorff formula [101] to express the time-ordered exponential (A.10) as

$$\begin{aligned} U(t) = \exp\Bigg\{ \frac{1}{\mathrm{i}\hbar}\int_0^t \mathrm{d}s\, \widetilde{H}_{\mathrm{sb}}(s) - \frac{1}{\hbar^2}\int_0^t \mathrm{d}s \int_0^t \mathrm{d}s' \\ \times f(s-s') \left[\theta(s-s') - \theta(s'-s)\right] \Bigg\}. \end{aligned} \tag{A.13}$$

The first term in the exponent can be written as

$$\exp\left\{\frac{1}{\mathrm{i}\hbar}\int_0^t \mathrm{d}s\, \widetilde{H}_{\mathrm{sb}}(s)\right\} = \prod_{\mathbf{k}} D_{\mathbf{k}}\Big(\sum_\nu X_\nu y_{\mathbf{k}\nu}\Big), \tag{A.14}$$

where we defined $y_{\mathbf{k}\nu} = g^*_{\mathbf{k}} \mathrm{e}^{-\mathrm{i}\mathbf{k}\cdot\mathbf{x}_\nu}(1 - \mathrm{e}^{\mathrm{i}\omega_{\mathbf{k}} t})/\omega_{\mathbf{k}}$ and the displacement operators $D_{\mathbf{k}}(X) = \exp\{X b^\dagger_{\mathbf{k}} - X^\dagger b_{\mathbf{k}}\}$. The second term in the exponent is a qubit operator and provides the time-dependent phase factor $\exp[\mathrm{i}\sum_{\nu\nu'} X_\nu X_{\nu'} \phi(t)]$ with

$$\phi(t) = \sum_{\mathbf{k}} |g_{\mathbf{k}}|^2 \frac{\omega_{\mathbf{k}} t - \sin(\omega_{\mathbf{k}} t)}{\omega^2_{\mathbf{k}}} \mathrm{e}^{\mathrm{i}\mathbf{k}\cdot\mathbf{x}_{\nu\nu'}}. \tag{A.15}$$

So far we have found for the propagator the expression

$$U(t) = \prod_{\mathbf{k}} D_{\mathbf{k}}\Big(\sum_\nu X_\nu y_{\mathbf{k}\nu}\Big) e^{\mathrm{i}\sum_{\nu\nu'} X_\nu X_{\nu'} \phi(t)}. \tag{A.16}$$

For the factorizing initial condition (A.6), the matrix elements of the reduced density operator become

$$\begin{aligned} \tilde{\rho}_{\mathbf{m},\mathbf{n}}(t) &= \mathrm{tr_b}\langle\mathbf{m}|U(t)\rho(0)\rho_{\mathrm{b}}U^\dagger(t)|\mathbf{n}\rangle \\ &= \rho_{\mathbf{m},\mathbf{n}}(0)\,\mathrm{tr_b}\left\{\rho_{\mathrm{b}}\langle\mathbf{n}|U^\dagger(t)|\mathbf{n}\rangle\langle\mathbf{m}|U(t)|\mathbf{m}\rangle\right\}. \end{aligned} \tag{A.17}$$

In the second equality of Eq. (A.17) we have used the cyclic property of the trace and the fact that the basis elements $|\mathbf{n}\rangle$ are eigenstates of the propagator. Inserting the expression (A.16) into Eq. (A.17), we find for density matrix element $\tilde{\rho}_{\mathbf{m},\mathbf{n}}(t)$ the phase

$$\phi_{\mathbf{m},\mathbf{n}}(t) = \phi(t) \sum_{\nu\nu'} \left(\langle \mathbf{m}| X_\nu X_{\nu'} |\mathbf{m}\rangle - \langle \mathbf{n}| X_\nu X_{\nu'} |\mathbf{n}\rangle \right) \tag{A.18}$$

$$= \sum_{\mathbf{k}} |g_{\mathbf{k}}|^2 \frac{\omega_{\mathbf{k}} t - \sin(\omega_{\mathbf{k}} t)}{\omega_{\mathbf{k}}^2} \sum_{\nu,\nu'} \mathrm{e}^{\mathrm{i}\mathbf{k}\cdot\mathbf{x}_{\nu\nu'}} \left[\chi_{\nu,m_\nu} \chi_{\nu',m_{\nu'}} - \chi_{\nu,n_\nu} \chi_{\nu',n_{\nu'}} \right] . \tag{A.19}$$

For the calculation of the remaining contributions in (A.17), we employ the relations $D_{\mathbf{k}}^\dagger(X) = D_{\mathbf{k}}(-X)$ and

$$D_{\mathbf{k}}(X) D_{\mathbf{k}}(Y) = \mathrm{e}^{(XY^\dagger - X^\dagger Y)/2} D_{\mathbf{k}}(X+Y), \tag{A.20}$$

which hold for any commuting qubit operators X and Y. Then we obtain for the matrix element

$$\tilde{\rho}_{\mathbf{m},\mathbf{n}}(t) = \rho_{\mathbf{m},\mathbf{n}}(0)\, \mathrm{e}^{\mathrm{i}\phi_{\mathbf{m},\mathbf{n}}(t)} \Big\langle \prod_{\mathbf{k}} \langle \mathbf{n}| D_{\mathbf{k}}^\dagger \Big(\sum_\nu X_\nu y_{\mathbf{k}\nu} \Big) |\mathbf{n}\rangle \langle \mathbf{m}| D_{\mathbf{k}} \Big(\sum_\nu X_\nu y_{\mathbf{k}\nu} \Big) |\mathbf{m}\rangle \Big\rangle_{\mathrm{b}} \tag{A.21}$$

$$= \rho_{\mathbf{m},\mathbf{n}}(0)\, \mathrm{e}^{\mathrm{i}[\phi_{\mathbf{m},\mathbf{n}}(t) + \eta_{\mathbf{m},\mathbf{n}}(t)]} \Big\langle \prod_{\mathbf{k}} D_{\mathbf{k}} \Big(\sum_\nu \left[\chi_{\nu,m_\nu} - \chi_{\nu,n_\nu} \right] y_{\mathbf{k}\nu} \Big) \Big\rangle_{\mathrm{b}} . \tag{A.22}$$

An additional phase $\eta_{\mathbf{m},\mathbf{n}}(t)$ stems from the commutator of the displacement operators $D_{\mathbf{k}}$ [see Eq. (A.20)] and reads

$$\eta_{\mathbf{m},\mathbf{n}}(t) = 2 \sum_{\mathbf{k}} |g_{\mathbf{k}}|^2 \frac{1 - \cos(\omega_{\mathbf{k}} t)}{\omega_{\mathbf{k}}^2} \sum_{\nu,\nu'} \chi_{\nu,m_\nu} \chi_{\nu',n_{\nu'}} \sin(\mathbf{k} \cdot \mathbf{x}_{\nu\nu'}) . \tag{A.23}$$

For the problems discussed in this thesis we either have $N = 1$ or we assume that the coupling and the dispersion is symmetric, i.e. $|g_{-\mathbf{k}}| = |g_{\mathbf{k}}|$ and $\omega_{-\mathbf{k}} = \omega_{\mathbf{k}}$. In both cases, the phase (A.23) vanishes.

It remains to evaluate the expectation value in Eq. (A.22). This is readily established by writing the bath state ρ_{b} in its P-function representation [see Eq. (A.7)] and noticing that expectation values of normal ordered products of annihilation and creation operators are identical to the moments of the P-function, where $b_{\mathbf{k}}^\dagger$ and $b_{\mathbf{k}}$ have to be replaced by $\beta_{\mathbf{k}}^*$ and $\beta_{\mathbf{k}}$, respectively [101]. Thus, by using the Baker-Campbell-Hausdorff formula

$$\exp(\lambda b_{\mathbf{k}}^\dagger - \lambda^* b_{\mathbf{k}}) = \exp(\lambda b_{\mathbf{k}}^\dagger) \exp(\lambda^* b_{\mathbf{k}}) \exp(-|\lambda|^2/2) \tag{A.24}$$

for each mode $\mathbf{k}$, we write bath expectation value in Eq. (A.22) in its normal-ordered form

$$\begin{aligned} &\exp\left[-\sum_{\mathbf{k}} \Big| \sum_\nu (\chi_{\nu,m_\nu} - \chi_{\nu,n_\nu}) y_{\mathbf{k}\nu} \Big|^2 \right] \\ &\quad \times \Big\langle \prod_k \exp\Big[\sum_\nu (\chi_{\nu,m_\nu} - \chi_{\nu,n_\nu}) (y_{\mathbf{k}\nu} \beta_{\mathbf{k}}^* + y_{\mathbf{k}\nu}^* \beta_{\mathbf{k}}) \Big] \Big\rangle_P \end{aligned} \tag{A.25}$$

where $\langle \ldots \rangle_P$ denotes the average with respect to the P-function,

$$\langle \cdots \rangle_P = \int \cdots \prod_{\mathbf{k}} P_{\mathbf{k}}(\beta_{\mathbf{k}}, \beta_{\mathbf{k}}^*) \mathrm{d}^2\beta_{\mathbf{k}} \,. \tag{A.26}$$

It is possible to express the P-function average in Eq. (A.25) with respect to the quantum characteristic function [101]

$$\mathcal{C}_{\mathbf{k}}(z) = \int \mathrm{e}^{z\beta_{\mathbf{k}}^* - z^*\beta_{\mathbf{k}}} P_{\mathbf{k}}(\beta_{\mathbf{k}}, \beta_{\mathbf{k}}^*) \mathrm{d}^2\beta_{\mathbf{k}} \,, \tag{A.27}$$

so that the exact expression for the reduced density matrix element (A.22) takes the form

$$\begin{aligned} \tilde{\rho}_{\mathbf{m},\mathbf{n}}(t) = \rho_{\mathbf{m},\mathbf{n}}(0)\, \mathrm{e}^{\mathrm{i}\phi_{\mathbf{m},\mathbf{n}}(t) - \sum_{\mathbf{k}} \left| \sum_\nu (\chi_{\nu,m_\nu} - \chi_{\nu,n_\nu}) y_{\mathbf{k}\nu} \right|^2} \\ \times \prod_{\mathbf{k}} \mathcal{C}_{\mathbf{k}} \Big(\sum_\nu \left[\chi_{\nu,m_\nu} - \chi_{\nu,n_\nu} \right] y_{\mathbf{k}\nu} \Big) \,. \end{aligned} \tag{A.28}$$

For the case of a Gaussian distribution (A.8) of the bath modes, it is possible to calculate the integral in the characteristic function (A.27) explicitly. The integration is performed easily in cartesian coordinates decomposing $\beta_{\mathbf{k}}$ in its real and imaginary part. We finally end up with

$$\tilde{\rho}_{\mathbf{m},\mathbf{n}}(t) = \rho_{\mathbf{m},\mathbf{n}}(0)\, \mathrm{e}^{-\Lambda_{\mathbf{m},\mathbf{n}}(t) + \mathrm{i}[\phi_{\mathbf{m},\mathbf{n}}(t) + \varphi_{\mathbf{m},\mathbf{n}}(t)]} \,, \tag{A.29}$$

with the phase $\phi_{\mathbf{m},\mathbf{n}}(t)$ defined in Eq. (A.19), and the phase

$$\varphi_{\mathbf{m},\mathbf{n}}(t) = 2 \sum_{\mathbf{k}} \sum_\nu \mathrm{Im} \left(\frac{\bar{\beta}_{\mathbf{k}} g_{\mathbf{k}}^*}{\omega_{\mathbf{k}}} \mathrm{e}^{\mathrm{i}\mathbf{k}\cdot\mathbf{x}_\nu} [1 - \mathrm{e}^{\mathrm{i}\omega_{\mathbf{k}} t}] \right) (\chi_{\nu,m_\nu} - \chi_{\nu,n_\nu}) \,, \tag{A.30}$$

which vanishes for a thermal initial state $\bar{\beta}_{\mathbf{k}} = 0$. The real-valued time-dependent damping reads

$$\Lambda_{\mathbf{m},\mathbf{n}}(t) = \sum_{\mathbf{k}} |g_{\mathbf{k}}|^2 \frac{1 - \cos(\omega_{\mathbf{k}} t)}{\omega_{\mathbf{k}}^2} \left[1 + 2n_{\mathbf{k}} \right] \left| \sum_\nu \left[\chi_{\nu,m_\nu} - \chi_{\nu,n_\nu} \right] \mathrm{e}^{\mathrm{i}\mathbf{k}\cdot\mathbf{x}_\nu} \right|^2 \,. \tag{A.31}$$

B

Damping rates, Lamb-shifts, and correlation functions

B.1 Solution of the integrals (3.22) and (3.19)

In this section, we outline the calculation of the integrals in the expressions for the damping amplitude (3.22) and the Lamb-shift (3.19). We introduce the dimensionless time $\tau = \omega_c t$, transit times $\tau_{\nu\nu'} = \omega_c t_{\nu\nu'}$, and temperature $\theta = k_B T/\hbar\omega_c$, and express the integral in Eq. (3.22) with respect to this scaled quantities. Taking into account the geometrical factors $G^{(d)}$ for $d = 1$ and $d = 3$ given in Eqs. (3.21)a,c, the damping amplitudes $\Lambda_{\mathbf{m},\mathbf{n}}$ involve integrals of the form

$$I^{\Lambda}_{\nu\nu'}(s',\tau) = \int_0^\infty \mathrm{d}\omega\, \omega^{s'} \mathrm{e}^{-\omega(1-\mathrm{i}\tau_{\nu\nu'})} \frac{1-\cos(\omega\tau)}{\omega^2} \coth\left(\frac{\omega}{2\theta}\right), \tag{B.1}$$

where for $d = 1$ we have to set $s' = s$ and take the real part of I^{Λ}, whereas for $d = 3$ we have to set $s' = s-1$ (since the geometrical factor $G^{(3)}(x)$ scales with $1/x$) and take the imaginary part of I^{Λ}. In the integral kernel we use the series expansion of the cosine

$$\frac{1-\cos(\omega\tau)}{\omega^2} = -\sum_{l=1}^{\infty} \frac{(-1)^l \tau^{2l} \omega^{2l-2}}{(2l)!}, \tag{B.2}$$

and perform the integration for each summand separately. We obtain

$$\begin{aligned} I^{\Lambda}_{\nu\nu'}(s',\tau) = -\sum_{l=1}^{\infty} \frac{(-1)^l \Gamma(2l+s'-1)\tau^{2l}}{(2l)!} \Big[& 2\theta^{2l+s'-1} \zeta[2l+s'-1, \theta(1-\mathrm{i}\tau_{\nu\nu'})] \\ & - (1-\mathrm{i}\tau_{\nu\nu'})^{-(2l+s'-1)} \Big]. \end{aligned} \tag{B.3}$$

Here, $\Gamma(x)$ and $\zeta(x,z)$ are the Euler Gamma function and the generalized Riemann zeta function, respectively. At this point, we can use the fact that the summation over l in Eq. (B.3) is of a standard form, so that we finally obtain expression (3.27). Likewise, for the Lamb-shift (3.19) we have to solve integrals of the form

$$I^{\phi}_{\nu\nu'}(s',\tau) = \int_0^\infty \mathrm{d}\omega\, \omega^{s'} \mathrm{e}^{-\omega(1-\mathrm{i}\tau_{\nu\nu'})} \frac{\omega\tau - \sin(\omega\tau)}{\omega^2}. \tag{B.4}$$

The calculation of this integral is straightforward and directly yields Eq. (3.30).

B.2 Correlation functions

The symmetric and anti-symmetric bath correlation functions (7.3) and (7.4), respectively, are the essential ingredients to a weak-coupling master equation approach. We found in Sect. 4.2.1 that, when integrated, they directly yield the *exact* rates for the damping and the Lamb-shift in the pure phase-noise model, c.f. Eqs. (4.14) and (4.15). Since we found explicit expressions (3.27) and (3.20) for the damping and the phase shift, we can directly obtain explicit expressions for the correlation functions by taking the second time derivate, respectively

$$\mathcal{S}_{\nu\nu'}(t) = \frac{\partial^2}{\partial t^2}\Lambda^{(d)}(t, t_{\nu\nu'})\,, \tag{B.5}$$

$$\mathcal{A}_{\nu\nu'}(t) = -\frac{\partial^2}{\partial t^2}\phi^{(d)}(t, t_{\nu\nu'})\,, \tag{B.6}$$

where the damping $\Lambda^{(d)}$ and the phase $\phi^{(d)}$ are given in Eqs. (3.25)–(3.26) and (3.28)–(3.29), respectively. For $\nu = \nu'$ they reduce to the usual correlation functions for which we find by an explicit calculation of the above time derivates

$$\begin{aligned}\mathcal{S}(t) = \mathcal{S}_{\nu\nu}(t) = \alpha\omega_{\mathrm{c}}^2\Gamma(s+1)\Bigg[&\frac{\cos[(s+1)\arctan(\omega_{\mathrm{c}}t)]}{(1+\omega_{\mathrm{c}}^2t^2)^{\frac{s+1}{2}}}\\ &+\left(\frac{2k_{\mathrm{B}}T}{\hbar\omega_{\mathrm{c}}}\right)^{s+1}\mathrm{Re}\,\zeta\Big(s+1, 1+\frac{k_{\mathrm{B}}T}{\hbar\omega_{\mathrm{c}}}[1+\mathrm{i}\omega_{\mathrm{c}}t]\Big)\Bigg]\,,\end{aligned} \tag{B.7}$$

$$\mathcal{A}(t) = \mathcal{A}_{\nu\nu}(t) = -\alpha\omega_{\mathrm{c}}^2\Gamma(s+1)\frac{\sin[(s+1)\arctan(\omega_{\mathrm{c}}t)]}{(1+\omega_{\mathrm{c}}^2t^2)^{\frac{s+1}{2}}}\,. \tag{B.8}$$

C

Quantum master equations

In this appendix, we revisit two common approaches to the reduced dynamics of a quantum system subject to the influence of a heat bath. The first one is the Nakajima-Zwanzig projector technique which leads to an integro-differential equation for the reduced density matrix, i.e. an equation of motion which is nonlocal in time. The second approach is termed "time convolutionless projection operator technique" and leads to a time-local equation of motion.

We assume that the dynamics of the total system and bath can be described by some microscopic Hamiltonian

$$H = H_0 + \epsilon H_{\mathrm{sb}}\,, \tag{C.1}$$

where H_0 is the Hamiltonian for the uncoupled system and bath and H_{sb} describes their interaction. Here, ϵ is a dimensionless expansion parameter. We will work in the interaction representation with respect to H_0 and denote operators in this picture with tilde. The Liouville-von Neumann equation for the full density matrix $\widetilde{R}$ then reads

$$\frac{\partial}{\partial t}\widetilde{R}(t) = \epsilon\mathcal{L}(t)\widetilde{R}(t)\,. \tag{C.2}$$

with the Liouvillian $\mathcal{L}(t)[\ldots] = [\widetilde{H}_{\mathrm{sb}}(t), \ldots]/\mathrm{i}\hbar$.

To derive a master equation for the reduced dynamics of the system, we will use the projector-operator formalism. We define the projector $\mathcal{P}$ in the usual way by

$$\mathcal{P} : R \mapsto \mathcal{P}R = \mathrm{tr}_{\mathrm{b}}\, R \otimes \rho_{\mathrm{b}} = \rho \otimes \rho_{\mathrm{b}}\,. \tag{C.3}$$

As the Liouvillian $\mathcal{L}(t)$ also $\mathcal{P}$ is a linear super-operator, i.e. its domain and co-domain is the set of all linear operators acting in the total Hilbert-space $\mathcal{H} = \mathcal{H}_{\mathrm{s}} \otimes \mathcal{H}_{\mathrm{b}}$ where $\mathcal{H}_{\mathrm{s}}$ and $\mathcal{H}_{\mathrm{b}}$ are the Hilbert spaces of system and bath, respectively. The trace in (C.3) is over the Hilbert space $\mathcal{H}_{\mathrm{b}}$ of the environment. Therefore the projector maps the environmental part of its argument down to a the density matrix ρ_{b} which serves as a reference state of the environment and can in principle be chosen arbitrarily. However, the choice depends on the specific application one has in mind and is often set to the stationary Gibbs state of the environment in thermal equilibrium. As $\mathcal{P}$ defines a projector, it satisfies $\mathcal{P}^2 = \mathcal{P}$. One also defines the complementary super-operator $\mathcal{Q} = \mathcal{I} - \mathcal{P}$ where $\mathcal{I}$ is the identity super-operator. One can easily show that $\mathcal{Q}^2 = \mathcal{Q}$ and $\mathcal{Q}\mathcal{P} = \mathcal{P}\mathcal{Q} = 0$.

As noted above, we will summarize two common approaches to master equations of reduced dynamics, i.e equations of motions for the reduced density matrix

$$\tilde{\rho}(t) = \langle \widetilde{R}(t) \rangle_{\mathrm{b}} \,, \tag{C.4}$$

with the average $\langle \ldots \rangle_{\mathrm{b}} = \mathrm{tr}_{\mathrm{b}}(\ldots \rho_{\mathrm{b}})$. In doing so we follow the presentation given in Ref. [100]. Our aim is to derive a closed equation for the relevant part $\mathcal{P}R$ of the total density matrix, because then the reduced density matrix is easily extracted out by definition.

By applying the operators $\mathcal{P}$ and $\mathcal{Q}$ to the Liouville-von Neumann equation we obtain two coupled differential equations for the relevant part and the irrelevant part $\mathcal{Q}\widetilde{R}$. Using $\mathcal{P} + \mathcal{Q} = \mathcal{I}$ one obtains

$$\frac{\partial}{\partial t}\mathcal{P}\widetilde{R}(t) = \epsilon \mathcal{P}\mathcal{L}(t)\widetilde{R}(t) = \epsilon \left(\mathcal{P}\mathcal{L}(t)\mathcal{P}\widetilde{R}(t) + \mathcal{P}\mathcal{L}(t)\mathcal{Q}\widetilde{R}(t) \right) , \tag{C.5}$$

$$\frac{\partial}{\partial t}\mathcal{Q}\widetilde{R}(t) = \epsilon \mathcal{Q}\mathcal{L}(t)\widetilde{R}(t) = \epsilon \left(\mathcal{Q}\mathcal{L}(t)\mathcal{Q}\widetilde{R}(t)_{\mathrm{I}} + \mathcal{Q}\mathcal{L}(t)\mathcal{P}\widetilde{R}(t) \right) . \tag{C.6}$$

C.1 Time-nonlocal form: Nakajima-Zwanzig projection operator formalism

To get a closed equation for $\mathcal{P}\widetilde{R}$ we solve the second expression formally for the irrelevant part treating the relevant part as inhomogeneity. Given an initial state $\widetilde{R}(t_0)$ at a time t_0, the irrelevant part reads

$$\mathcal{Q}\widetilde{R}(t) = \mathcal{G}(t, t_0)\mathcal{Q}\widetilde{R}(t_0) + \epsilon \int_{t_0}^{t} \mathrm{d}t' \, \mathcal{G}(t, t')\mathcal{Q}\mathcal{L}(t')\mathcal{P}\widetilde{R}(t') \tag{C.7}$$

with the propagator

$$\mathcal{G}(t, t') = \mathcal{T} \exp\left\{ \epsilon \int_{t'}^{t} \mathrm{d}s \, \mathcal{Q}\mathcal{L}(s) \right\} . \tag{C.8}$$

where $\mathcal{T}$ is the time ordering operator.[1] Note that the propagator satisfies the equation

$$\frac{\partial}{\partial t}\mathcal{G}(t, t') = \epsilon \mathcal{Q}\mathcal{L}(t)\mathcal{G}(t, t'), \quad \mathcal{G}(t', t') = \mathcal{I} \,. \tag{C.9}$$

Inserting now (C.7) into (C.5) we obtain the Nakajima-Zwanzig master equation

$$\begin{aligned} \frac{\partial}{\partial t}\mathcal{P}\widetilde{R}(t) = {} & \epsilon \mathcal{P}\mathcal{L}(t)\mathcal{P}\widetilde{R}(t) + \epsilon \mathcal{P}\mathcal{L}(t)\mathcal{G}(t, t_0)\mathcal{Q}\widetilde{R}(t_0) \\ & + \epsilon^2 \int_{t_0}^{t} \mathrm{d}t' \, \mathcal{P}\mathcal{L}(t)\mathcal{G}(t, t')\mathcal{Q}\mathcal{L}(t')\mathcal{P}\widetilde{R}(t') \,. \end{aligned} \tag{C.10}$$

This equation is in a so-called time-nonlocal (tnl) form because values of the density operator $R(t')$ and hence the state of the system at former times $t' < t$ explicitly enter the equation.

[1] As usual, $\mathcal{T}$ means chronological time ordering, i.e. products of (super)operators are ordered so that their time arguments increase from right to left.

It is often the case that the odd moments of the interaction $\widetilde{H}_{\mathrm{sb}}(t)$ with respect to the reference state ρ_{b} vanish,

$$\left\langle \widetilde{H}_{\mathrm{sb}}(t_1)\widetilde{H}_{\mathrm{sb}}(t_2)\dots\widetilde{H}_{\mathrm{sb}}(t_{2n-1})\right\rangle_{\mathrm{b}} = 0, \quad n = 1, 2, \dots, \tag{C.11}$$

from which follows that

$$\mathcal{P}\mathcal{L}(t_1)\mathcal{L}(t_2)\dots\mathcal{L}(t_{2n-1})\mathcal{P} = 0\,. \tag{C.12}$$

Using this assumption for $n = 1$, the first summand in the Nakajima-Zwanzig master equation (C.10) vanishes and we can write it in more compact notation

$$\frac{\partial}{\partial t}\mathcal{P}\widetilde{R}(t) = \mathcal{D}_{\mathrm{tnl}}(t, t_0)\mathcal{Q}\widetilde{R}(t_0) + \int_{t_0}^{t} \mathrm{d}t'\, \mathcal{K}_{\mathrm{tnl}}(t, t')\mathcal{P}\widetilde{R}(t')\,, \tag{C.13}$$

with the inhomogeneity

$$\mathcal{D}_{\mathrm{tnl}}(t, t_0) = \epsilon\mathcal{P}\mathcal{L}(t)\mathcal{G}(t, t_0)\mathcal{Q}\,, \tag{C.14}$$

and with the memory kernel

$$\mathcal{K}_{\mathrm{tnl}}(t, t') = \epsilon^2\mathcal{P}\mathcal{L}(t)\mathcal{G}(t, t')\mathcal{Q}\mathcal{L}(t')\mathcal{P}\,. \tag{C.15}$$

In the present form, the Nakajima-Zwanzig master equation is in general still too complicated to be accessible by analytical or numerical computations. Therefore, appropriate perturbation expansion are needed. There are a variety of possibilities for doing so and for weak system-bath coupling which we assume here, it is convenient to expand around the coupling strength ϵ.

Assuming a factorizing initial condition $\widetilde{R}(t_0) = \widetilde{\rho}(t_0) \otimes \rho_{\mathrm{b}}$ we have $\mathcal{Q}\widetilde{R}(t_0) = 0$ and the inhomogeneity in the Nakajima-Zwanzig master equation vanishes. If we now want to expand the memory kernel up to second order in the coupling parameter ϵ we have to expand the propagator $\mathcal{G}$ to zeroth order only, i.e. approximate it by the identity operator because of the prefactor ϵ^2 in (C.15),

$$\mathcal{K}_{\mathrm{tnl}}(t, t') = \epsilon^2\mathcal{P}\mathcal{L}(t)\mathcal{Q}\mathcal{L}(t')\mathcal{P} + \mathrm{O}(\epsilon^3) = \epsilon^2\mathcal{K}^{(2)}_{\mathrm{tnl}}(t, t') + \mathrm{O}(\epsilon^3) \tag{C.16}$$

with the second order generator $\mathcal{K}^{(2)}_{\mathrm{tnl}}(t, t') = \mathcal{P}\mathcal{L}(t)\mathcal{L}(t')\mathcal{P}$, where we again used $\mathcal{Q} = \mathcal{I} - \mathcal{P}$ and $\mathcal{P}\mathcal{L}(t)\mathcal{P} = 0$. With this modification we find the weak-coupling master equation

$$\frac{\partial}{\partial t}\mathcal{P}\widetilde{R}(t) = \int_{t_0}^{t} \mathrm{d}t'\, \mathcal{K}^{(2)}_{\mathrm{tnl}}(t, t')\mathcal{P}\widetilde{R}(t')\,. \tag{C.17}$$

Using the definition of the projection operator $\mathcal{P}$, the equation for the reduced density matrix reads

$$\frac{\partial}{\partial t}\tilde{\rho}(t) = -\frac{\epsilon^2}{\hbar^2}\int_{t_0}^{t} \mathrm{d}t'\ \mathrm{tr}_{\mathrm{b}}\left[\widetilde{H}_{\mathrm{sb}}(t), \left[\widetilde{H}_{\mathrm{sb}}(t'), \tilde{\rho}(t')\rho_{\mathrm{b}}\right]\right]\,. \tag{C.18}$$

C.2 Time-local form: time-convolutionless projection operator method

It is possible to remove the time convolution in the Nakajima-Zwanzig equation by using a so-called time-convolutionless projector operator technique which was introduced by Shibata et al. [177]. This alternative approach provides a systematic expansion in the coupling strength as well and, originally designed by van Kampen [173, 174], is called cumulant expansion. The technique was then utilized by Breuer et al. [181], in particular for a systematic expansions of the inhomogeneity which arises by considering non-factorizing initial conditions.

The trick to remove the explicit dependence on the history of the relevant part $\mathcal{P}R$ from the master equation is to introduce the inverse of the propagator (C.8) by

$$\mathcal{G}^{-1}(t,t') = \mathcal{T}_{\rightarrow} \exp\left\{-\epsilon \int_{t'}^{t} \mathrm{d}s\, \mathcal{Q}\mathcal{L}(s)\right\}, \tag{C.19}$$

where $\mathcal{T}_{\rightarrow}$ denotes antichronological time-ordering. Now we express the relevant part at former times $t' < t$ with the help of the exact back-propagation

$$\mathcal{P}\widetilde{R}(t') = \mathcal{P}\mathcal{G}^{-1}(t,t')\widetilde{R}(t) = \mathcal{P}\mathcal{G}^{-1}(t,t')\left(\mathcal{P}+\mathcal{Q}\right)\widetilde{R}(t)\,. \tag{C.20}$$

Inserting this expression in the equation (C.7) for the irrelevant part we get

$$\mathcal{Q}\widetilde{R}(t) = \mathcal{G}(t,t_0)\mathcal{Q}\widetilde{R}(t_0) + \mathcal{E}(t,t_0)\left(\mathcal{P}+\mathcal{Q}\right)\widetilde{R}(t)\,, \tag{C.21}$$

with the superoperator

$$\mathcal{E}(t,t_0) = \epsilon \int_{t_0}^{t} \mathrm{d}t'\, \mathcal{G}(t,t')\mathcal{Q}\mathcal{L}(t')\mathcal{P}\mathcal{G}^{-1}(t,t')\,. \tag{C.22}$$

This equation may be rewritten as

$$\left[1-\mathcal{E}(t,t_0)\right]\mathcal{Q}\widetilde{R}(t) = \mathcal{G}(t,t_0)\mathcal{Q}\widetilde{R}(t_0) + \mathcal{E}(t,t_0)\mathcal{P}\widetilde{R}(t)\,, \tag{C.23}$$

which means that provided that the super-operator $[1-\mathcal{E}(t,t_0)]$ can be inverted, the irrelevant part in principle can determined by the knowledge of the relevant part and the initial condition $\mathcal{Q}\widetilde{R}(t_0)$. Note that $\mathcal{E}(t,t_0) \to 0$ for $t \to t_0$ so that the inverse of $[1-\mathcal{E}(t,t_0)]$ exists for small time intervals $t-t_0$. For larger time intervals, the inverse typically also exists for small couplings because $\mathcal{E}(t,t_0) \to 0$ for $\epsilon \to 0$. However, for larger coupling strengths Eq. (C.23) may no longer be solved for $\mathcal{Q}\widetilde{R}(t)$ uniquely [100, 272].

Assuming the inverse $[1-\mathcal{E}(t,t_0)]^{-1}$ exists we can solve (C.11) for the irrelevant part and insert it into the equation (C.5). Using again the assumption of vanishing odd moments of the interaction (C.11) and (C.12) we find the following time-local (tl) master equation

$$\frac{\mathrm{d}}{\partial t}\mathcal{P}\widetilde{R}(t) = \mathcal{D}_{\mathrm{tl}}(t,t_0)\mathcal{Q}\widetilde{R}(t_0) + \mathcal{L}_{\mathrm{tl}}(t,t_0)\mathcal{P}\widetilde{R}(t)\,, \tag{C.24}$$

with the inhomogeneity

$$\mathcal{D}_{\mathrm{tl}}(t,t_0) = \epsilon\mathcal{P}\mathcal{L}(t)\left[1-\mathcal{E}(t,t_0)\right]^{-1}\mathcal{G}(t,t_0)\mathcal{Q}\,, \tag{C.25}$$

and the time-local generator

$$\mathcal{L}_{\mathrm{tl}}(t,t_0) = \epsilon\mathcal{P}\mathcal{L}(t)\left[1-\mathcal{E}(t,t_0)\right]^{-1}\mathcal{P}\,. \tag{C.26}$$

As in the previous section, we want to find now an expansion of the master equation for weak system-bath coupling. To do so, the super-operator $\mathcal{E}(t,t_0)_{\mathrm{I}}$ is be expanded into a geometric series

$$\left[1-\mathcal{E}(t,t_0)\right]^{-1} = \sum_{n=0}^{\infty}\mathcal{E}^n(t,t_0)\,, \tag{C.27}$$

so that $\mathcal{L}_{\mathrm{tl}}(t,t_0) = \epsilon\mathcal{P}\mathcal{L}(t)\mathcal{P} + \epsilon\mathcal{P}\mathcal{L}(t)\mathcal{E}(t,t_0)\mathcal{P} + O(\mathcal{E}^2)$. Using Eq. (C.12), the first term $\epsilon\mathcal{P}\mathcal{L}(t)\mathcal{P}$ vanishes and the term linear in $\mathcal{E}$ can be expanded to lowest order in ϵ,

$$\mathcal{E}(t,t_0) = \epsilon\int_{t_0}^{t}\mathrm{d}t'\,\mathcal{Q}\mathcal{L}(t')\mathcal{P} + O(\epsilon^2) = \epsilon\int_{t_0}^{t}\mathrm{d}t'\,\mathcal{L}(t')\mathcal{P} + \mathrm{O}(\epsilon^2) \tag{C.28}$$

Therefore, the second-order time-local generator reads

$$\mathcal{L}_{\mathrm{tl}}^{(2)}(t,t_0) = \int_{t_0}^{t}\mathrm{d}t'\,\mathcal{P}\mathcal{L}(t)\mathcal{L}(t')\mathcal{P}\,. \tag{C.29}$$

Inserting this expansion into Eq. (C.24) and assuming again a factorizing initial condition so that the inhomogeneity vanishes, we arive at the following second-order time-local master equation for the reduced density matrix

$$\frac{\partial}{\partial t}\tilde{\rho}(t) = -\frac{\epsilon^2}{\hbar^2}\int_{t_0}^{t}\mathrm{d}t'\;\mathrm{tr}_{\mathrm{b}}\left[\widetilde{H}_{\mathrm{sb}}(t),\left[\widetilde{H}_{\mathrm{sb}}(t'),\tilde{\rho}(t)\rho_{\mathrm{b}}\right]\right]\,. \tag{C.30}$$

Note the difference between Eq. (C.30) and the corresponding second order equation (C.18) obtained from the Nakajima-Zwanzig master equation: in the time-local form, density matrices at former times do not explicitly enter the equation. However, the time-local master equation is still non-Markovian because the coefficients in these equations are time-dependent and explicitly refer to the preparation time t_0. As both types of weak-coupling master equations considered here are equations of second order in the coupling strength, they may be expected to approximate the exact dynamics with the same accuracy [181], in the sense that they can and in general will yield different time evolutions but their relative error to the exact solution should be of the same order. Nevertheless, there is no general agreement in the literature about this statement and the time-nonlocal form is often believed to be more general.

The time-local and time-nonlocal dissipative generators in second order are the very same

$$\mathcal{L}_{\mathrm{tl}}^{(2)}(t,t_0) = \int_{t_0}^{t}\mathrm{d}t'\,\mathcal{K}_{\mathrm{tnl}}^{(2)}(t,t')\,. \tag{C.31}$$

Therefore, starting with the master equation (C.18) one is lead to Eq. (C.30) by replacing $\tilde{\rho}(t')$ with $\tilde{\rho}(t)$ in the integral kernel. In interaction picture, the system's state

changes solely due to the coupling to the environment. This change is at least of order ϵ. Therefore, in replacing the time argument t' in $\tilde{\rho}(t')$ one is left with an error of order ϵ which is neglected in second-order perurbation theory since the memory kernels considered above are themselves already of second order. This approximation is often called "first Markov-approximation" [101] although the nomenclature is somewhat misleading: the resulting equation is time-local, but in general still non-Markovian, as noted above. By considering the long time limit $t - t_0 \to \infty$ of the generator (C.31) which amounts to a "coarse-graining" of time, one is lead to a Markovian master equation equivalent to the Bloch-Redfield theory.

Bibliography

[1] M. A. Nielsen and I. L. Chuang, *Quantum Computing and Quantum Information* (Cambridge University Press, Cambridge, 2000).

[2] J. Stolze and D. Suter, *Quantum Computing* (Wiley-VCH, Weinheim, 2004).

[3] P. W. Shor, *Scheme for reducing decoherence in quantum computer memory*, Phys. Rev. A **52**, R2493 (1995).

[4] J. Kempe, *Approaches to quantum error correction*, Séminaire Poincaré **2**, 1 (2005).

[5] A. W. Steane, *A tutorial on quantum error correction*, in *Proceedings of the International School of Physics "Enrico Fermi", CLXII, Quantum Computers, Algorithms and Chaos*, edited by G. Casati, D. L. Shepelyansky, and P. Zoller, 1 (IOS Press, Amsterdam, 2006).

[6] G. M. Palma, K.-A. Suominen, and A. K. Ekert, *Quantum computers and dissipation*, Proc. R. Soc. Lond. A **452**, 567 (1996).

[7] P. Zanardi and M. Rasetti, *Noiseless quantum codes*, Phys. Rev. Lett. **79**, 1085 (1997).

[8] D. A. Lidar, I. L. Chuang, and K. B. Whaley, *Decoherence-free subspaces for quantum computation*, Phys. Rev. Lett. **81**, 2594 (1998).

[9] D. A. Lidar and K. B. Whaley, *Decoherence-free subspaces and subsystems*, in *Irreversible Quantum Dynamics*, edited by F. Benatti and R. Floreanini, vol. 622 of *Lecture Notes in Physics*, 83–120 (Springer, Berlin, 2003).

[10] E. Schrödinger, *Die gegenwärtige Situation in der Quantenmechanik*, Naturwissenschaften **23**, 807 (1935).

[11] J. D. Trimmer, *The present situation in quantum mechanics: A translation of Schrödingers 'cat paradox' paper*, Proc. Am. Phil. Soc. **124**, 323 (1980).

[12] A. Einstein, B. Podolsky, and N. Rosen, *Can quantum-mechanical description of physical reality be considered complete?*, Phys. Rev. **47**, 777 (1935).

[13] C. H. Bennett, G. Brassard, C. Crépeau, R. Jozsa, A. Peres, and W. K. Wootters, *Teleporting an unknown quantum state via dual classical and Einstein-Podolsky-Rosen channels*, Phys. Rev. Lett. **70**, 1895 (1993).

[14] A. Ekert, *Quantum cryptography based on Bell's theorem*, Phys. Rev. Lett. **67**, 661 (1991).

[15] N. Gisin, G. Ribordy, W. Tittel, and H. Zbinden, *Quantum cryptography*, Rev. Mod. Phys. **74**, 145 (2002).

[16] R. P. Feynman, *Simulating physics with computers*, Int. J. Theo. Phys. **21**, 467 (1982).

[17] E. Bernstein and U. Vazirani, *Quantum complexity theory*, in *Proceedings of the 25th Annual ACM Symposium on Theory of Computing*, 11 (ACM Press, New York, 1993).

[18] D. Deutsch, *Quantum theory, the Church-Turing principle and the universal quantum computer*, Proc. R. Soc. Lond. A **400**, 97 (1985).

[19] D. Deutsch, *Quantum computational networks*, Proc. R. Soc. Lond. A **425**, 73 (1989).

[20] R. P. Feynman, *Feynman Lectures on Computing* (Addison-Wesley, 1996).

[21] S. Lloyd, *A potentially realizable quantum computer*, Science **406**, 1047 (1993).

[22] E. Farhi, J. Goldstone, and S. G. M. Sipser, *Quantum Computation by Adiabatic Evolution*, arXiv:quant-ph/0001106 (2000).

[23] R. Raussendorf and H. J. Briegel, *A one-way quantum computer*, Phys. Rev. Lett. **86**, 5188 (2001).

[24] R. Raussendorf, D. E. Browne, and H. J. Briegel, *Measurement-based quantum computation on cluster states*, Phys. Rev. A **68**, 022312 (2003).

[25] M. H. Freedman, A. Kitaev, M. J. Larsen, and Z. H. Wang, *Topological quantum computation*, Bull. Am. Math. Soc. **40**, 31 (2003).

[26] D. Aharonov, W. van Dam, J. Kempe, Z. Landau, S. Lloyd, and O. Regev, *Adiabatic quantum computation is equivalent to standard quantum computation*, SIAM Journal of Computing **37**, 166 (2007).

[27] A. Y. Kitaev, *Fault-tolerant quantum computation by anyons*, Ann. Phys. **303**, 2 (2003).

[28] R. W. Ogburn and J. Preskill, *Topological quantum computation*, in *Quantum Computing and Quantum Communications: First NASA International Conference, QCQC'98*, edited by G. Goos, J. Hartmanis, and J. van Leeuwen, Lecture Notes in Computer Science (Springer, Berlin, 1999).

[29] D. Deutsch and R. Jozsa, *Rapid solution of problems by quantum computing*, Proc. R. Soc. Lond. A **439**, 553 (1992).

[30] D. Coppersmith, *An approximate Fourier transform useful in quantum factoring*, IBM Reserach Report No. RC19642 (1994).

[31] L. K. Grover, *A fast quantum mechanical algorithm for database search*, in *Proceedings of the 28th Annual ACM Symposium on Theory of Computing*, 212 (ACM Press, New York, 1996).

[32] L. K. Grover, *Quantum mechanics helps in searching for needle in a haystack*, Phys. Rev. Lett. **79**, 325 (1997).

[33] P. Shor, *Polynomial-time algorithms for prime factorizing and discrete logarithms on a quantum computer*, in *Proceedings of the 35th Annual Symposium on Foundations of Computer Science* (IEEE Press, Piscataway, NJ, 1994).

[34] A. Singh, *The Code Book* (Anchor Book, 2000).

[35] R. Jozsa and N. Linden, *On the Role of Entanglement in Quantum-Computational Speed-Up*, Proc. R. Soc. Lond. A **459**, 2011 (2003).

[36] S. Wallentowitz, I. A. Walmsley, and J. H. Eberly, *How big is a quantum computer?*, arXiv:quant-ph/0009069 (2000).

[37] A. Ekert, R. Jozsa, and P. Marcer, *Quantum algorithms: Entanglement-enhanced information processing*, Phil. Trans. R. Soc. Lond. A **356**, 1769 (1998).

[38] R. Horodecki, P. Horodecki, M. Horodecki, and K. Horodecki, *Quantum entanglement*, arXiv:quant-ph/0702225 (2007).

[39] P. Knight, *Quantum information processing without entanglement*, Science **287**, 441 (2000).

[40] D. Kenigsberg, T. Mor, and G. Ratsaby, *Quantum advantage without entanglement*, Quant. Inf. Comp. **6**, 606 (2006).

[41] *Quantum information Science and Technology Roadmap*, Tech. rep., URL `http://qist.lanl.gov`.

[42] L. Vandersypen and I. Chuang, *NMR techniques for quantum control and computation*, Rev. Mod. Phys. **76**, 1037 (2004).

[43] L. Vandersypen, M. Steffen, G. Breyta, C. Yannoni, M. Sherwood, and I. Chuang, *Experimental realization of Shor's quantum factoring algorithm using nuclear magnetic resonance*, Nature **414**, 883 (2001).

[44] D. Leibfried, R. Blatt, C. Monroe, and D. Wineland, *Quantum dynamics of single trapped ions*, Rev. Mod. Phys. **75**, 281 (2003).

[45] P. Kok, W. J. Munro, K. Nemoto, T. C. Ralph, J. P. Dowling, and G. J. Milburn, *Linear optical quantum computing*, Rev. Mod. Phys. **79**, 135 (2007).

[46] D. P. DiVincenzo, *The physical implementation of quantum computation*, Fortschr. Phys. **48**, 771 (2000).

[47] H. J. Krenner, S. Stufler, M. Sabathil, E. C. Clark, P. Ester, M. Bichler, G. Abstreiter, J. J. Finley, and A. Zrenner, *Recent advances in exciton-based quantum information processing in quantum dot nanostructures*, New J. Phys. **7**, 184 (2005).

[48] H. Häffner, W. Hänsel, C. F. Roos, J. Benhelm, D. Check-Al-Kar, M. Chwalla, T. Körber, U. D. Rapol, M. Riebe, P. O. Schmidt, C. Becher, O. Gühne, W. Dür, and R. Blatt, *Scalable multiparticle entanglement of trapped ions*, Nature **438**, 643 (2005).

[49] Y. Makhlin, G. Schön, and A. Shnirman, *Quantum-state engineering with Josephson-junction devices*, Rev. Mod. Phys. **73**, 357 (2001).

[50] D. Bimberg, M. Grundmann, and N. Ledentskov, *Quantum Dot Heterostructures* (Wiley, 1998).

[51] G. Chen, N. H. Bonadeo, D. G. Steel, D. Gammon, D. S. Katzer, D. Park, and L. J. Sham, *Optically induced entanglement of excitons in a single quantum dot*, Science **289**, 1906 (2000).

[52] M. Bayer, P. Hawrylak, K. Hinzer, S. Fafard, M. Korkusinski, Z. R. Wasilewski, O. Stern, and A. Forchel, *Coupling and Entangling of Quantum States in Quantum Dot Molecules*, Science **19**, 451 (2001).

[53] V. Cerletti, W. A. Coish, O. Gywat, and D. Loss, *Recipes for spin-based quantum computing*, Nanotechnology **16**, R27 (2005).

[54] E. A. Stinaff, M. Scheibner, A. S. Bracker, I. V. Ponomarev, V. L. Korenev, M. E. Ware, M. F. Doty, T. L. Reinecke, and D. Gammon, *Optical signatures of coupled quantum dots*, Science **311**, 636 (2006).

[55] Q. Xie, A. Madhukar, P. Chen, and N. P. Kobayashi, *Vertically self-organized InAs quantum box islands on GaAs(100)*, Phys. Rev. Lett. **75**, 2542 (1995).

[56] H. J. Krenner, M. Sabathil, E. C. Clark, A. Kress, D. Schuh, M. Bichler, G. Abstreiter, and J. J. Finley, *Direct observation of controlled coupling in an individual quantum dot molecule*, Phys. Rev. Lett. **94**, 057402 (2005).

[57] H. J. Krenner, E. C. Clark, T. Nakaoka, M. Bichler, C. Scheurer, G. Abstreiter, and J. J. Finley, *Optically probing spin and charge interactions in a tunable artificial molecule*, Phys. Rev. Lett. **97**, 076403 (2006).

[58] R. Hanson, L. P. Kouwenhoven, J. R. Petta, S. Tarucha, and L. M. K. Vandersypen, *Spins in few-electron quantum dots*, Rev. Mod. Phys. **79**, 1217 (2007).

[59] M. Ciorga, A. S. Sachrajda, P. Hawrylak, C. Gould, P. Zawadzki, S. Jullian, Y. Feng, and Z. Wasilewski, *Addition spectrum of a lateral dot from Coulomb and spin-blockade spectroscopy*, Phys. Rev. B **61**, R16315 (2000).

[60] L. P. Kouwenhoven, D. G. Austing, and S. Tarucha, *Few-electron quantum dots*, Rep. Prog. Phys. **64**, 701 (2001).

[61] R. H. Blick and H. Lorenz, *Possible definition of quantum bits in coupled quantum dots*, in *Proceedings of the IEEE International Symposium on Circuits and Systems*, edited by J. Calder, vol. II, 245 (2000).

[62] L. Fedichkin, M. Yanchenko, and K. A. Valiev, *Coherent charge qubits based on GaAs quantum dots with built-in barrier*, Nanotechnology **11**, 387 (2000).

[63] W. G. van der Wiel, T. Fujisawa, S. Tarucha, and L. P. Kouwenhoven, *A double quantum dot as an artificial two-level system*, Jpn. J. Appl. Phys. **40**, 2100 (2001).

[64] T. Hayashi, T. Fujisawa, H. D. Cheong, Y. H. Jeong, and Y. Hirayama, *Coherent Manipulation of Electronic States in a Double Quantum Dot*, Phys. Rev. Lett. **91**, 226804 (2003).

[65] J. R. Petta, A. C. Johnson, C. M. Marcus, M. P. Hanson, and A. C. Gossard, *Manipulation of a single charge in a double quantum dot*, Phys. Rev. Lett. **93**, 186802 (2004).

[66] J. Gorman, D. G. Hasko, and D. A. Williams, *Charge-qubit operation of an isolated double quantum dot*, Phys. Rev. Lett. **95**, 090502 (2005).

[67] T. Brandes and B. Kramer, *Spontaneous emission of phonons by coupled quantum dots*, Phys. Rev. Lett **83**, 3021 (1999).

[68] L. Fedichkin and A. Fedorov, *Error rate of a charge qubit coupled to an acoustic phonon reservoir*, Phys. Rev. A **69**, 032311 (2004).

[69] Z.-J. Wu, K.-D. Zhu, X.-Z. Yuan, Y.-W. Jiang, and H. Zheng, *Charge qubit dynamics in a double quantum dot coupled to phonons*, Phys. Rev. B **71**, 205323 (2005).

[70] M. J. Storcz, U. Hartmann, S. Kohler, and F. K. Wilhelm, *Intrinsic phonon decoherence and quantum gates in coupled lateral quantum-dot charge qubits*, Phys. Rev. B **72**, 235321 (2005).

[71] S. Vorojtsov, E. R. Mucciolo, and H. U. Baranger, *Phonon decoherence of a double quantum dot*, Phys. Rev. B **71**, 205322 (2005).

[72] L. Fedichkin and V. Privman, *Quantitative Treatment of Decoherence*, in *Electron Spin Resonance and Related Phenomena in Low Dimensional Structures*, edited by M. Fanciulli, Topics in Applied Physics (Springer, 2007).

[73] D. Loss and D. P. DiVincenzo, *Quantum computation with quantum dots*, Phys. Rev. A **57**, 120 (1998).

[74] D. P. DiVincenzo, D. Bacon, J. Kempe, G. Burkhard, and K. B. Whaley, *Universal quantum computation with the exchange interaction*, Nature **408**, 339 (2000).

[75] A. Khaetskii and Y. V. Nazarov, *Spin relaxation in semiconductor quantum dots*, Phys. Rev. B **61**, 12639 (2000).

[76] V. N. Golovach, A. Khaetskii, and D. Loss, *Phonon-induced decay of the electron spin in quantum dots*, Phys. Rev. Lett. **93**, 016601 (2004).

[77] I. A. Merkulov, A. L. Efros, and M. Rosen, *Electron spin relaxation by nuclei in semiconductor quantum dots*, Phys. Rev. B **65**, 205309 (2002).

[78] A. V. Khaetskii, D. Loss, and L. Glazman, *Electron Spin Decoherence in Quantum Dots due to Interaction with Nuclei*, Phys. Rev. Lett. **88**, 186802 (2002).

[79] A. Khaetskii, D. Loss, and L. Glazman, *Electron spin evolution induced by interaction with nuclei in a quantum dot*, Phys. Rev. B **67**, 195329 (2003).

[80] W. A. Coish and D. Loss, *Hyperfine interaction in a quantum dot: Non-Markovian electron spin dynamics*, Phys. Rev. B **70**, 195340 (2004).

[81] N. Mason, M. J. Biercuk, and C. M. Marcus, *Local Gate Control of a Carbon Nanotube Double Quantum Dot*, Science **303**, 655 (2004).

[82] M. J. Biercuk, S. Garaj, N. Mason, J. M. Chow, and C. M. Marcus, *Gate-defined quantum dots on carbon nanotubes*, Nano Lett. **5**, 1267 (2005).

[83] S. Sapmaz, P. Jarillo-Herrero, L. Kouwenhoven, and H. van der Zant, *Quantum dots in carbon nanotubes*, Semicond. Sci. Technol. **23**, S52 (2006), and Refs. therein.

[84] C. B. Simmons, M. Thalakulam, N. Shaji, L. J. Klein, H. Qin, R. H. Blick, D. E. Savage, M. G. Lagally, S. N. Coppersmith, and M. A. Eriksson, *Single-electron quantum dot in Si/SiGe with integrated charge sensing*, Appl. Phys. Lett. **91**, 213103 (2007).

[85] R. G. Clark, R. Brenner, T. M. Buehler, V. Chan, N. J. Curson, A. S. Dzurak, E. Gauja, H. S. Goan, A. D. Greentree, T. Hallam, A. R. Hamilton, L. C. L. Hollenberg, D. N. Jamieson, J. C. McCallum, G. J. Milburn, J. L. O'Brien, L. Oberbeck, C. I. Pakes, S. D. Prawer, D. J. Reilly, F. J. Ruess, S. R. Schofield, M. Y. Simmons, F. E. Stanley, R. P. Starrett, C. Wellard, and C. Yang, *Progress in silicon-based quantum computing*, Phil. Trans. R. Soc. Lond. A **361**, 1451 (2003).

[86] B. Kane, *A silicon-based nuclear spin quantum computer*, Nature (London) **393**, 133 (1998).

[87] S. D. Barrett and G. J. Milburn, *Measuring the decoherence rate in a semiconductor charge qubit*, Phys. Rev. B **68**, 155307 (2003).

[88] L. C. L. Hollenberg, A. S. Dzurak, C. Wellard, A. R. Hamilton, D. J. Reilly, G. J. Milburn, and R. G. Clark, *Charge-based quantum computing using single donors in semiconductors*, Phys. Rev. B **69**, 113301 (2004).

[89] D. A. Lidar, D. Bacon, and K. B. Whaley, *Concatenating decoherence-free subspaces with quantum error correcting codes*, Phys. Rev. Lett. **828**, 4556 (1999).

[90] W. K. Wootters and W. Z. Zurek, *A single quantum cannot be cloned*, Nature **299**, 802 (1982).

[91] T. Fujisawa, T. H. Oosterkamp, W. G. van der Wiel, B. Broer, R. Aguado, S. Tarucha, and L. P. Kouwenhoven, *Spontaneous emission spectrum in double quantum dot devices*, Science **282**, 932 (1998).

[92] M. Thorwart, J. Eckel, and E. R. Mucciolo, *Non-Markovian dynamics of double quantum dot charge qubits due to acoustic phonons*, Phys. Rev. B **72**, 235320 (2005).

[93] J. Eckel, S. Weiss, and M. Thorwart, *Phonon-induced decoherence and dissipation in donor-based charge qubits*, Eur. Phys. J. B **53**, 91 (2006).

[94] A. O. Caldeira and A. J. Leggett, *Path Integral Approach To Quantum Brownian Motion*, Physica A **121**, 587 (1983).

[95] V. B. Magalinskiĭ, *Dynamical model in the theory of the Brownian motion*, Zh. Eksp. Teor. Fiz. **36**, 1942 (1959), [Sov. Phys. JETP **9**, 1381 (1959)].

[96] R. P. Feynman and F. L. Vernon, *The theory of a general quantum system interacting with a linear dissipative system*, Ann. Phys. (N.Y.) **24**, 118 (1963).

[97] A. J. Leggett, S. Chakravarty, A. T. Dorsey, M. P. A. Fischer, A. Garg, and W. Zwerger, *Dynamics of the dissipative two-state system*, Rev. Mod. Phys. **59**, 1 (1987).

[98] P. Hänggi, P. Talkner, and M. Borkovec, *Reaction-rate theory: fifty years after Kramers*, Rev. Mod. Phys. **62**, 251 (1990).

[99] U. Weiss, *Quantum Dissipative Systems* (World Scientific, Singapore, 1998), 2nd edn.

[100] H.-P. Breuer and F. Petruccione, *The Theory of Open Quantum Systems* (Oxford University Press, Oxford, 2002).

[101] C. W. Gardiner and P. Zoller, *Quantum Noise* (Springer, Berlin, 2004), 3rd edn.

[102] P. Ullersma, *An exactly solvable model for Brownian motion. 1. Derivation of Langevin equation*, Physica **32**, 27 (1966).

[103] P. Ullersma, *An exactly solvable model for Brownian motion. 2. Derivation of Fokker-Planck equation and master equation*, Physica **32**, 56 (1966).

[104] P. Ullersma, *An exactly solvable model for Brownian motion. 3. Motion of a heavy mass in a linear chain*, Physica **32**, 74 (1966).

[105] P. Ullersma, *An exactly solvable model for Brownian motion. 4. Susceptibility and Nyquists theorem*, Physica **32**, 90 (1966).

[106] A. O. Caldeira and A. J. Leggett, *Quantum Tunnelling in a Dissipative System*, Ann. Phys. **149**, 374 (1983).

[107] G. W. Ford and M. Kac, *On the Quantum Langevin Equation*, J. Stat. Phys. **46**, 803 (1987).

[108] G. W. Ford, J. T. Lewis, and R. F. O'Connell, *Quantum Langevin equation*, Phys. Rev. A **37**, 4419 (1988).

[109] G. W. Ford, J. T. Lewis, and R. F. O'Connell, *Independent Oscillator Model of a Heat Bath: Exact Diagonalization of the Hamiltonian*, J. Stat. Phys. **53**, 439 (1988).

[110] L. Mandel and E. Wolf, *Optical Coherence and Quantum Optics* (Cambridge University Press, Cambridge, 1995).

[111] C. Cohen-Tannoudji, J. Dupont-Roc, and G. Grynberg, *Photons and Atoms* (Wiley, 1989).

[112] M. Göppert-Mayer, Ann. Phys. **9**, 273 (1931).

[113] W. G. Unruh, *Maintaining coherence in quantum computers*, Phys. Rev. A **51**, 992 (1995).

[114] G. D. Mahan, *Many-Particle Physics* (Plenum Press, New York, 1990).

[115] W. P. Schleich, *Quantum Optics in Phase Space* (Wiley-VCH, 2001).

[116] V. F. Gantmakher and Y. B. Levinson, *Carrier Scattering in Metals and Semiconductors* (North-Holland, Amsterdam, 1987).

[117] A. Grodecka, L.Jacak, P. Machnikowski, and K. Roszak, *Phonon impact on the coherent control of quantum states in semiconductor quantum dots*, in *Quantum Dots: Research Developments*, edited by P. A. Ling, 47 (Nova Science, New York, 2005).

[118] B. Krummheuer, *Reines Dephasieren und Phononendynamik in Halbleiter-Quantenpunkten*, Ph.D. thesis, Westfälische Wilhelms-Universität Münster (2005).

[119] G. D. Mahan, in *Polarons in Ionic Crystals and Polar Semiconductors*, edited by J. T. Devreese, 533 (North-Holland, 1972).

[120] B. Krummheuer, V. M. Axt, T. Kuhn, I. D'Amico, and F. Rossi, *Pure dephasing and phonon dynamics in GaAs- and GaN-based quantum dot structures: Interplay between material parameters and geometry*, Phys. Rev. B **71**, 235329 (2005).

[121] L. M. Woods, T. L. Reinecke, and Y. Lyanda-Geller, *Spin relaxation in quantum dots*, Phys. Rev. B **66**, 161318 (2002).

[122] H. Bruus, K. Flensberg, and H. Smith, *Magnetoconductivity of Quantum Wires with Elastic and Inelastic Scattering*, Phys. Rev. B **48**, 11144 (1993).

[123] T. Brandes and T. Vorrath, *Adiabatic transfer of electrons in coupled quantum dots*, Phys. Rev. B **66** (2002).

[124] P. Stano, *Controlling electron quantum dot qubits by spin-orbit interactions*, Ph.D. thesis, Universtät Regensburg (2007).

[125] L. Roth, *g Factor and Donor Spin-Lattice Relaxation for Electrons in Germanium and Silicon*, Phys. Rev. **118**, 1534 (1960).

[126] H. Hasegawa, *Spin-Lattice Relaxation of Shallow Donor States in Ge and Si through a Direct Phonon Process*, Phys. Rev. **118**, 1523 (1960).

[127] D. M. Frenkel, *Spin relaxation in GaAs-$Al_xGa_{1-x}As$ heterostructures in high magnetic fields*, Phys. Rev. B **43**, 14228 (1991).

[128] C. Calero, E. M. Chudnosvsky, and D. A. Garanin, *Field dependence of the electron spin relaxation in quantum dots*, Phys. Rev. Lett. **95**, 166603 (2005).

[129] V. Privman and D. Solenov, *Coherence and entanglement in two-qubit dynamics: Interplay of the induced exchange interaction and quantum noise due to thermal bosonic environment*, in *Quantum Information and Computation V*, edited by E. J. Donkor, A. R. Pirich, and H. E. Brandt, vol. 6573, 1 (2007).

[130] D. Mozyrsky, S. Kogan, V. N. Gorshkov, and G. P. Berman, *Time scales of phonon-induced decoherence of semiconductor spin qubits*, Phys. Rev. B **65**, 245213 (2002).

[131] M. I. D'yakonov, V. A. Marushchak, V. I. Perel', and A. N. Titkov, *The effect of strain on the spin relaxation of conduction electrons in III-V semiconductors*, Sov. Phys. JETP **63**, 655 (1986).

[132] W. Apel and Y. A. Bychkov, *Spin Relaxation in Quantum Hall Systems*, Phys. Rev. Lett. **82**, 3324 (1999).

[133] A. V. Khaetskii, *Spin relaxation in semiconductor mesoscopic systems*, Physica E **10**, 27 (2001).

[134] R. Winkler, S. J. Papadakis, E. P. D. Poortere, and M. Shayegan, *Spin-Orbit coupling in two-dimensional electron and hole systems*, in *Advances in Solid State Physics 41* (Springer, 2001).

[135] W. Zawadzki and P. Pfeffer, *Spin splitting of subband energies due to inversion asymmetry in semiconductor heterostructures*, Semicond. Sci. Technol. **19**, R1 (2004).

[136] I. Zutić, J. Fabian, and S. D. Sarma, *Spintronics: Fundamentals and applications*, Rev. Mod. Phys. **76**, 323 (2004).

[137] P. Pfeffer and W. Zawadzki, *Spin splitting of conduction subbands in GaAs-$Ga_{0.7}Al_{0.3}As$ heterostructures*, Phys. Rev. B **52**, R14332 (1995).

[138] G. Pikus and A. Titkov, *Optical orientation*, chap. Spin Relaxation under Optical Orientation in Semiconductors, 73 (North-Holland, 1984).

[139] L. Meier, G. Salis, I. Shorubalko, E. Gini, S. Schön, and K. Ensslin, *Measurement of rashba and dresselhaus spin–orbit magnetic fields*, Nature Phys. **3**, 650 (2007).

[140] J. Lehmann and D. Loss, *Cotunneling current through quantum dots with phonon-assisted spin-flip processes*, Phys. Rev. B **73**, 045328 (2006).

[141] D. V. Bulaev and D. Loss, *Spin relaxation and anticrossing in quantum dots: Rashba versus Dresselhaus spin-orbit coupling*, Phys. Rev. B **71**, 205324 (2005).

[142] H. Grabert, U. Weiss, and P. Talkner, *Quantum Theory of the Damped Harmonic Oscillator*, Z. Phys. B **55**, 87 (1984).

[143] H. Grabert, U. Weiss, and P. Hänggi, *Quantum Tunneling in Dissipative Systems at Finite Temperatures*, Phys. Rev. Lett. **25**, 2193 (1984).

[144] H. Grabert, P. Schramm, and G.-L. Ingold, *Quantum Brownian motion: The funtional integral approach*, Phys. Rep. **168**, 115 (1988).

[145] P. Riseborough, P. Hänggi, and U. Weiss, *Exact results for a damped quantum mechanical harmonic oscillator*, Phys. Rev. A **31**, 471 (1985).

[146] C. Zerbe and P. Hänggi, *Brownian parametric quantum oscillators with dissipation*, Phys. Rev. E **52**, 1533 (1995).

[147] M. Wubs, K. Saito, S. Kohler, Y. Kayanuma, and P. Hänggi, *Gauging a quantum heat bath with dissipative Landau-Zener transitions*, Phys. Rev. Lett. **97**, 200404 (2006).

[148] J. Luczka, *Spin in contact with thermostat: Exact reduced dynamics*, Physica A **167**, 919 (1990).

[149] N. G. van Kampen, *A soluble model for quantum mechanical dissipation*, J. Stat. Phys. **78**, 299 (1995).

[150] L.-M. Duan and G.-C. Guo, *Conditions for independent decoherence*, Quantum Semiclass. Opt. **10**, 611 (1998).

[151] D. Mozyrsky and V. Privman, *Adiabatic decoherence*, J. Stat. Phys. **91**, 787 (1998).

[152] D. Braun, F. Haake, and W. T. Strunz, *Universality of Decoherence*, Phys. Rev. Lett. **86**, 002913 (2001).

[153] T. Yu and J. H. Eberly, *Phonon decoherence of quantum entanglement: Robust and fragile states*, Phys. Rev. B **66**, 193306 (2002).

[154] J. H. Reina, L. Quiroga, and N. F. Johnson, *Decoherence of quantum registers*, Phys. Rev. A **65**, 032326 (2002).

[155] B. Krummheuer, V. M. Axt, and T. Kuhn, *Theory of pure dephasing and the resulting absorption line shape in semiconductor quantum dots*, Phys. Rev. B **65**, 195313 (2002).

[156] T. Yu and J. H. Eberly, *Qubit disentanglement and decoherence via dephasing*, Phys. Rev. B **68**, 165322 (2003).

[157] D. Tolkunov, V. Privman, and P. K. Aravind, *Decoherence of a measure of entanglement*, Phys. Rev. A **71**, 060308 (2005).

[158] D. Braun, *Decoherence in system of many two-level atoms*, Phys. Rev. Lett. **96**, 230502 (2006).

[159] R. Doll, M. Wubs, P. Hänggi, and S. Kohler, *Limitation of decoherence due to spatial qubit separation*, Europhys. Lett. **76**, 547 (2006).

[160] R. Doll, M. Wubs, P. Hänggi, and S. Kohler, *Incomplete pure dephasing of N-qubit entangled W states*, Phys. Rev. B **76**, 045317 (2007).

[161] R. Doll, M. Wubs, S. Kohler, and P. Hänggi, *Fidelity and entanglement of a spatially extended linear three-qubit register*, Int. J. Quantum Inf. (in press), arXiv:0802.1930 (2008).

[162] D. Solenov, D. Tolkunov, and V. Privman, *Entanglement and quantum noise due to a thermal bosonic field*, Phys. Rev. B **75**, 035134 (2007).

[163] S. Banerjee and R. Gosh, *Dynamcis of decoherence without dissipation in a squeezed thermal bath*, arXiv:quant-ph/0703054 (2007).

[164] A. Shnirman and G. Schön, *Relation between dehasing and renormalization phenomena in quantum two-level systems*, in *Quantum computing and quantum bits in mesoscopics systems*, edited by A. J. Leggett, B. Ruggiero, and P. Silvestrini, 211 (Kluwer Academic, New York, 2004).

[165] A. Perelomov, *Generalized Coherent States and Their Applications*, Theoretical and Mathematical Physics (Springer, Berlin, 1986).

[166] D. Braun, *Creation of Entanglement by Interaction with a Common Heat Bath*, Phys. Rev. Lett. **89**, 277901 (2002).

[167] K. Blum, *Density Matrix Theory and Applications* (Plenum Press, New York, 1996), 2nd edn.

[168] R. Doll, D. Zueco, M. Wubs, S. Kohler, and P. Hänggi, *On the conundrum of deriving exact solutions from approximate master equations*, Chem. Phys. (in press), doi:10.1016/j.chemphys.2007.09.003 (2007).

[169] N. G. van Kampen, *Stochastic Processes in Physics and Chemistry* (North-Holland, Amsterdam, 2001).

[170] A. Fuliński, *Master equations without time convolution*, Phys. Lett. A **25**, 13 (1967).

[171] A. Fuliński and W. J. Kramarczyk, *On the exact master equations*, Physica **39**, 575 (1968).

[172] M. Tokuyama and H. Mori, *Statistical-mechanical theory of random frequency modulations and generalized Brownian motions*, Prog. Theor. Phys. **55**, 411 (1976).

[173] N. G. van Kampen, *A cumulant expansion for stochastic linear differential euqations. I.*, Physica **74**, 215 (1974).

[174] N. G. van Kampen, *A cumulant expansion for stochastic linear differential euqations. II.*, Physica **17**, 239 (1974).

[175] P. Hänggi and H. Thomas, *Time Evolution, Correlations, and Linear Response of Non-Markov Processes*, Z. Phys. B **26**, 85 (1977).

[176] H. Grabert, P. Talkner, and P. Hänggi, *Microdynamics and time-evolution of macroscopic non-Markovian systems*, Z. Phys. B **26**, 389 (1977).

[177] F. Shibata, Y. Takahashi, and N. Hashitsume, *A generalized stochastic Liouville equation. Non-Markovian versus memoryless master equation.*, J. Stat. Phys. **17**, 171 (1977).

[178] F. Shibata and N. Hashitsume, J. Phys. Soc. Jpn. **44**, 1435 (1978).

[179] P. Hänggi, *Correlation Functions and Masterequations of Generalized (Non-Markovian) Langevin Equations*, Z. Phys. B **31**, 407 (1978).

[180] P. Hänggi and H. Thomas, *Stochastic Processes: Time Evolution, Symmetries and Linear Response*, Phys. Rep. **88**, 206 (1982).

[181] H. P. Breuer, B. Kappler, and F. Petruccione, *The time-convolutionless projector operator technique in the quantum theory of dissipation and decoherence.*, Ann. Phys. **291**, 483 (2001).

[182] S. Nakajima, *On quantum theory of transport phenomena*, Prog. Theo. Phys. **20**, 948 (1958).

[183] R. Zwanzig, *Ensemble method in the theory of irreversibility*, J. Chem. Phys. **33**, 1338 (1960).

[184] F. Haake, *Quantum Statistics in Optics and Solid-State Physics*, vol. 66 of *Springer Tracts in Modern Physics* (Springer, Berlin, 1973).

[185] K. M. Fonseca-Romero, P. Talkner, and P. Hänggi, *Is the dynamics of open quantum systems always linear?*, Phys. Rev. A **69**, 052109 (2004).

[186] R. Kubo, *Generalized cumulant expansion method*, J. Phys. Soc. Jpn. **17**, 1100 (1962).

[187] S. Chaturvedi and F. Shibata, *Time-convolutionless projection operator formalism for elimination of fast variables. Applications to Brownian motion*, Z. Phys. B **35**, 297 (1979).

[188] K. Kraus, *General state changes in quantum theory*, Ann. Phys. **64**, 311 (1970).

[189] G. Lindblad, *On the generators of quantum dynamical semigroups*, Commun. Math. Phys. **48**, 119 (1976).

[190] H. Risken, *The Fokker-Planck Equation*, vol. 18 of *Springer Series in Synergetics* (Springer, Berlin, 1984).

[191] J. Marcinkiewicz, *Sur une propriété de la loi de Gauß*, Math. Z **44**, 612 (1938).

[192] R. F. Pawula, *Approximation of the linear Boltzmann equation by the Fokker-Planck equation*, Phys. Rev. **162**, 186 (1967).

[193] P. Hänggi and P. Talkner, *A remark on truncation schemes of cumulant hierarchies*, J. Stat. Phys. **22**, 65 (1980).

[194] A. K. Rajagopal and E. C. G. Sudarshan, *Some generalizations of the Marcinkiewicz theorem and its implications to certain approximation schemes in many-particle physics*, Phys. Rev. A **10**, 1852 (1974).

[195] U. M. Titulaer, *Marcinkiewicz's theorem and approximation schemes for many-particle correlation functions: Comment on a paper by Rajagopal and Sudarshan*, Phys. Rev. A **11**, 2204 (1975).

[196] R. Schack and A. Schenzle, *Moment hierarchies and cumulants in quantum optics*, Phys. Rev. A **41**, 3847 (1990).

[197] B. Yoon, J. M. Deutch, and J. H. Freed, *A comparison of generalized cumulant and projection operator methods in spin-relaxation theory*, J. Chem. Phys. **62**, 4687 (1975).

[198] F. Shibata and T. Arimitsu, *Expansion formulas in nonequilibrium statistical mechanics*, J. Phys. Soc. J. **49**, 891 (1980).

[199] D. Solenov and V. Privman, *Models of short-time decoherence*, Proc. SPIE **5436**, 172 (2004).

[200] Y. J. Yan and R. X. Xu, *Quantum mechanics of dissipative systems*, Annu. Rev. Phys. Chem. **126**, 114102 (2005).

[201] A. Royer, *Combining projection superoperators and cumulant expansions in open quantum dynamics with initial correlations and fluctuating Hamiltonians end environments*, Phys. Lett. A **315**, 335 (2003).

[202] H.-P. Breuer, D. Burgarth, and F. Petruccione, *Non-Markovian dynamics in a spin star system: Exact solution and approximation techniques*, Phys. Rev. B **70**, 045323 (2004).

[203] H. Krovi, O. Oreshkov, M. Ryazanov, and D. A. Lidar, *Non-Markovian dynamics of a qubit coupled to an Ising spin bath*, Phys. Rev. A **76**, 052117 (2007).

[204] S. Mukamel, I. Oppenheim, and J. Ross, *Statistical reduction for strongly driven simple quantum systems*, Phys. Rev. A **17**, 1988 (1978).

[205] D. R. Reichman, F. H. Brown, and P. Neu, *Cumulant expansion and the spin-boson problem*, Phys. Rev. E **55**, 2328 (1997).

[206] M. Schröder, M. Schreiber, and U. Kleinekathöfer, *Reduced dynamics of coupled harmonic and anharmonic oscillators using higher-order perturbation theory*, J. Chem. Phys. **126**, 114102 (2007).

[207] D. A. Lidar, Z. Bihary, and K. B. Whaley, *From completely positive maps to the quantum Markovian semigroup master equation*, Chem. Phys. **268**, 35 (2001).

[208] L. A. Khalfin, *Phenomenological theory of K.deg.-mesons and the nonexponentiality of the decay law*, JETP Lett. **8**, 65 (1968).

[209] B. Misra and E. C. G. Sudarshan, *The Zeno's paradox in quantum theory*, J. Math. Phys. **18**, 756 (1977).

[210] W. H. Zurek, *Reversibility and Stability of Information Processing Systems*, Phys. Rev. Lett. **53**, 391 (1984).

[211] L. Vaidman, L. Goldenberg, and S. Wiesner, *Error prevention scheme with four particles*, Phys. Rev. A **54**, R1745 (1996).

[212] N. Erez, Y. Aharonov, B. Reznik, and L. Vaidman, *Correcting quantum errors with the Zeno effect*, Phys. Rev. A **69**, 062315 (2004).

[213] E. Brion, V. M. Akulin, D. Comparat, I. Dumer, G. Harel, N. Kébaïli, G. Kurizki, I. E. Mazets, and P. Pillet, *Decoherence, Entanglement and Information Protection in Complex Quantum Systems Verlag*, chap. Coherence Protection by the Quantum Zeno Effect, 137 (Springer Netherlands, 2005).

[214] S. Tasaki, A. Tokuse, P. Facchi, and S. Pascazio, *Control of decoherence: Dynamical decoupling versus quantum Zeno effect: A case study for trapped ions*, Int. J. Quant. Chem. **98**, 160 (2004).

[215] P. Facchi, S. Tasaki, S. Pascazio, H. Nakazato, A. Tokuse, and D. A. Lidar, *Control of decoherence: Analysis and comparison of three different strategies*, Phys. Rev. A **71**, 022302 (2005).

[216] O. Oreshkov and T. A. Brun, *Continuous quantum error correction for non-Markovian decoherence*, Phys. Rev. A **76**, 022318 (2007).

[217] A. Vagov, V. M. Axt, and T. Kuhn, *Impact of pure dephasing on the nonlinear optical response of single quantum dots and dot ensembles*, Phys. Rev. B **67**, 115338 (2003).

[218] A. Vagov, V. M. Axt, T. Kuhn, W. Langbein, P. Borri, and U. Woggon, *Nonmonotonous temperature dependence of the initial decoherence in quantum dots*, Phys. Rev. B **70**, 201305 (2004).

[219] W. K. Wootters, *Entanglement of formation of an arbitrary state of two qubits*, Phys. Rev. Lett. **80**, 2245 (1998).

[220] D. Bacon, D. A. Lidar, and K. B. Whaley, *Robustness of decoherence-free subspaces for quantum computation*, Phys. Rev. A **60**, 1944 (1999).

[221] J. B. Altepeter, P. G. Hadley, S. M. Wendelken, A. J. Berglund, and P. G. Kwiat, *Experimental investigation of a two-qubit decoherence-free subspace*, Phys. Rev. Lett. **92**, 147901 (2004).

[222] A. Ferreira, A. Guerreiro, and V. Vedral, *Macroscopic thermal entanglement due to radiation pressure*, Phys. Rev. Lett. **96**, 060407 (2006).

[223] W. Dür, G.Vidal, and J. I. Cirac, *Three qubits can be entangled in two inequivalent ways*, Phys. Rev. A **62**, 062314 (2000).

[224] J. Joo, Y.-J. Park, S. Oh, and J. Kim, *Quantum teleportation via a W state*, New J. Phys. **5**, 136 (2003).

[225] P. Agrawal and A. Pati, *Perfect teleportation and superdense coding with W states*, Phys. Rev. A **74**, 062320 (2006).

[226] Y.-J. Han, Y.-S. Zhang, and G.-C. Guo, *W state and Greenberger-Horne-Zeilinger state in quantum three-person prisoner's dilemma*, Phys. Lett. A **295**, 61 (2002).

[227] M. Eibl, N. Kiesel, M. Bourennane, C. Kurtsiefer, and H. Weinfurter, *Experimental realization of a three-qubit entangled state*, Phys. Rev. Lett. **92**, 077901 (2004).

[228] C. F. Roos, M. Riebe, H. Häffner, W. Hänsel, J. Benhelm, G. P. T. Lancaster, C. Becher, F. Schmidt-Kaler, and R. Blatt, *Control and measurement of three-qubit entangled states*, Science **304**, 1478 (2004).

[229] H. Mikami, Y. Li, K. Fukuoka, and T. Kobayashi, *New high-efficiency source of a three-photon W state and its full characterization using quantum state tomography*, Phys. Rev. Lett. **95**, 150404 (2005).

[230] V. N. Gorbachev, A. A. Rodichkina, A. I. Trubilko, and A. I. Zilba, *On preparation of the entangled W-states from atomic ensembles*, Phys. Lett. A **310**, 339 (2003).

[231] D. Bruss, N. Datta, A. Ekert, L. C. Kwek, and C. Macchiavello, *Multipartite entanglement in quantum spin chains*, Phys. Rev. A **72**, 014301 (2005).

[232] K. Saito, M. Wubs, S. Kohler, P. Hänggi, and Y. Kayanuma, *Quantum state preparation in circuit QED via Landau-Zener tunneling*, Europhys. Lett. **76**, 22 (2006).

[233] M. Wubs, S. Kohler, and P. Hänggi, *Entanglement creation in circuit QED via Landau–Zener sweeps*, Physica E **40**, 187 (2007).

[234] D. Kielpinski, *Mesoscopic entanglement of noninteracting qubits using collective spontaneous emission*, N. J. Phys. **9**, 408 (2007).

[235] A. R. R. Carvalho, F. Mintert, and A. Buchleitner, *Decoherence and Multipartite Entanglement*, Phys. Rev. Lett. **93**, 230501 (2004).

[236] C. Simon and J. Kempe, *Robustness of multiparty entanglement*, Phys. Rev. A **65**, 052327 (2002).

[237] W. Dür and H.-J. Briegel, *Stability of macroscopic entanglement under decoherence*, Phys. Rev. Lett. **92**, 180403 (2004).

[238] J. F. Poyatos, J. I. Cirac, and P. Zoller, *Complete characterization of a quantum process: The two-bit quantum gate*, Phys. Rev. Lett. **78**, 390 (1997).

[239] F. Mintert, A. R. R. Carvalhoa, M. Kuś, and A. Buchleitner, *Measures and dynamics of entangled states*, Phys. Rep. **415**, 207 (2005).

[240] R. Lohmayer, A. Osterloh, J. Siewert, and A. Uhlmann, *Entangled three-qubit states without concurrence and three-tangle*, Phys. Rev. Lett. **97**, 260502 (2006).

[241] R. Klesse and S. Frank, *Quantum error correction in spatially correlated quantum noise*, Phys. Rev. Lett. **95**, 230503 (2005).

[242] B. M. Terhal and G. Burkard, *Fault-tolerant quantum computation for local non-Markovian noise*, Phys. Rev. A **71**, 012336 (2005).

[243] P. Aliferis, D. Gottesman, and J. Preskill, *Quantum accuracy threshold for concatenated distance-3 codes*, Quant. Inf. Comput. **6**, 97 (2006).

[244] J. Kempe, D. Bacon, D. A. Lidar, and K. B. Whaley, *Theory of decoherence-free fault-tolerant universal quantum computation*, Phys. Rev. A **6304**, 042307 (2001).

[245] R. I. Karasik, K.-P. Marzlin, B. C. Sanders, and K. B. Whaley, *Multiparticle decoherence-free subspaces in extended systems*, Phys. Rev. A **76**, 012331 (2007).

[246] Y. C. Cheng and R. J. Silbey, *Markovian approximation in the relaxation of open quantum systems*, J. Phys. Chem. B **109**, 21399 (2005).

[247] R. Dicke, *Coherence in spontaneous radiation processes*, Phys. Rev. **93**, 99 (1954).

[248] Z. Ficek and R. Tanas, *Entangled states and collective nonclassical effects in two-atom systems*, Phys. Rep. **372**, 369 (2002).

[249] M. Scheibner, T. Schmidt, L. Worschech, A. Forchel, G. Bacher, T. Passow, and D. Hommel, *Superradiance of quantum dots*, Nature Physics **3**, 106 (2007).

[250] T. Brandes, *Coherent and collective quantum optical effects in mesoscopic systems*, Phys. Rep. **408**, 315 (2005).

[251] S. Iijima, *Helical microtubules of graphitic carbon*, Nature **354**, 56 (1991).

[252] M. S. Dresselhaus and P. C. Eklund, *Phonons in carbon nanotubes*, Adv. Phys. **49**, 705 (2000).

[253] J. Hone, B. Batlogg, Z. Benes, A. T. Johnson, and J. E. Fischer, *Quantized Phonon Spectrum of Single-Wall Carbon Nanotubes*, Science **289**, 1730 (2000).

[254] C. Chang, D. Okawa, H. Garcia, A. Majumdar, and A. Zettl, *Nanotube phonon waveguide.*, Phys Rev Lett **99**, 045901 (2007).

[255] P. W. Milonni and P. L. Knight, *Retardation in the resonant interaction of two identical atoms*, Phys. Rev. A **10**, 1096 (1974).

[256] P. W. Milonni and P. L. Knight, *Retarded interaction of two nonidentical atoms*, Phys. Rev. A **11**, 1090 (1975).

[257] H. T. Dung and K. Ujihara, *Analytical solution for retardation in two-atom systems*, Phys. Rev. A **59**, 2524 (1999).

[258] K. Ujihara and H. T. Dung, *Two-atom spontaneos emission in a planar microcavity*, Phys. Rev. A **66**, 053807 (2002).

[259] G. Ordonez and S. Kim, *Complex collective states in a one-dimensional two-atom system*, Phys. Rev. A **70**, 032702 (2004).

[260] M. Governale, M. Grifoni, and G. Schön, *Decoherence and dephasing in coupled Josephson-junction qubits*, Chem. Phys. **268**, 273 (2001).

[261] I. Rau, G. Johansson, and A. Shnirman, *Cavity quantum electrodynamics in superconducting circuits: Susceptibility at elevated temperatures*, Phys. Rev. B **70**, 054521 (2004).

[262] E. Hairer, S. P. Norsett, and G. Wanner, *Solving Ordinary Differential Equations I. Nonstiff Problems*, Springer Series in Comput. Mathematics (Springer, 1993).

[263] T. Yu and J. H. Eberly, *Finite-time disentanglement via spontaneos emission*, Phys. Rev. Lett. **93**, 140404 (2004).

[264] M. P. Almeida, F. de Melo, M. Hor-Meyll, A. Salles, S. P. Walborn, P. H. S. Ribeiro, and L. Davidovich, *Environment-induced sudden death of entanglement*, Science **316**, 579 (2007).

[265] J. H. Eberly and T. Yu, *The End of an Entanglement*, Science **316**, 555 (2007).

[266] Z. Ficek and R. Tanas, *Dark periods and revivals of entanglement in a two qubit system*, Phys. Rev. A **74**, 024304 (2006).

[267] K. Roszak and P. Machnikowski, *Complete disentanglement by partial pure dephasing*, Phys. Rev. A **73**, 022313 (2006).

[268] T. Yu and J. H. Eberly, *Many-Body Separability of Warm Qubits*, arXiv:0707.3215 [quant-ph] (2007).

[269] M. O. Terra Cunha, *The geometry of entanglement sudden death*, New J. Phys. **9**, 237 (2007).

[270] M. J. Storcz and F. K. Wilhelm, *Decoherence and gate performance of coupled solid-state qubits*, Phys. Rev. A **67**, 042319 (2003).

[271] C. Dekker, *Carbon nanotubes as molecular quantum wires*, Phys. Today **52**, 22 (1999).

[272] J. Salo, S. Stenholm, G. Kurizki, and A. G. Kofman, *The varieties of master equations*, in *Decoherence, Entanglement and Information Protection in Complex Quantum Systems*, edited by V. M. Akulin, A. Sarfati, G. Kurizki, and S. Pellegrin, 239 (Springer, Dordrecht, 2005).

Index

Acknowledgments

First, I would like to thank Prof. Dr. Peter Hänggi for giving me the opportunity to work in his research group on the fascinating topic of quantum information processing. This work would have been impossible without his experience and his continual support.

I am deeply indebted to PD. Dr. Sigmund Kohler for supervising the present thesis. His constant enthusiasm and high standards were extremely valuable. It was a great pleasure to work with him and I'm thankful for his advices and the motivation he supplied to make me aim higher.

I would also like to express my sincere appreciation to Prof. Dr. Stefan Kehrein for co-refereeing this thesis and Prof. Dr. Achim Wixforth for being part of the examination board.

Furthermore, I would like to express my gratitude to Dr. Martijn Wubs and Dr. David Zueco for the productive discussions we had, and the insightful feedback they provided during my work. They have been a resource for many issues and a great support.

For the careful proof-reading and the helpful comments about the present work I am very thankful to Franz Kaiser and Sekhar Burada. Last but not least my thanks go to all former and present members of the "Theorie I" group for creating an environment that was both very warm personally and very stimulating scientifically. Many thanks especially to Gert-Ludwig Ingold, Karl-Heinz Höck, Michael Schindler, Eric Lutz, Michael Strass, Gerhard Schmid, Ralf Utermann, and Daniela Schneider.

Financial support by the Deutsche Forschungsgemeinschaft through the Sonderforschungsbereich 631 "Solid-State Based Quantum Information Processing: Physical Concepts and Materials Aspects" is gratefully acknowledged.